**Academic year 2023-2024**

# Advanced Protection Concepts in Future Distribution Grids with a High Level of Distributed Generation


**Full Name of Student:** *Taulant Aliu*

**Core Provider:** *The Carl von Ossietzky University of Oldenburg*
**Specialisation:** *University of Zaragoza*

**Host Organization:** *DLR – German Airspace Center* | *Carl-von-Ossietzky Street 15, 26129 Oldenburg, Germany*

**Academic Supervisor:** *Daniel Jung*


**Submission Date:** 16.02.2025

# Table of Contents


Table of Contents ........ 2
Figures ........ 4
Tables ........ 6
List of Abbreviations ........ 7
Abstract ........ 8
Declaration ........ 9
Acknowledgements ........ 10
1. Introduction ........ 11
1.1 Motivation ........ 11
1.2. Objective ........ 12
2. Power System Protection ........ 13
2.1. Introduction to Power System Protection ........ 13
2.2. Traditional Protection Schemes ........ 16
2.2.1. Overcurrent Protection ........ 16
2.2.2. Distance Protection ........ 19
3. Fault Analysis in Distribution Grids with High DG Penetration ........ 23
3.1. Fault Types ........ 23
3.2. Impact of DG on Fault Current Levels ........ 24
4. Advanced Protection Concepts and Techniques ........ 26
4.1. Challenges in Protection Device Coordination ........ 27
5. Methodology ........ 31
5.1. Tools Used ........ 31
5.2. Cigre MS Grid Model ........ 32
5.3. The Loads ........ 34
5.4. Photovoltaic (PV) Generation Profiles ........ 35
5.5. Relay coordination ........ 36
5.5.1. Distance Protection ........ 37
5.5.2. Overcurrent Protection ........ 40

5.6. Definition and Configuration of Simulation Cases for Protection Analysis ........ 42
6. Results ........ 44
6.1. Overcurrent protection results ........ 44
6.1.1. Base Case – Without PV Generation ........ 44
6.1.2. Analysis of PV Generation Increase on Bus 12 ........ 47
6.1.3 Analysis of PV Generation Increase on Bus 13 ........ 49
6.1.4 Analysis of PV Generation Increase on Bus 14 ........ 51
6.2. Distance Protection Results ........ 53
6.3. Built-In Model Limitations ........ 55
6.4. Simplified PV Inverter Model ........ 57
6.4.1. Model Description ........ 57
6.4.2. Testing Framework ........ 59
6.5. Results from the Simplified PV Model ........ 61
6.5.1. Downstream Placement – Distance Protection ........ 61
6.5.2. Upstream Placement – Distance Protection ........ 62
6.5.3. Downstream Placement – Overcurrent Protection ........ 63
6.5.4. Upstream Placement – Overcurrent Protection ........ 64
7. Discussion ........ 65
7.1. Discussion on Overcurrent Protection Results ........ 65
7.2. Discussion on Distance Protection Results ........ 66
7.3. Future Work ........ 67
8. Conclusion ........ 69
References ........ 70
Appendices ........ 73

# Figures

Figure 1. Criteria for Selecting Overcurrent Relay [9] ....17
Figure 2 Protection problem for protective relays [9] ....17
Figure 3 Standard inverse-time overcurrent relay characteristics [9] ....18
Figure 4. The Mho graphic representation [11]....20
Figure 5. Illustration of distance protection zones with associated time delays and coverage [12] ....22
Figure 6. Representation of the zones in the complex impedance plane [12] ....22
Figure 7. Fault current waveform showing AC and DC components [13]....25
Figure 8. Parallel distribution feeders with their interconnected DG units [17] ....28
Figure 9. Illustration of fault-induced false tripping in a distribution network with distributed generation (DG) [8] ....28
Figure 10. Illustration of blinding of protection in a medium voltage network with distributed generation (DG) [19] ....29
Figure 11. Effect of DG units on distance relays [19]....29
Figure 12. Effect of infeed in distance protection [12]....30
Figure 13. The Cigre benchmark model [24] ....33
Figure 14. Active and reactive power demand profiles for residential (top) and industrial (bottom) loads generated with quasi simulation for a one week period....35
Figure 15. Active and reactive power generation profiles for the PV system at Bus 4 over a one-week period. ....36
Figure 16. RX Plot of Relay 1a with short circuit calculations [26] ....38
Figure 17. The Time Distance Plot for the Short Circuit path between bus 1 and bus 7 ....39
Figure 18. The reach plot of relay 1a....39
Figure 19. The Time Over Current plots of overcurrent protection relay OC1a (blue curve) and OC2a (green curve) ....41
Figure 20. Short-circuit current magnitudes and relay trip timings on line 12-13 under base case conditions (no PV generation)....45
Figure 21. Short-circuit current magnitudes and relay OC1a trip times versus fault location on line 12-13 ....46
Figure 22. Short-circuit current magnitudes (Iks) and relay trip times (OC1a and OC2a) for various fault locations along line 13-14 (Case 1) ....46
Figure 23. Short-circuit currents (Iks) and relay trip times for line 12-13. Top plots show variations with PV generation (Cases 1–5), and bottom plots show variations with fault location (% of line length)....47
Figure 24. Short-circuit current (Iks) and relay trip times (OC1a and OC2a) for line 13-14 under increasing PV generation levels (Cases 1–5) and varying fault locations. ....48
Figure 25. Short-circuit current (Iks) and relay trip times (OC1a and OC2a) for line 12-13 with PV generation at Bus 13. ....49
Figure 26. Short-circuit current (Iks) and relay trip times (OC1a and OC2a) for line 13-14 with PV generation at Bus 13. ....50
Figure 27. Short-circuit current (Iks) and relay trip times (OC1a) for line 12-13 with PV generation at Bus 14....52

Figure 28. Short-circuit current (Iks) and relay trip times (OC1a and OC2a) for line 13-14 with PV generation at Bus 14. ....53
Figure 29. Visualization of real and imaginary components of current and voltage during fault conditions, captured using PowerFactory measurement tools....54
Figure 30. Figure XX: Internal Structure of the Built-In PowerFactory DSL Model for PV Systems ....56
Figure 31. The PV inverter modeled as an AC Current Source ....57
Figure 32. The controller of the PV inverter....58
Figure 33. The control frame diagram of the PV inverter ....58
Figure 34. The grid model designed to test the PV inverter for a) upstream connection and b) downstream connection ....59
Figure 35. a) Impedance Magnitude vs. PV Current Contribution (Downstream PV Placement); b)Resistance and Reactance Trends (R-X Plane) for Downstream PV Placement....61
Figure 36. a) Impedance Magnitude vs. PV Current Contribution (Upstream PV Placement); b)Resistance and Reactance Trends (R-X Plane) for Upstream PV Placement ....62
Figure 37. Relationship between PV current setpoints and overcurrent protection performance for downstream PV placement : (a) Fault current magnitudes (Isc) versus cases and (b) Overcurrent relay trip times (OCtrip) versus cases. ....63
Figure 38. Relationship between PV current setpoints and overcurrent protection performance for downstream PV placement : (a) Fault current magnitudes (Isc) versus cases and (b) Overcurrent relay trip times (OCtrip) versus cases. ....64

# Tables


Table 1. Characteristics of the Cigre Model's lines ....33
Table 2. The loads of the model [24] ....33
Table 3 Transformer Specifications and Parameters. ....34
Table 4. Overcurrent relay parameters ....41
Table 5. Overview of PV Generation Scenarios in Grid area 1 ....42
Table 6. PV Generation Scenarios For Distance Protection Analysis In Grid area 2 ....43
Table 7. Fault Current Magnitudes and Relay Trip Timings for Short-Circuit Simulations on Line 12-13 ....45
Table 8. Short-Circuit Current Magnitudes (Iks) and Relay Trip Times for Line 13-14 at Various Fault Locations. ....46
Table 9. Short-circuit current magnitudes (Iks) and relay OC1a trip times for various fault locations on line 12-13 under increasing PV generation levels at Bus 12 (Cases 1–5). ....47
Table 10. Short-Circuit Currents (Iks) and Relay OC1a Trip Times for Line 13-14 ....48
Table 11. Short-Circuit Currents (Iks) and Relay OC2a Trip Times for Line 13-14 ....48
Table 12. Short-Circuit Currents (Iks) and Relay OC1a Trip Times for Line 12-13 with PV Generation at Bus 13 ....49
Table 13. Short-Circuit Currents (Iks) and Relay OC1a Trip Times for Line 13-14 with PV Generation at Bus 13 ....50
Table 14. Short-Circuit Currents (Iks) and Relay OC2a Trip Times for Line 13-14 with PV Generation at Bus 13 ....50
Table 15. Short-Circuit Currents (Iks) and Relay OC1a Trip Times for Line 12-13 with PV Generation at Bus 14 ....51
Table 16. *Short-Circuit Currents (Iks) and Relay OC1a Trip Times for Line 13-14 with PV Generation at Bus 14* ....52
Table 17. *Short-Circuit Currents (Iks) and Relay OC2a Trip Times for Line 13-14 with PV Generation at Bus 14* ....52
Table 18. Impedance and Derived Parameters for Relay 3a in the Base Case (Without PV Generation) ....54
Table 19. Impedance and Derived Parameters for Relay 5a in the Base Case (Without PV Generation) ....55
Table 20. Impedance and Derived Parameters for Relay 9a in the Base Case (Without PV Generation) ....55
Table 21. PV Inverter Current Setpoints for Fault Simulation Cases ....60
Table 22. Distance Protection Relay Impedance, Angle, Resistance, and Reactance for Downstream PV Placement ....61
Table 23. Distance Protection Relay Impedance, Angle, Resistance, and Reactance for Upstream PV Placement ....62
Table 24. Fault current magnitudes (Isc) and overcurrent relay trip times (OCtrip) for downstream PV placement with varying PV current setpoints (Ipv) ....63
Table 25. Fault current magnitudes (Isc) and overcurrent relay trip times (OCtrip) for downstream PV placement with varying PV current setpoints (Ipv). ....64
Table 26. Scenarios, Effects, and Proposed Solutions for Addressing Protection Challenges in PV-Integrated Power Systems [29] ....68

# List of Abbreviations

DG - Distributed Generation
RES - Renewable Energy Sources
PV - Photovoltaic
OCPD - Overcurrent Protection Device
CT - Current Transformer
VT - Voltage Transformer
MV - Medium Voltage
LV - Low Voltage
HV - High Voltage
IED - Intelligent Electronic Device
PMU - Phasor Measurement Unit
DER - Distributed Energy Resources
WAMS - Wide-Area Monitoring System
DSE - Dynamic State Estimation
RED - Renewable Energy Directive
EU - European Union
AC - Alternating Current
DC - Direct Current
RC - Reclosing Circuit
ROCOF - Rate of Change of Frequency
IEEE - Institute of Electrical and Electronics Engineers
IEC - International Electrotechnical Commission

# Abstract

The increasing penetration of photovoltaic (PV) generation in modern power systems raises critical questions about the effectiveness of traditional protection schemes. How does the location of PV generation influence fault current contributions and relay tripping times? What are the limitations of distance protection in systems with high PV penetration, and how can these be addressed? This thesis seeks to answer these questions by investigating overcurrent and distance protection in medium-voltage grids with distributed PV generation. Using the Cigre MS grid model in PowerFactory, various fault scenarios were simulated to evaluate the impacts of PV integration on protection coordination and relay operation.

The results reveal that upstream PV generation enhances fault current contributions and reduces relay tripping times, while downstream PV leads to delayed fault clearance, potentially compromising system stability. For distance protection, the inability to model accurate short-circuit contributions from grid-following inverters highlights significant challenges in adapting traditional schemes for renewable integration. The study emphasizes the need for advanced technologies such as phasor measurement units (PMUs) and robust communication infrastructures to enable adaptive protection schemes capable of addressing these limitations.

By exploring the limitations of current models and identifying key areas for improvement, this thesis provides a foundation for addressing protection challenges in renewable-integrated grids. Furthermore, it sets the stage for future research into grid-forming inverters, representing the next frontier in renewable energy integration and protection engineering.

# Declaration

I, Taulant Aliu, hereby declare that this thesis/report, entitled "Advanced Protection Concepts in Future Distribution Grids with a High Level of Distributed Generation", is my original work, conducted under the guidance and supervision of Daniel Jung at DLR – The German Aerospace Center, Energy System Technologies Department.

All sources of information, data, and material used in this work have been acknowledged and referenced appropriately, adhering to academic and professional standards. I further confirm that this work has not been previously submitted, in whole or in part, for any degree or qualification at this or any other institution.

During the preparation of this thesis, I utilized ChatGPT-4o, an AI language model developed by OpenAI, to assist in improving the writing style, enhancing clarity, and checking grammar and spelling. All content generated by the AI tool was thoroughly reviewed, edited, and validated by me to ensure its accuracy and alignment with the objectives of this work.

I take full responsibility for the content of this thesis and affirm that it complies with the ethical standards of research, writing, and reporting.

Signed:

Taulant Aliu

Date:

16.02.2025

# Acknowledgements

I would like to express my sincere gratitude to the DLR – German Aerospace Center, particularly the Energy System Technology Department, for providing me with the opportunity, resources, and guidance to carry out this research. I am especially thankful to my supervisor, Daniel Jung, for his unwavering support, insightful feedback, and expert guidance throughout this project. His encouragement and advice have been invaluable in shaping this work. I am equally grateful to my co-supervisor, Nauman Beg, for his technical expertise and constructive feedback, which significantly enhanced the quality of this research. I am also deeply thankful to Frank Schuldt, my first examiner, for his constructive criticism and valuable input throughout the process doing this research.

This thesis would not have been possible without the foundation laid by the European Master in Renewable Energy program. I am thankful to my core university, the University of Oldenburg, and my specialization university, the University of Zaragoza, for their academic and professional support throughout my studies.

On a personal note, I am profoundly grateful to my family—my parents, fiancé, siblings, and my little nephew—whose unwavering love, support, and encouragement have been my greatest source of strength and motivation throughout this journey.

To everyone who has contributed, directly or indirectly, to the completion of this thesis, I offer my deepest gratitude.

# 1. Introduction

## 1.1 Motivation

The global energy sector is undergoing a major transformation, driven by the increasing integration of renewable energy sources and the shift towards decentralized power generation. Climate change concerns and the need to reduce carbon emissions have accelerated the adoption of Distributed Generation (DG), particularly from renewable sources such as wind, solar, and biomass. This shift has not only altered the conventional structure of power systems, which were originally designed for large, centralized power plants, but has also introduced new technical challenges that must be addressed to ensure reliable and stable grid operation.

In Europe, the transition to green energy is supported by ambitious policies such as the European Union’s Renewable Energy Directive (RED) [1] and the European Green Deal [2], which aim to achieve significant decarbonization by promoting renewable energy use and improving energy efficiency. Since its introduction in 2009 and subsequent revision in 2018, RED has set binding targets requiring at least 32% of the EU's energy to come from renewables by 2030. National policies such as Germany’s Energiewende [3] and Denmark’s wind energy initiatives [4] have significantly increased the penetration of DG technologies across the continent, fundamentally reshaping power systems.

However, this transition has introduced challenges in fault detection, protection coordination, and grid stability, particularly in the presence of inverter-based renewable generation. Unlike traditional synchronous generators, inverter-based DG contributes much lower fault currents, complicating the operation of overcurrent and distance protection systems [5]. Bidirectional power flows introduced by DG also lead to phenomena such as blinding of protection and sympathetic tripping. These technical issues are further intensified by the intermittent nature of renewable generation, which causes rapid changes in power output, challenging conventional protection systems.

Another critical challenge is the reduction in system inertia due to the displacement of traditional synchronous machines. Inverter-based DG lacks mechanical inertia, leading to faster frequency deviations during disturbances and increasing the risk of frequency instability [5]. Voltage regulation, historically managed centrally, has also become more complex due to DG integration in distribution networks, where reverse power flows during periods of high generation and low demand can cause overvoltages, while low generation during peak demand can result in undervoltage conditions [5].

To address these challenges, modern power systems are adopting advanced protection schemes and smart grid technologies. Adaptive relays and Phasor Measurement Units (PMUs) allow real-time monitoring of grid conditions and enable protection schemes to dynamically adjust to changing conditions [5]. These technologies are essential for managing the variability introduced by renewable generation and ensuring reliable fault detection and isolation.

Despite these advancements, significant research gaps remain. Current protection systems often struggle to address the variability and complexity introduced by high levels of DG penetration. This thesis focuses on exploring the protection challenges associated with DG integration, with particular attention to overcurrent and distance protection. The research investigates how varying levels of PV generation affect fault detection and relay performance, providing insights into adapting protection systems for modern grids. Furthermore, by addressing the limitations of current protection systems, this work sets the stage for future studies on grid-forming inverters, which represent the next frontier in renewable energy integration and protection engineering.

## 1.2. Objective

The primary objective of this research is to evaluate the behavior and limitations of overcurrent and distance protection schemes in medium-voltage (MV) grids with high penetration of photovoltaic (PV) generation. To achieve this, the research is structured around several key aims.

First, the study focuses on developing a detailed model of a reference medium-voltage grid. This model incorporates unique residential load profiles and PV generation profiles, which are critical for accurately simulating the dynamics of a grid with significant distributed generation (DG). The modeling process aims to capture the intermittent nature of solar PV systems, ensuring a realistic representation of their integration into the grid.

Next, the research conducts a comprehensive fault analysis to assess the performance of overcurrent and distance protection schemes under various grid scenarios. For overcurrent protection, the study analyzes the impact of PV generation on fault current magnitudes and relay tripping times, particularly as PV penetration levels and locations are varied. The analysis identifies key limitations of traditional overcurrent protection schemes in handling the bidirectional power flows and reduced fault current contributions introduced by PV systems. For distance protection, the focus is on evaluating relay behavior in base case scenarios without PV generation. This approach provides a benchmark for traditional grid conditions while highlighting the challenges of modeling PV contributions under fault conditions.

The research also explores how PV generation affects relay coordination and protection system reliability. It examines the redistribution of fault currents caused by PV integration and its impact on relay performance. Challenges such as delayed tripping times and coordination issues are analyzed in detail, with particular attention to the role of current transformer (CT) saturation and its influence on fault current measurements and relay operations.

Finally, the study emphasizes the need for advanced solutions to address the challenges posed by increasing PV penetration. Adaptive protection schemes, supported by technologies such as Phasor Measurement Units (PMUs), are proposed as critical tools for enhancing fault detection and relay coordination in modern grids. Furthermore, the research serves as a stepping stone for future investigations into grid-forming inverters, which represent the next frontier in renewable energy integration and protection engineering. By addressing the limitations of current models and proposing pathways for improvement, this work provides valuable insights into developing resilient and adaptive protection systems for modern power grids.

This research is not only technically significant but also strategically important, as it contributes to ensuring the stability and reliability of power systems in the face of increasing renewable integration. The findings and methodologies developed in this study aim to guide future work in grid protection and to support the global transition to sustainable energy systems.

# 2. Power System Protection

## 2.1. Introduction to Power System Protection

Power system protection is a critical aspect of electrical engineering, tasked with ensuring the safety, reliability, and operational continuity of electrical power systems. As electrical grids become increasingly complex due to the integration of renewable energy, decentralized generation, and digital technologies, the role of protection systems has expanded significantly. Initially, power system protection focused on safeguarding equipment and minimizing outages, but in modern grids, it also plays a pivotal role in optimizing performance, improving efficiency, and maintaining stability during disturbances.

The primary objective of power system protection is to detect and isolate faults while ensuring the minimal interruption of service. Protection systems achieve this by detecting abnormal conditions such as short circuits, overloads, or equipment failures, and then initiating the appropriate corrective actions. These actions typically include tripping circuit breakers to isolate the affected portion of the grid, thereby limiting the impact of the fault on the broader system. Furthermore, modern protection systems are designed with additional objectives like minimizing downtime, reducing equipment damage, and ensuring personnel safety.

As electrical grids evolve, protection systems must also adapt to new challenges, including increased system complexity, integration of variable renewable energy sources, and the implementation of distributed energy resources (DERs). In the past, protection systems were primarily electromechanical, but today, digital relays and intelligent systems have revolutionized protection methodologies. The current shift towards microprocessor-based protection and smart grid technologies brings about new capabilities such as real-time monitoring, adaptive protection schemes, and enhanced coordination between different layers of the grid infrastructure [6]

Power systems are prone to various faults, including short circuits, ground faults, and overload conditions, which can lead to significant disruptions if not managed effectively. The principles of power system protection are designed to ensure that such faults are isolated swiftly while minimizing the impact on the rest of the system. A well-designed protection system isolates only the faulted section, allowing the rest of the grid to continue operating normally. This is achieved through a combination of fault detection mechanisms, relay systems, and circuit breakers, which work in concert to ensure that faults are cleared quickly and efficiently [6]

The key aspects of protection systems can be broken down into three critical attributes:

- Reliability
- Speed
- Selectivity

Reliability in protection systems ensures correct operation during faults and inaction under normal conditions. It is defined by dependability (operation when required) and security (avoiding unnecessary actions). These objectives often conflict—enhancing one can reduce the other—making balance critical in designing robust protection schemes [6].

Dependable protection systems operate within their designated fault area and remain secure against maloperation caused by phenomena like voltage regulation or inrush currents. Redundant elements, such as backup relays or dual trip coils, enhance reliability by ensuring continued operation in the event of primary system failure. Critical applications, such as high-voltage systems, may implement “two-out-of-three” tripping arrangements to balance reliability and security [7]. For busbar protection, duplicate systems are common, preventing widespread outages due to busbar faults [7] .

Speed is critical in minimizing fault impacts, such as equipment damage and arc flash hazards. Faster fault clearance reduces these risks, particularly in high-voltage transmission and industrial systems. Modern digital relays significantly outperform traditional electromechanical relays, detecting faults and initiating actions in microseconds [6]. From a stability perspective, fast fault clearance ensures synchronism between interconnected systems, especially under heavy loading, which increases the risk of instability during prolonged faults [7].

Selectivity isolates faults to minimize disruptions while maintaining system functionality. In radial systems, this is achieved through time-coordinated overcurrent relays, where downstream devices trip faster than upstream ones. While this introduces a slight delay in fault clearance, advanced unit protection schemes, such as differential protection, provide faster response times without relying on time grading [7].

Simplicity and cost-effectiveness remain essential in protection system design. Complex schemes can be difficult to maintain, potentially compromising reliability. Historically, electromechanical systems prioritized simplicity, but modern grids, integrating renewable energy and distributed generation (DG), demand advanced strategies that remain economical and maintainable [6].

The integration of renewable energy and DG has introduced new challenges. Traditional systems, designed for unidirectional power flow, now contend with bidirectional flows, varying fault currents, and reduced inertia. Protection schemes must adapt to these changes. For example, DG-connected systems may experience blinding of protection, where fault current drops below relay thresholds, or false tripping, where healthy feeders are disconnected unnecessarily due to altered fault current paths [8]. These scenarios emphasize the need for adaptive and flexible protection strategies.

The evolution of protection systems, driven by technological advancements and grid decentralization, highlights the need for innovative approaches. Emerging technologies, such as phasor measurement units (PMUs) and wide-area monitoring systems (WAMS), provide real-time data for fault detection and system stability enhancement. Adaptive protection schemes and communication-based systems offer promising solutions for addressing the challenges posed by modern grids [7].

One of the most critical changes in modern protection systems is the shift from electromechanical relays to digital or microprocessor-based relays. Traditional electromechanical relays operate using mechanical components that move in response to electrical signals, which limit their speed, accuracy, and flexibility. In contrast, microprocessor-based relays leverage advanced computing technologies to process data faster, implement more complex algorithms, and offer enhanced diagnostic capabilities [6].

Digital relays can be programmed to perform multiple protection functions within a single device, reducing the need for numerous dedicated relays for different protective tasks. This multifunctionality not only simplifies system design but also enhances flexibility and scalability, making digital relays well-suited for modern power systems that require adaptive protection. Additionally, microprocessor-based relays are capable of real-time data analysis, which allows them to adapt to changing system conditions, detect more complex fault scenarios, and provide more accurate fault location information [6].

Another major benefit of digital relays is their ability to integrate with communication networks, enabling the development of wide-area protection systems. These systems can coordinate protection across large areas of the grid, using real-time data from multiple points in the system to improve fault detection and isolation. This is particularly important in modern grids where the increased complexity and variability introduced by renewable energy sources require more sophisticated protection strategies [6].

## 2.2. Traditional Protection Schemes

Traditional power system protection schemes form the foundational layer of electrical system protection and have been the standard for several decades. These schemes primarily use electromechanical relays to detect abnormal electrical conditions such as overcurrent, under-voltage, and frequency imbalances. The fundamental design philosophy behind traditional protection schemes is centered on simplicity, reliability, and robustness. In these systems, relays are tasked with monitoring key parameters of electrical circuits and operating circuit breakers when they detect fault conditions, thereby preventing the spread of disturbances across the entire grid.

While traditional protection schemes have been widely implemented and are still in use today, they face several limitations in the context of modern electrical grids. As the complexity of power systems increases, with the integration of renewable energy sources, distributed generation, and smart grid technologies, the ability of traditional protection systems to maintain high levels of reliability and selectivity is increasingly challenged.

One of the primary limitations of traditional protection schemes is their reliance on preset thresholds for operation. In modern grids, where operating conditions can change rapidly due to fluctuating renewable energy inputs, these preset thresholds may no longer provide the optimal level of protection. Moreover, traditional schemes typically do not have the ability to adapt in real-time to changing system conditions, which can result in either delayed fault clearing or unnecessary tripping of protective devices [6].

### 2.2.1. Overcurrent Protection

Overcurrent protection is a fundamental component of power system protection and is designed to detect abnormal current levels and isolate faults quickly to prevent damage. This protection scheme operates based on the principle that under normal conditions, the current remains within a defined range, and any significant deviation indicates a fault. When an overcurrent occurs, the relay detects the excessive current and sends a trip signal to the circuit breaker, which isolates the faulted section of the network. Overcurrent protection is implemented using overcurrent relays, which operate by detecting when the current exceeds a preset threshold. These relays can be configured with various characteristics to optimize their response times and fault detection capabilities, depending on the system requirements.

Based on the available information regarding short-circuit and load flow currents, a minimum operating criterion for overcurrent protection can be determined. Figure 1 below illustrates the criteria used for selecting overcurrent relay tap settings.

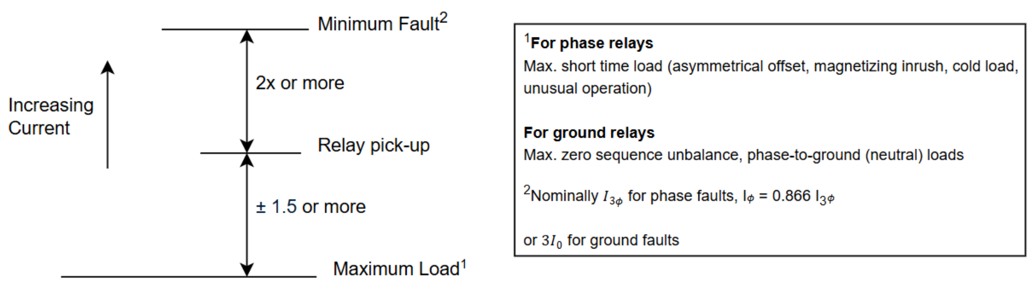


Figure 1. Criteria for Selecting Overcurrent Relay [9]

The minimum operating value, commonly referred to as the "pickup" value, represents the lowest current level at which the relay begins to operate. For an overcurrent protection relay, the pickup value is the minimum current that initiates the relay's timing process, ultimately leading to the closure of its contacts.

The operation of overcurrent and distance relays near the boundary of a protection zone is less precise compared to differential protection, leading to potential issues such as underreach or overreach for faults near this boundary. This can create a protection challenge, as illustrated in Figure 2.

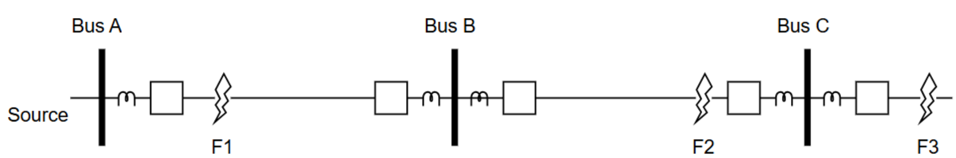


Figure 2 Protection problem for protective relays [9]

From the perspective of selectivity, ensuring a high level of service continuity requires that protective devices at each bus (A, B, C) operate only for faults within their designated protection zone. For example, Relay A at Bus A is responsible for protecting the line AB, Relay B at Bus B protects the line BC, and Relay C at Bus C protects the line C. Short-circuit currents are typically higher in magnitude the closer they are to the power source. In Figure 2, fault F1, being nearer to the source, results in a higher magnitude current compared to faults F2 and F3. However, differentiating between faults F2 and F3 presents a challenge, as these faults occur in close proximity, resulting in nearly equal current magnitudes.

The standard approach to resolving this issue involves conducting a protection coordination study, using time-current grading to ensure proper relay operation and fault isolation.

In modern applications, relays have adjustable taps that determine the minimum current required for operation. The pickup value, expressed as multiples of the tap setting, dictates when the relay will activate. For instance, a relay set on tap 2 will operate at 2.0 A (with manufacturer tolerances). These taps allow relays to function over a range of current magnitudes, providing flexibility in coordinating protection. Figure 3 shows typical inverse-time overcurrent relay characteristics, highlighting the relationship between time and current at various pickup settings. The relay begins timing once the pickup value is reached, and, depending on the current magnitude, it operates with an inverse-time characteristic, meaning it responds faster at higher current levels and slower at lower levels.

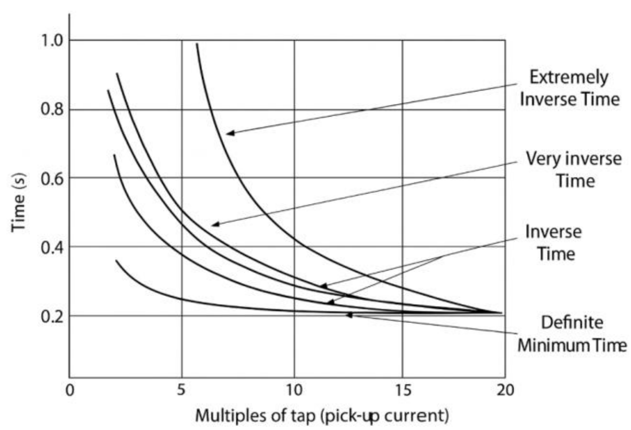


Figure 3 Standard inverse-time overcurrent relay characteristics [9]

To calculate the trip time for overcurrent relays, the Long Time Inverse (LTI) curve, as specified by the IEEE standard, was utilized. The trip time (t) is determined using the equation 1:

$$t = k\left[\frac{A}{\left(\frac{I}{I_{pickup}}\right)^{C} - 1} + B\right] \quad \text{(Equation 1)}$$

where I is the measured fault current, $I_{pickup}$ is the relay's pickup current, and A,B,C are constants specific to the selected curve type. The constant k represents a time multiplier that adjusts the overall delay to align with system requirements. The LTI curve is particularly suited for applications requiring a delay proportional to the inverse of the fault current, ensuring rapid operation under severe fault conditions while providing slower responses to minor overloads. [10]

### 2.2.2. Distance Protection

Distance protection, commonly used in transmission line protection, operates by measuring the impedance between the relay location and the fault. The principle behind this approach is that the impedance of a transmission line is proportional to its length. When a fault occurs, the impedance drops suddenly, indicating that the fault is closer to the relay. By comparing voltage and current measurements, the relay can calculate the impedance and determine the fault's location. If the impedance falls below a preset threshold, the relay activates to isolate the faulted section of the line [11].

Unlike overcurrent protection, which relies primarily on current magnitude, distance protection is effective for longer transmission lines because it can accurately pinpoint the fault location. This selectivity makes it critical for maintaining the stability of larger, interconnected power systems [11]. Distance relays are typically configured with a reach setting, a fraction of the total transmission line length that defines the relay's protective zone. For instance, a relay may be set to protect 80% to 90% of the line, ensuring that it operates quickly for faults within this range but delays tripping for faults beyond this zone [11].

One of the key advantages of distance protection is that it is not significantly affected by system conditions, such as changes in load or generation, making it a highly reliable method for transmission line protection. However, traditional distance relays can face challenges when faults occur near the boundary of their protective zone, potentially leading to underreach or overreach. These limitations have driven the development of more advanced distance protection schemes that incorporate communication between relays at different ends of the transmission line to enhance selectivity and coordination [11].

Distance relays operate by calculating the impedance between the relay location and the fault to determine if a fault lies within the relay’s protective zone. The basic principle involves measuring the ratio of voltage to current at the relay location, which provides the apparent impedance:

$$\frac{V_R}{I_{RS}} = Z_{RS} = h_S Z_L \qquad \text{(Equation 2)}$$

where $V_R$ = voltage at the relay

$I_{RS}$ = current at the relay

$Z_L$ = total line impedance

$h_s$ = fraction of line impedance to balance point

This reach setting defines the percentage of the line that the relay is responsible for protecting. If the apparent impedance falls below this value, the relay will trip, indicating a fault within its zone. For faults located farther from the relay, beyond the set reach, the impedance will increase, preventing unnecessary tripping. However, relay performance can be affected by factors such as high fault resistance or source impedance, which can cause the relay to underreach or overreach. These scenarios are commonly analyzed using R-X plots that graphically represent the relay's operating zone in terms of real and reactive impedance components.

In distance protection, the R-X plot is a valuable tool for visualizing the impedance seen by the relay during fault conditions. The plot represents the relationship between the resistance and the reactance of the measured impedance. For a given transmission line, the line impedance is depicted as a vector originating from the plot's origin and extending along the line's characteristic angle. The relay's protective zone is typically represented as a mho circle or other geometric shape that encloses the portion of the line the relay is set to protect.

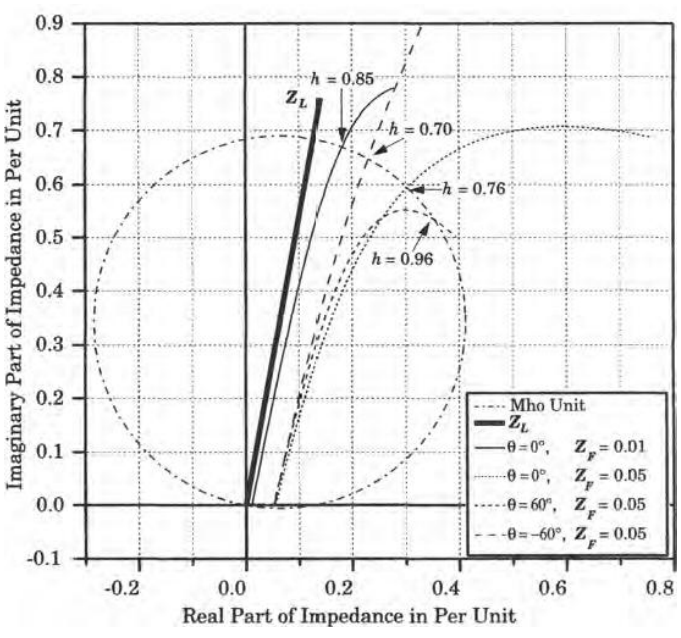


Figure 4. The Mho graphic representation [11]

As illustrated in Figure 4, the mho circle represents the operating zone of the distance relay, with the line impedance and potential faults plotted on the same graph. Faults occurring within the protective zone (inside the mho circle) will trigger the relay to trip, while faults outside this zone will not. Figure also demonstrates how different system conditions, such as fault resistance, can affect the impedance measured by the relay, potentially causing underreach or overreach.

In figure, the value h represents the fractional distance from the relay to the fault, expressed as a proportion of the total line impedance. For instance, h = 0.9 means the fault is located at 90% of the line length between the two buses. This reach setting defines the maximum distance the relay will protect. Faults closer to the relay (with smaller h values) will be detected and isolated more quickly, whereas faults beyond the reach setting will be handled by relays further down the line.

Additionally, the value $Z_f$ refers to the fault impedance, which can vary based on fault type and location. Higher $Z_f$ values may cause the relay to underreach, meaning it might fail to detect faults that are within its intended zone. Conversely, lower fault impedances are more likely to result in correct relay operation. These variations are critical for determining whether the relay will successfully isolate the fault within its protective zone [11].

The R-X plot allows engineers to visualize and analyze how the relay's performance varies with different fault conditions and system impedances. It provides a clear representation of the relationship between the relay's operating zone and the fault's position along the transmission line, offering valuable insight into the behavior of distance relays under varying system conditions [11].

Distance relays typically operate in multiple zones to ensure comprehensive protection across the entire transmission line. These zones are set based on the distance from the relay to the fault, with each zone covering a different percentage of the total line length and having its own time delay. Zone 1, for example, is usually set to protect about 80% to 85% of the line length and operates with no intentional time delay, ensuring immediate tripping for faults within this zone. Zone 2 is set to cover 100% of the line, plus an additional margin—often 50% of the shortest adjacent line—and operates with a time delay (T2) to coordinate with other relays on adjacent lines. Zone 3 typically covers a greater distance, including two full line lengths and a portion of the third line, with a longer time delay (T3), providing backup protection for faults that occur outside the primary zones. The visual representation of these zones and their coverage of the lines are portraid in figure 5. The coordination of these time delays ensures that faults are cleared sequentially, allowing the relay nearest to the fault to trip first, while relays farther away provide backup protection with appropriate time delays [11] [12]

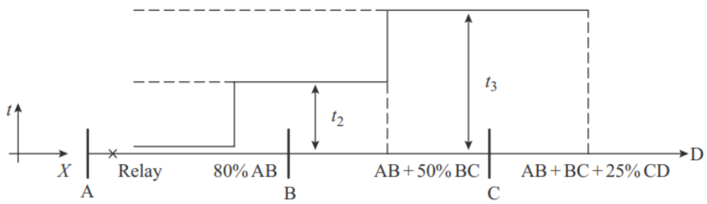


Figure 5. Illustration of distance protection zones with associated time delays and coverage [12]

The R-X plot in Figure 6 shows how these zones are represented in the complex impedance plane, with each zone having a distinct operating characteristic. This allows for clear differentiation between faults within different zones, ensuring that the correct relay responds to each fault. The directional unit supervises the tripping for each zone, ensuring that only faults in the forward direction trigger the relay, providing selective and coordinated fault clearance across the transmission system [11] [12].

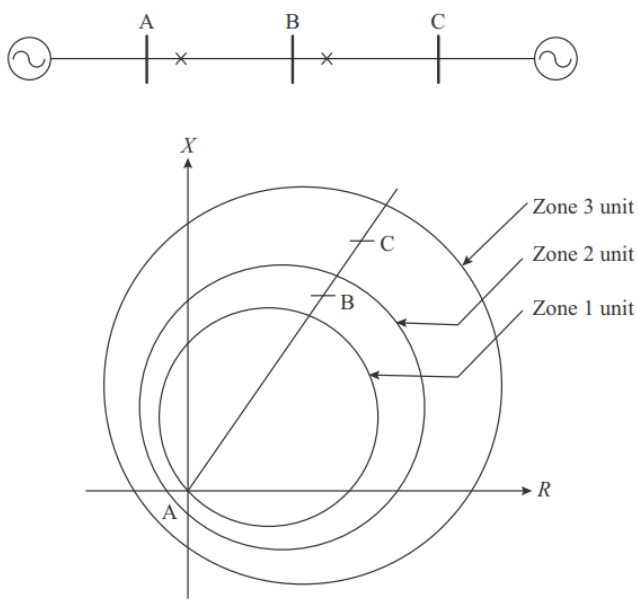


Figure 6. Representation of the zones in the complex impedance plane [12]

# 3. Fault Analysis in Distribution Grids with High DG Penetration

With the increasing integration of Distributed Generation (DG) into power systems, fault analysis in distribution grids has become more complex. DGs, which include renewable energy sources like solar photovoltaic (PV) and wind turbines, significantly alter the dynamics of fault conditions. Traditionally, fault analysis and protection system design were based on predictable fault current contributions from centralized generation sources. However, the introduction of multiple, decentralized DG units affects fault current levels and complicates the coordination and sensitivity of protection devices. This section explores the types of faults that occur in distribution grids, the impact of DG on fault current levels, and methodologies for conducting short circuit analysis in grids with high DG penetration.

## 3.1. Fault Types

Faults in power systems are typically classified into two broad categories: symmetrical and asymmetrical faults. These faults result from various conditions, including equipment failures, short circuits, and environmental disturbances such as lightning strikes or vegetation contact with overhead lines. Faults disrupt normal system operation by creating abnormal currents, which must be promptly detected and cleared to prevent equipment damage, power outages, and safety hazards.

Symmetrical faults, also known as three-phase faults, are the most severe but least common types of faults in power systems. In this type of fault, all three phases (L1, L2, and L3) are short-circuited either to each other or to the ground. The fault currents are balanced, meaning that the magnitude of the fault current is the same in each phase, but the phase angles are separated by 120 degrees. While symmetrical faults are relatively rare (typically accounting for less than 5% of all faults), their high fault currents can cause significant damage to equipment, and the system must be designed to handle such extreme conditions.

Asymmetrical faults, also known as unbalanced faults, occur much more frequently and include single-line-to-ground (SLG) faults, line-to-line (LL) faults, and double-line-to-ground (DLG) faults. These faults are characterized by unbalanced fault currents in the three phases. Asymmetrical faults can occur due to various reasons, such as insulation failure, broken conductors, or contact with foreign objects like trees or animals and can be grouped into:

- Single-Line-to-Ground (SLG) Fault: This occurs when one phase contacts the ground. It is the most common type of fault in distribution systems, accounting for around 60% of all faults.

- Line-to-Line (LL) Fault: This occurs when two phases come into contact with each other. It results in a high fault current between the two faulted phases.
- Double-Line-to-Ground (DLG) Fault: This type involves two phases short-circuited to each other and the ground. The fault current is distributed through the two faulted phases and the ground.

Asymmetrical fault analysis is more complex than symmetrical fault analysis because of the unbalanced nature of the fault currents. The method of symmetrical components is also used here to simplify the analysis by converting the unbalanced three-phase system into three balanced sets of sequence components: positive, negative, and zero sequences [12].

## 3.2. Impact of DG on Fault Current Levels

The penetration of DG into distribution grids introduces new challenges for fault current analysis and protection system design. DG units, particularly inverter-based sources like solar PV and some types of wind turbines, contribute fault currents that are significantly different from those produced by traditional synchronous generators. The nature and magnitude of fault current contributions from DGs depend on several factors, including the type of DG technology, its location within the network, and its operating characteristics.

Calculation of fault currents becomes more complex due to the presence of multiple fault current sources. Traditional short circuit analysis methodologies, such as symmetrical components, are still used but must be adapted to account for the contributions of DG. The symmetrical component method decomposes the unbalanced fault currents into three sets of balanced currents—positive, negative, and zero sequence—which allows for the analysis of symmetrical and asymmetrical faults [6].

The behavior of fault current can be understood through both its AC and DC components. The steady-state AC short circuit current is described by the following equation:

$$\mathrm{i_{ac}(t)} = \frac{\mathrm{V_s}}{\mathrm{R}}\left(1 - \mathrm{e}^{-\left(\frac{t}{T}\right)}\right) \qquad \text{Equation 3}$$

where T is the time constant determined by the inductance (L) and resistance (R) of the network:

$$\mathrm{T} = \frac{\mathrm{L}}{\mathrm{R}} = \frac{\mathrm{X_L}}{\mathrm{R_\omega}} \qquad \text{Equation 4}$$

In addition to the AC component, a DC fault component arises from the stored energy in network inductors and capacitors. This DC component, which spikes at the inception of the fault, is given by:

$$i_{dc}(t) = I_0 e^{-(\frac{t}{T})} \text{ Equation 5}$$

The total fault current is a combination of these AC and DC components and can be represented as:

$$i_f(t) = i_{ac}(t) + i_{dc}(t) = \frac{V_s}{R} + \left(I_0 - \frac{V_s}{R}\right) e^{-(\frac{t}{T})} \text{ Equation 6}$$

As shown in Fig. 7, the DC component causes a spike in the fault current at the inception of the fault, which decays over time. The rate of decay is determined by the time constant T [13]

Synchronous generators, often used in genset and combined heat and power (CHP) DG units, contribute fault current according to their internal impedance and network topology. Their behavior is governed by three reactances: subtransient, transient, and synchronous, each relevant at different fault stages. Subtransient reactance dominates in the first cycle after fault inception, typically lasting ~0.1 s, followed by transient and then synchronous reactances, which become relevant after 0.5–2 s and in steady-state conditions, respectively [14].

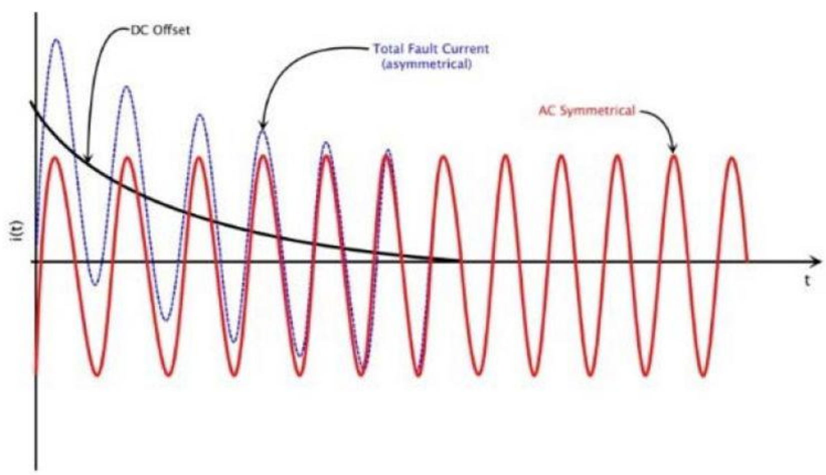


Figure 7. Fault current waveform showing AC and DC components [13]

Induction generators, commonly used in wind turbines and other small DG units, contribute significantly to the fault current at the beginning of a fault. However, the current decays quickly as the machine's stator flux diminishes without an external excitation source. The fault current decays to zero in steady-state conditions, as shown in figure 7, due to the self-exciting nature of induction machines [14].

In contrast, inverter-based DG units (such as PV systems) contribute far less to fault currents. Studies have shown that the contribution of inverters to fault currents does not typically exceed 200% of their rated current, and they are usually disconnected within a few cycles of fault inception. According to IEEE standards, if the terminal voltage of an inverter drops below 0.5 pu, the PV unit disconnects within six cycles [15].

Short circuit analysis is directly relevant to the design of protection schemes, as it determines the magnitude and direction of fault currents that protective devices must detect and interrupt. In systems with high DG penetration, protection schemes must be designed to accommodate the variability in fault current levels and ensure that devices remain sensitive to faults without being prone to false trips.

To address these challenges, advanced protection schemes, such as adaptive protection, are being developed. These systems can dynamically adjust their settings based on real-time measurements of system conditions, including fault current levels, to maintain optimal protection performance. Additionally, communication-based protection schemes, such as those using IEC 61850, enable better coordination between protection devices by allowing them to share real-time data on system conditions. This ensures that devices can operate in a coordinated manner, even in complex systems with multiple DG sources [6]

# 4. Advanced Protection Concepts and Techniques

As power systems evolve with the increasing penetration of distributed generation and the growing complexity of microgrids and smart grids, traditional protection schemes are often insufficient to meet the demands of modern networks. Advanced protection concepts and techniques have emerged to address these challenges, offering more dynamic, flexible, and intelligent methods of protecting power systems. These techniques are particularly critical for ensuring system reliability, stability, and safety in environments where traditional protection settings may not be appropriate due to fluctuating power flows, bidirectional fault currents, and evolving grid conditions.

Adaptive protection is an advanced method where protection settings are dynamically adjusted in response to real-time changes in network conditions. Unlike conventional protection schemes, which rely on static settings that are determined during the system design phase, adaptive protection continuously monitors the power system and modifies protection parameters based on the current operating state of the grid. This approach is particularly valuable in distribution grids with high DG penetration, where network conditions can change rapidly due to the variability of renewable energy sources like wind and solar power.

The theoretical basis for adaptive protection lies in the real-time analysis of grid conditions, such as load levels, fault currents, and voltage fluctuations. Protection relays are equipped with communication capabilities and sensors that feed real-time data into algorithms designed to adjust relay settings based on the prevailing conditions. For example, in grids with significant DG integration, adaptive protection can increase the sensitivity of relays during periods of low generation from renewable sources and decrease it during periods of high generation. This ensures that the protection system remains responsive to faults while avoiding unnecessary trips or miscoordination caused by the variability of DG [6].

In grids with high DG penetration, adaptive protection addresses several key challenges. One of the main issues is the variation in fault current levels due to the presence of multiple DG sources. Traditional protection settings may be too conservative or too lenient, leading to delayed fault clearance or frequent false tripping. Adaptive protection schemes can adjust relay settings in real time, improving the selectivity and coordination of protective devices while maintaining system stability. Moreover, adaptive protection can also respond to changes in network topology, such as the switching in and out of lines or DG units, ensuring that the protection system adapts to these changes without requiring manual intervention [6].

### 4.1. Challenges in Protection Device Coordination

Variations in the fault current level at any point within the power system can significantly impact the operation and reliability of protection devices (PDs). The integration of distributed generation (DG) units introduces a range of challenges that can disrupt the proper functioning of these devices. This section examines the potential adverse effects that DG integration may have on PDs, emphasizing how these impacts can undermine system stability and protection coordination. [16]

These impacts can be categorized as follows [16]:

- Reverse power flow
- Unintended tripping
- Protection blinding
- Unwanted islanding
- Unsynchronized reclosing
- Loss of connection to the main power supply

In conventional distribution networks, power flows unidirectionally from the transmission grid to downstream loads. However, with DG integration, the direction of power flow can reverse, depending on the size and output of the DG units. For example, as illustrated in

Figure 8, DG1 can cause reverse current flow through CB1 or Fuse1 if its capacity exceeds local load demand. Reverse power flow can exceed device settings, leading to undesired tripping and network instability. The severity of this issue increases with higher DG penetration, particularly in feeders with limited load diversity [17].

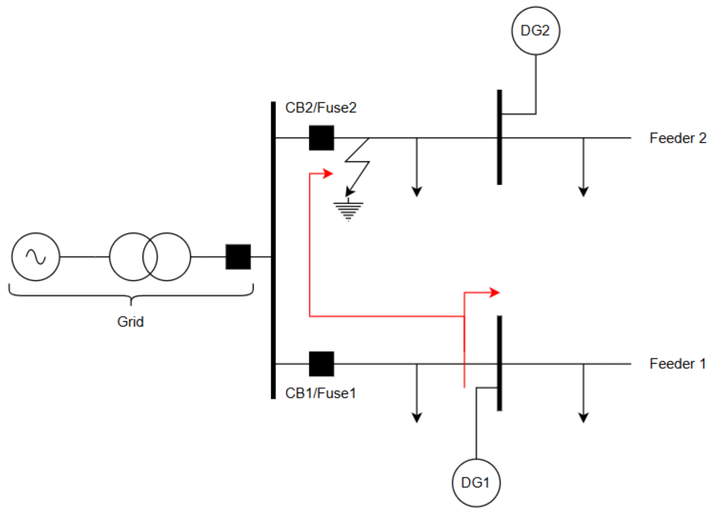


Figure 8. Parallel distribution feeders with their interconnected DG units [17]

False Tripping occurs when a PD operates inappropriately, disconnecting a healthy feeder or activating a backup device prematurely. As shown in Figure 9, DG units downstream of a recloser can increase fault current through a fuse, causing it to blow during temporary faults. This behavior, known as sympathetic tripping, disrupts service unnecessarily. Similarly, Figure 8 highlights how faults on feeder 2 can lead to false activation of CB1 (circuit breaker) or Fuse1 on feeder 1, especially if DG capacity contributes significant fault current. In complex systems, such as looped or multi-feeder networks, false tripping can cascade, disconnecting multiple healthy feeders and exacerbating power outages [8] [18].

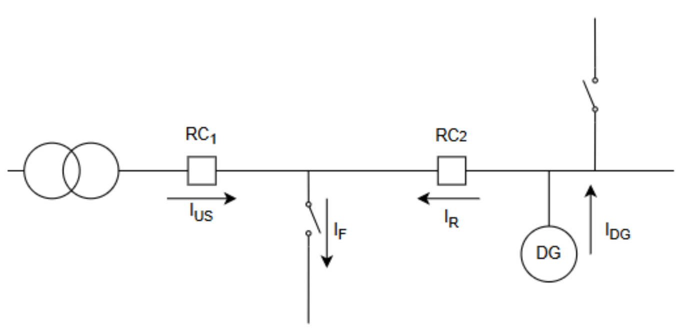


Figure 9. Illustration of fault-induced false tripping in a distribution network with distributed generation (DG) [8]

Blinding of protection occurs when DG reduces the fault current seen by a relay to levels below its pickup settings, preventing fault detection. For example, as depicted in Figure 10, the fault current measured by an overcurrent protection device (OCPD) decreases when DG contributes power, resulting in delayed or failed operation. This issue is particularly problematic in high-impedance networks or when DG units significantly offset grid fault contributions. Distance relays are also affected, as shown in Figure 11, where DG causes under-reach conditions, shifting protection zones and impairing fault detection. These effects necessitate recalibration of relay settings to maintain reliability [19].

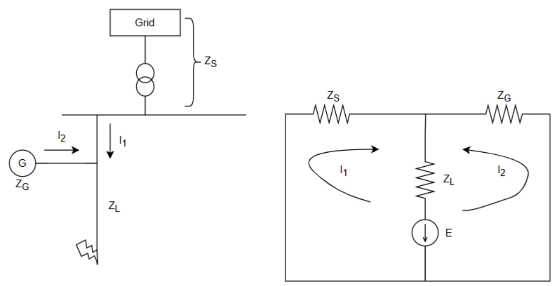


Figure 10. Illustration of blinding of protection in a medium voltage network with distributed generation (DG) [19]

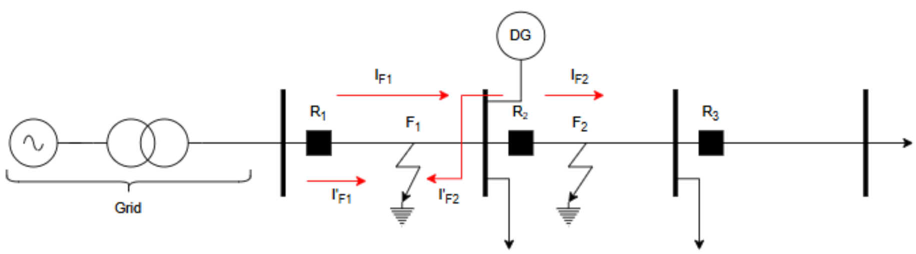


Figure 11. Effect of DG units on distance relays [19]

Unwanted Islanding : Unwanted islanding occurs when a portion of the grid becomes unintentionally isolated but remains energized by DG units. Unlike planned islanding, this condition poses significant safety risks, particularly for maintenance personnel working on live equipment. Additionally, traditional protection systems struggle to detect faults in islanded sections due to reduced short-circuit levels, leading to prolonged fault clearance. Unwanted islanding also compromises voltage and frequency stability, further endangering system reliability [19].

Unsynchronized reclosing : Reclosing operations are designed to restore power following temporary faults, but DG complicates this process. As illustrated in Figure 9, DG can sustain fault currents after the main circuit breaker (CB) trips, preventing complete fault clearance. When the recloser attempts to restore power, it may close out of synchronization with the grid, causing damage to synchronous generators and degrading power quality. Inverter-based DG units, while less susceptible to such damage, still require coordination to ensure reliable reclosing operations. Adaptive reclosing strategies are essential to mitigate these risks in DG-integrated networks [20] [21]

Infeed Effect : Distance relays have a unique advantage in that they can differentiate between faults occurring in various sections of a network based on the measured impedance. This functionality involves assessing the fault current observed by the relay relative to the voltage at its location to calculate the line impedance to the fault. However, when there are one or more sources of generation within the protection zone, such as distributed generation (DG), the phenomenon known as the "infeed effect" must be considered. This effect occurs because these sources can contribute to the fault current without being directly detected by the distance relay [22].

When analyzing the example in Figure 12, it becomes evident that the actual impedance to the fault is $Z_A+Z_B$. However, due to the infeed effect, the impedance seen by the relay is altered, appearing as $Z_A + Z_B + (I_B/I_A)$. For a fault occurring beyond busbar B, the distance relay perceives an impedance higher than the true fault impedance. This phenomenon, known as the “infeed effect,” is particularly significant when distributed generation (DG) is integrated into the network.

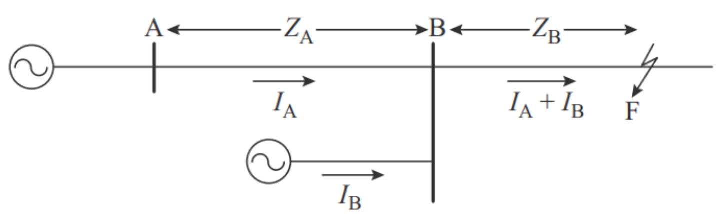


Figure 12. Effect of infeed in distance protection [12]

The impact of DG is a reduction in the effective reach of the distance relay. As described in [23], when a fault occurs downstream of a bus where DG is connected, the upstream relay measures an impedance higher than the actual fault impedance. To address this, relay settings for Zones 2 and 3 must be adapted.

$$Z_{relay} = Z_A + (1+K)Z_B \quad \text{Equation 7}$$

The infeed constant K is used in these adjustments, with specific constants $K_2$ and $K_3$ being calculated for each zone.

$$K = \frac{I_{total\ infeed}}{I_{relay}} \quad \text{Equation 8}$$

These constants account for infeed on both the adjacent and remote lines, as detailed in the calculation methods found in [12].

The underreach issue caused by DG requires precise recalibration of relay settings to ensure accurate operation. By carefully calculating the infeed constants, the impact on zone reach can be minimized or even eliminated. Adaptive distance protection schemes for distribution systems with DG have been proposed, such as the method discussed in [23], which focuses on dynamically adjusting Zone 2 settings based on the relay’s protective characteristics.

Loss of main power : Loss of main power refers to the disconnection of the main grid, causing a section of the network to operate in islanded mode. In such scenarios, DG units may supply insufficient fault current to trigger protection devices, delaying fault clearance and risking equipment damage. This challenge highlights the need for coordinated protection settings and advanced detection mechanisms to ensure safety and reliability in islanded networks [19].

# 5. Methodology

This section outlines the methods, tools, and assumptions used throughout the study. The objective of this study is to model, simulate, and analyze a medium voltage (20 kV) grid by customizing load profiles, integrating photovoltaic (PV) systems, and coordinating relay settings for protection.

## 5.1. Tools Used

Digsilent PowerFactory 2024 was used for the simulation and analysis of the medium voltage grid. PowerFactory is a leading software tool for power system analysis, offering comprehensive capabilities for modeling, including :

- Power flow analysis
- Short-circuit analysis
- Relay coordination
- Dynamic simulation of grid systems.

Its extensive feature set makes it particularly suitable for simulating complex power system behaviors under various operating and fault conditions, ensuring accurate analysis of relay protection schemes and PV integration.

### 5.2. Cigre MS Grid Model

The Cigre MS grid model, used as the foundation for this study, represents a typical medium voltage (20 kV) rural distribution network. The model is derived from a real-world German MV distribution network and has been widely used as a benchmark for studying the integration of distributed energy resources (DER) and renewable energy systems. Figure 13 shows the topology of the model.

The network is structured into two distinct feeder zones :

- Zone 1 : Features overhead lines, spanning 9.88 km.
- Zone 2 : Comprised of cable lines, with a total length of 15.07 km.

The details and characteristics of the lines in the model are presented in Table 1.

Zone 1 is configured in a radial topology, while Zone 2 starts as a radial configuration upstream but transitions into a meshed grid downstream. The overall network includes 14 nodes, with various loads connected as specified in Table 2. Both zones are interconnected via a disconnector switch, S1, which provides the option to transform the topology of the model into a ring.

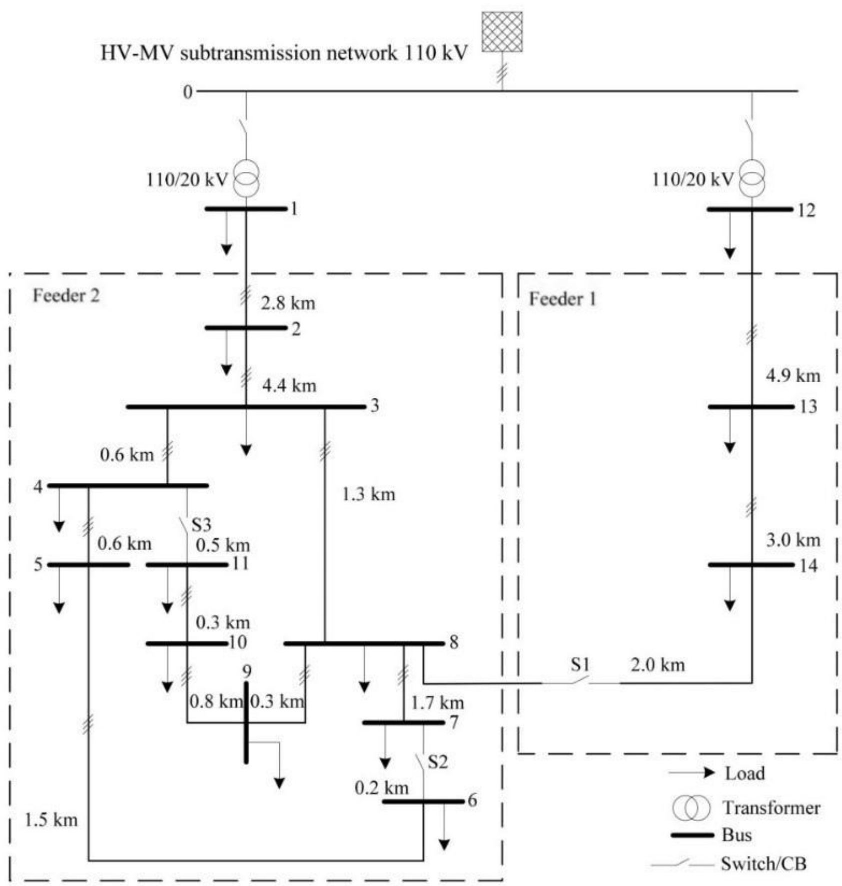

Figure 13. The Cigre benchmark model [24]

Table 1. Characteristics of the Cigre Model's lines

| Name | Length [km] | Type | Nominal Current [kA] | Positive Sequence Impedance Z1 [Ohm] | Pos. Seq. Impedance, Angle [deg] |
|---|---|---|---|---|---|
| LL 13-14 | 2.990 | OHL | 0.32 | 1.8769390 | 35.6650 |
| LL 11-4 | 0.490 | Cable | 0.32 | 0.4281986 | 55.0187 |
| LL 1-2 | 2.820 | Cable | 0.32 | 2.4643270 | 55.0187 |
| LL 9-10 | 0.770 | Cable | 0.32 | 0.6728835 | 55.0187 |
| LL 8-9 | 0.320 | Cable | 0.32 | 0.2796399 | 55.0187 |
| LL 7-8 | 1.670 | Cable | 0.32 | 1.4593710 | 55.0187 |
| LL 6-7 | 0.240 | Cable | 0.32 | 0.2097299 | 55.0187 |
| LL 5-6 | 1.540 | Cable | 0.32 | 1.3476700 | 55.0187 |
| LL 4-5 | 0.560 | Cable | 0.32 | 0.4893680 | 55.0187 |
| LL 3-8 | 1.300 | Cable | 0.32 | 1.1360370 | 55.0187 |
| LL 3-4 | 0.610 | Cable | 0.32 | 0.5330636 | 55.0187 |
| LL 2-3 | 4.420 | Cable | 0.32 | 3.8625260 | 55.0187 |
| LL 14-8 | 2.000 | OHL | 0.32 | 1.2554780 | 35.6650 |
| LL 12-13 | 4.890 | Cable | 0.32 | 3.0696430 | 55.0187 |
| LL 10-11 | 0.330 | Cable | 0.32 | 0.2883787 | 55.0187 |

Table 2. The loads of the model [24]

| Node | Residential | | Commercial/Industrial | |
|---|---|---|---|---|
| | Apparent Power S [kVA] | Power factor | Apparent Power S [kVA] | Power factor |
| 1 | 15300 | 0.98 | 5100 | 0.95 |
| 2 | --- | --- | --- | --- |
| 3 | 285 | 0.97 | 265 | 0.85 |
| 4 | 445 | 0.97 | --- | --- |
| 5 | 750 | 0.97 | --- | --- |
| 6 | 565 | 0.97 | --- | --- |
| 7 | --- | --- | 90 | 0.85 |
| 8 | 605 | 0.97 | --- | --- |
| 9 | --- | --- | 675 | 0.85 |
| 10 | 490 | 0.97 | 80 | 0.85 |
| 11 | 340 | 0.97 | --- | --- |
| 12 | 15300 | 0.98 | 5280 | 0.95 |
| 13 | --- | --- | 40 | 0.85 |
| 14 | 215 | 0.97 | 390 | 0.85 |

The grid model is connected to an external 110 kV network through two 25 MVA transformers, labeled TR1 and TR2. These transformers facilitate the connection of the medium voltage grid to the higher voltage transmission system, ensuring a robust supply of power to the distribution network while also handling fluctuations in demand and generation. The data for the transformers are represented in Table 3.

Table 3 Transformer Specifications and Parameters.

| Name | Rated Power [MVA] | Rated Voltage HV [kV] | Rated Voltage LV [kV] | Short Circuit Voltage uk [%] | Copper Losses [kW] | Vector Group HV Side | Vector Group LV Side |
|---|---|---|---|---|---|---|---|
| Transformer 0-1 | 25.000 | 110 | 20 | 12.0004200 | 25.0000 | D | YN |
| Transformer 0-12 | 25.000 | 110 | 20 | 12.0004200 | 25.0000 | D | YN |

### 5.3. The Loads

The residential loads used in this study are based on a dataset of 74 high-resolution load profiles derived from a research project conducted by HTW Berlin [25]. These profiles, which represent the electrical consumption of single-family households in Germany, provide minute-by-minute data, capturing the fluctuating nature of residential electricity consumption [25]. The original dataset was collected as part of two different measurement campaigns : one conducted by the Institute for Future Energy Systems (IZES) and another by the Vienna University of Technology. The dataset was refined to synthesize representative load profiles by extending low-resolution data (15-minute intervals) into second-level resolution using an innovative time-series synchronization technique.

To improve the representativeness of these profiles, the 74 individual load profiles are combined to create a new composite load profile that better reflects the diversity and variability of real-world residential electricity consumption. A Python script was developed to merge these profiles dynamically, allowing for various combinations and aggregations based on the desired total load values, as per Table 2. Each residential load node in the Cigre network was assigned a combination of load profiles generated. This combination approach ensures that the aggregated load profile reflects typical household consumption patterns while also capturing the inherent randomness in electricity usage.

In order to impose stress on the grid and assess how the protective systems would handle high-demand situations, the code was designed to allow for peaks to surpass the rated load by 30%. This decision was motivated by the need to simulate extreme conditions that might occur during peak demand periods (see Figure 14 for the generated residential and industrial load profiles).

For the industrial load, no detailed load profiles were available. Therefore, the industrial load was modeled as constant, in accordance with the load values specified in Table 2. This constant load assumption simplifies the simulation for industrial nodes while still contributing to the overall demand in the network.

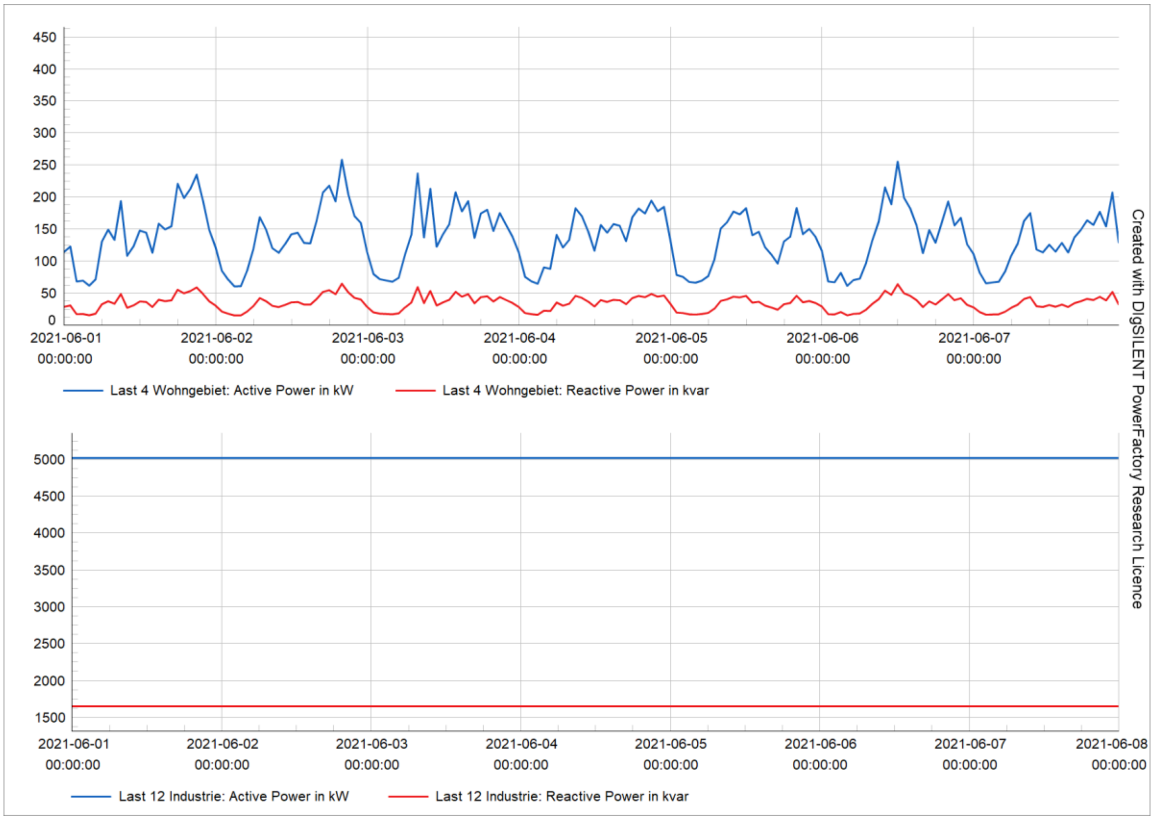


Figure 14. Active and reactive power demand profiles for residential (top) and industrial (bottom) loads generated with quasi simulation for a one week period

### 5.4. Photovoltaic (PV) Generation Profiles

To simulate the impact of distributed generation on the medium voltage (MV) grid, PV generators were added to each node in the Cigre MV network. A total of 30 PV generation profiles were used to represent the variability in solar power production across different residential nodes. The irradiation data were picked from the HTW database [25] while the resolution data were generated from project ROLLEN [26].

To assign the appropriate generation capacity to each PV generator, a Python script was developed to combine the generation profiles in line with the values specified for residential nodes in Table 2. This approach ensured that the PV generation was proportional to the residential demand at each node, maintaining balance between the energy consumption and production. Each generation profile was inserted under the load profile feature within the PV element in power factory.

Similar to the load profiles, the PV generation profiles were designed to allow peaks that surpass the rated capacity by 30%. This assumption was made to simulate conditions where optimal solar irradiance leads to exceptionally high-power generation, testing the grid's ability to handle such spikes without destabilizing (see Figure 15 for the generated PV profiles).

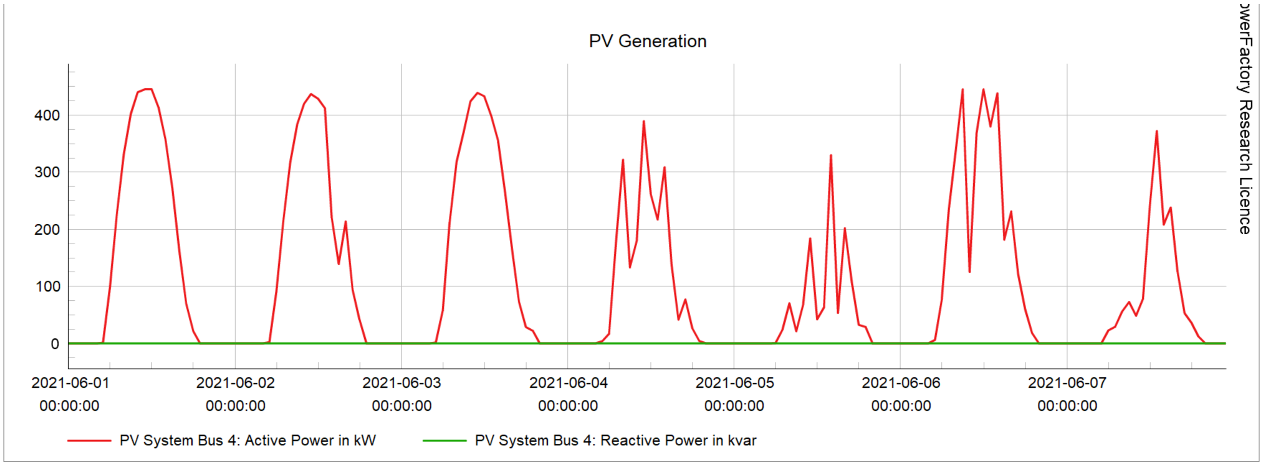


Figure 15. Active and reactive power generation profiles for the PV system at Bus 4 over a one-week period.

### 5.5. Relay coordination

To evaluate the behavior of relay protections in a grid with increased PV generation, two distinct protection systems were implemented: overcurrent relay protection in Zone 1 and distance relay protection in Zone 2. Zone 1, configured in a radial topology, utilizes overcurrent protection devices. The objective in this zone is to analyze the performance of overcurrent relays under scenarios both with and without PV generation, observing how fault detection and grid stability are affected by distributed energy sources.

Zone 2, which features a topology transitioning from radial upstream to meshed downstream, is protected using distance relays on each line. The aim here is to assess the effectiveness of distance protection in scenarios with varying levels of PV generation, analyzing the response to faults and the impact on grid stability in a more complex network.

PowerFactory's extensive library of relay devices was utilized for this study. The software offers a range of relays from major manufacturers such as ABB, Siemens, and Schneider, along with models for mho and polygonal distance relays, overcurrent relays, and under-voltage relays. These relays can be configured with custom settings to match the protection requirements of each zone. When integrated into the network at designated terminals, complete with associated circuit breakers, they enable detailed testing of protection schemes.

By adding relays to the network, the study can simulate and analyze the protection system's response to different fault conditions and operational scenarios. This includes testing tripping times across various fault locations and assessing the impact of DG on system protection. Such simulations are vital for understanding potential challenges introduced by PV generation and for developing solutions to maintain reliable and effective protection.

To ensure accurate protection and measurement, Current Transformers (CTs) and Voltage Transformers (VTs) were incorporated at the locations where relays were installed. Specifically, for distance relays, both CTs and VTs are necessary, while overcurrent relays only require CTs. In this study, a CT ratio of 300A/1A and a VT ratio of 132,000V/1V were used.

### 5.5.1. Distance Protection

Initially, the intention was to use manufacturer-specific relay models to represent the protective devices in the grid at the specific locations in the system model. However, during the modeling phase, significant challenges arose. The behavior of these relays was often unpredictable and difficult to interpret, particularly with the Siemens model 7SJ70. This model featured numerous functions and commands that were complex to decipher and cumbersome to calculate accurately. Due to these difficulties, a decision was made to switch to a simpler model to represent the distance relay function. As a result, relays from GEC Alsthom with MHO characteristic model were chosen for this study.

In Zone 2, distance protection relays were installed at the end of each line. All these distance relays are from the manufacturer GEC Alsthom and are configured using the MHO characteristic model. The relays are labeled 1a, 1b, 2a, 2b, 3a, 3b, 4a, 4b, 5a, 5b, 6a, 6b, 7a, 7b, 8a, 8b, 9a, 9b, 10a, 10b, 11a, 11b, 12a, and 12b. Their respective zone parameters are detailed in the table included in the appendices (appendix 3 and appendix 4).

Tripping times for these digital relays are carefully set to ensure proper grading and coordination. The grading time, $\Delta t$, is set at 0.3 seconds for digital protection. Zone 1 is configured to trip instantaneously ($t_1 = 0$ s), Zone 2 trips at $t_2 = 0.3$ s, and Zone 3 trips at $t_3 = 0.6$ s [27]. These settings ensure a clear and reliable coordination of tripping times across the zones, preventing any overlap or miscoordination in the relay's operation.

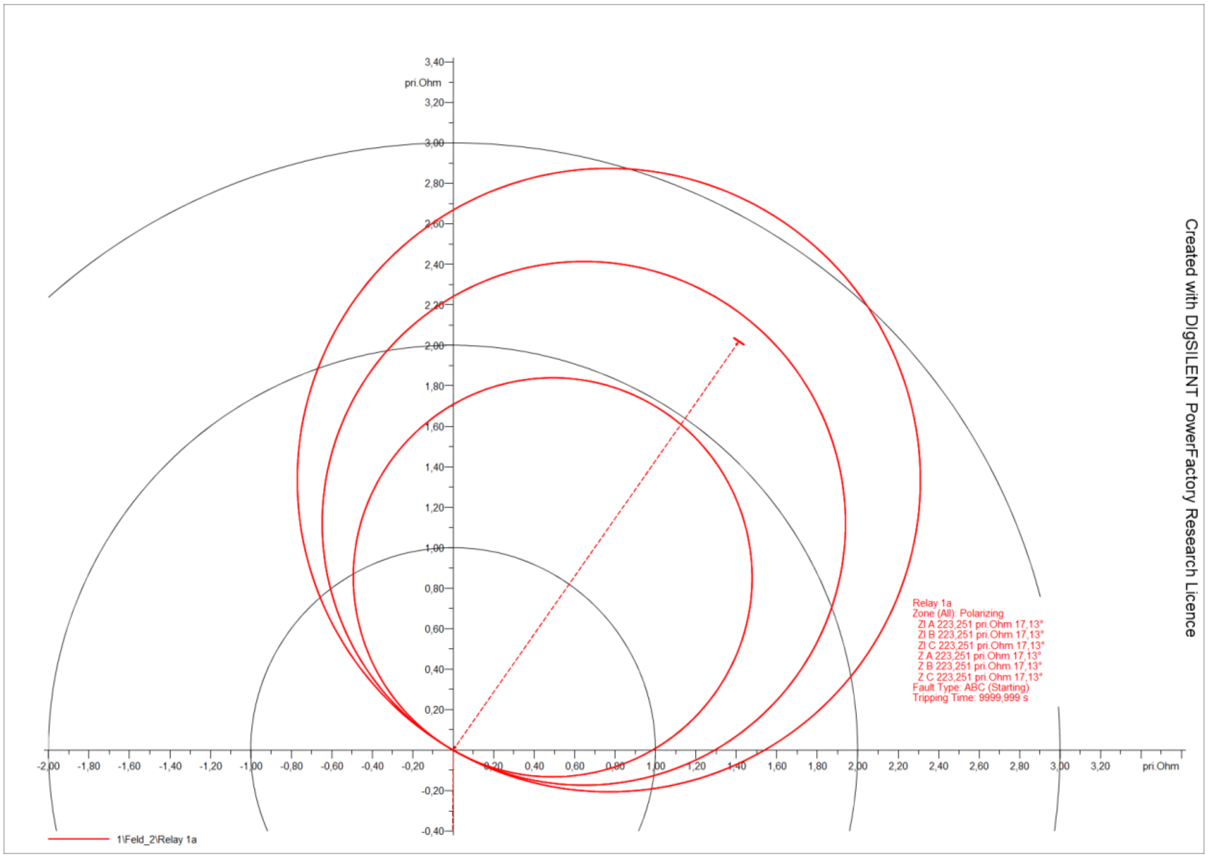


Figure 16. RX Plot of Relay 1a with short circuit calculations [27]

Figure 16 presents the R-X plot for relay 1a, illustrating the relay's characteristics. This plot highlights the calculated zone impedances and delineates which parts of the system each zone covers. Additionally, the plot provides the results of short-circuit calculations and includes important information such as the relay's name, the measured impedances as seen from its location, fault type, trip time, and the specific zone that is tripped.

The directionality of the relays is configured to detect faults occurring in the forward direction from the relay's position, ensuring accurate and reliable fault detection within the intended areas of the grid.

Additionally, the time-distance plot in Figure 17 visually represents the relay zones and tripping times along the short-circuit path from bus 1 to bus 7. The plot shows relay operation times for faults occurring along this path, with the upper half indicating clockwise direction operation times and the lower half representing anti-clockwise direction operation times. The x-axis denotes line impedances, with busbars marked along the path, while the y-axis shows the operating time.

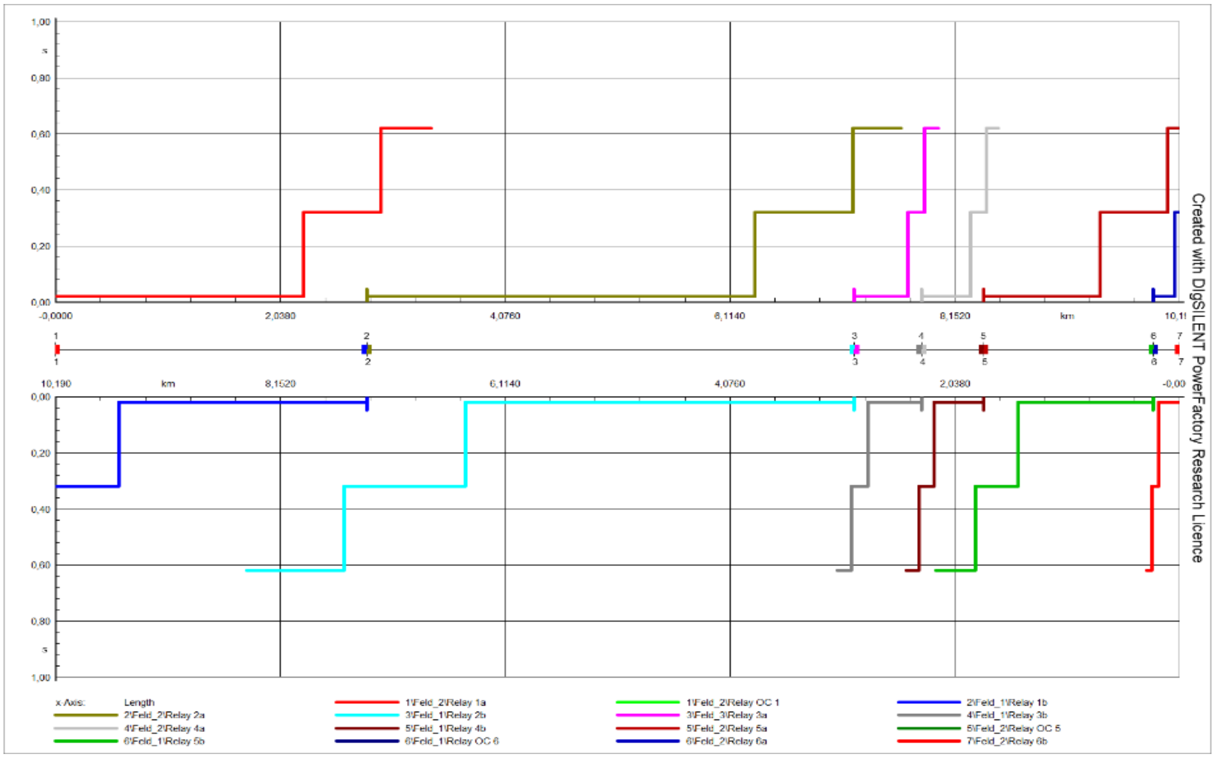

Figure 17. The Time Distance Plot for the Short Circuit path between bus 1 and bus 7

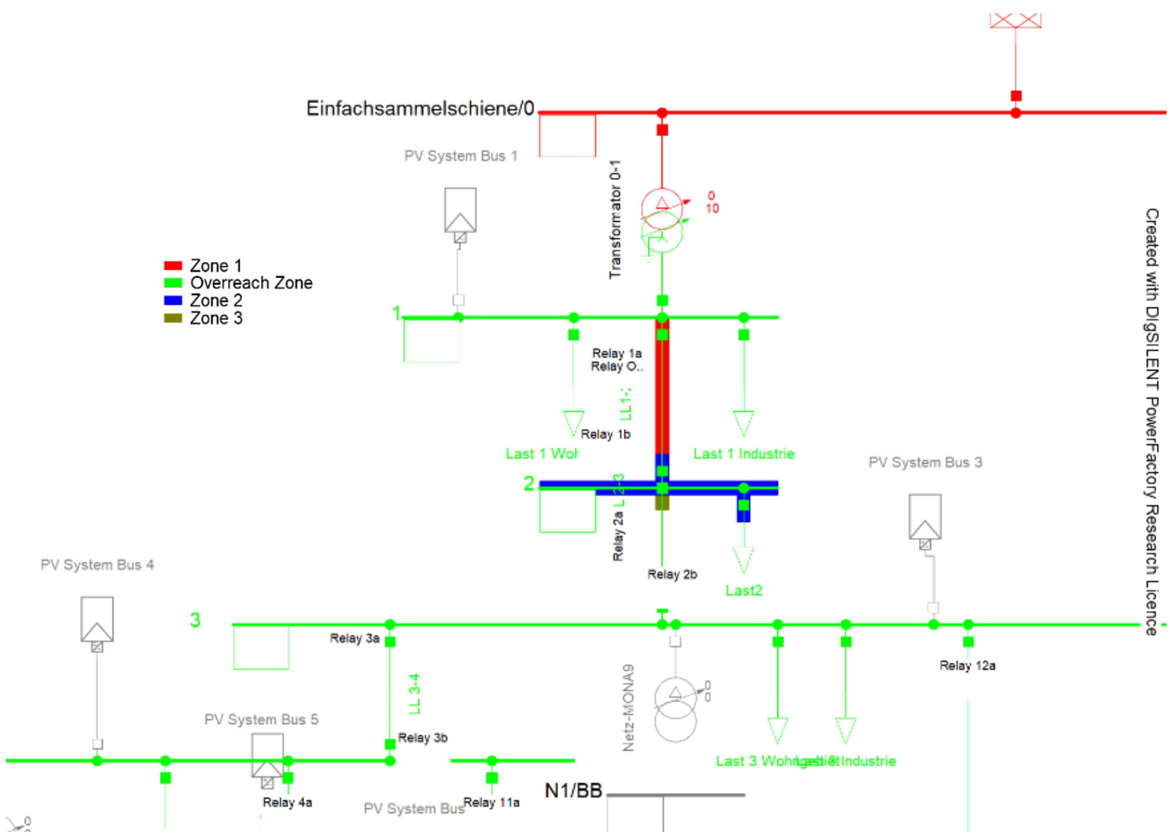


Figure 18. The reach plot of relay 1a

PowerFactory provides a powerful visualization tool known as the reach plot for analyzing the behavior and coverage of distance relays. This plot graphically represents the relay's reach in terms of impedance, clearly delineating the protective zones. By utilizing the reach plot, users can visually assess the extent to which each zone of the distance relay protects different segments of the network under fault conditions. This is crucial for ensuring that relay settings are correctly configured to secure the intended portions of the grid while avoiding overreach or underreach.

The reach plot for relay 1a is presented in Figure 18. This figure illustrates the impedance boundaries and the coverage provided by each zone of relay 1a, highlighting its effectiveness in detecting and isolating faults. This visual analysis enhances the understanding of the relay coordination and ensures that the protection scheme is robust and well-calibrated, even in the presence of distributed generation.

### 5.5.2. Overcurrent Protection

In Zone 1, overcurrent protection was selected to ensure reliable fault detection and grid stability within the radial topology. The relays used for this purpose are the ABB model SPAJ 131C, strategically placed on Line 12-13 and Line 13-14. To enable accurate current measurement and relay operation, Current Transformers (CTs) have been installed at each relay location, as outlined in Section 5.5.

The ABB SPAJ 131C model provides two stages of overcurrent detection : I> (50) and I>> (51). The first stage, I> operates based on a Normal Inverse characteristic, which allows for time-coordinated fault clearing depending on the magnitude of the fault current. The second stage, I>>, utilizes a definite time characteristic, offering a fixed response time for high-magnitude fault currents. This dual-stage approach ensures that the protection system can respond effectively to a wide range of fault scenarios.

Once the appropriate relays were selected, the next step involved calculating the pickup current settings. The pickup current must be determined to ensure the shortest operating time under conditions of maximum fault current while remaining sensitive enough to trigger at the minimum expected fault current. This calculation ensures that the relays are configured to send timely pickup signals, providing effective protection while minimizing the risk of misoperation or delays.

The specific parameters for the ABB SPAJ 131C overcurrent relays are detailed in Table 4. This table includes critical settings such as the pickup currents for both stages, the time multiplier for the Normal Inverse characteristic of I> and the fixed time delay for the definite characteristic of I>>.

Table 4. Overcurrent relay parameters

| | Protection Device | Location | Branch | Manufacturer | Model | CT | Stage (Phase) | Current pri.A | Current sec.A | Current p.u. | Time | Characteristic | Directional |
|---|---|---|---|---|---|---|---|---|---|---|---|---|---|
| 1 | Relay OC1a | 12 | LL 12-13 | ABB | SPAJ 131C | Current Transformer | I> [51] | 1655 | 5.52 | 5.52 | 1.00 | Normal Inverse | None |
| | | | | | | | I>> [50] | 3600 | 12.00 | 12.00 | 0.06 | Definite | None |
| 2 | Relay OC2a | 13 | LL13-14 | ABB | SPAJ 131C(1) | Current Transformer | I> [51] | 960 | 3.20 | 3.20 | 0.10 | Normal Inverse | None |
| | | | | | | | I>> [50] | 2125 | 7.08 | 7.08 | 0.05 | Definite | None |

PowerFactory provides a feature to generate time-overcurrent plots, which are essential for visualizing and analyzing the performance of overcurrent relays in relation to the damage curves of the protected equipment. The time-overcurrent plots for relays OC1a and OC2a are presented in Figures 19. On the left side of each figure, you can also see the single-line diagram that shows the placement of the relays within the network, providing context for their locations and the elements they protect.

These plots illustrate the operating times of each relay across different current levels, clearly showing how the relays respond to varying fault conditions. In the plots, you can observe the damage curves of the transformer, which include the inrush current limits. The overcurrent relay curves are positioned beneath and to the left of the damage curves, ensuring that the relays are set to trip before the current reaches a damaging level for the transformer. The trip times for the relays are calculated based on the methods described in 2.2.1., providing a clear demonstration of how the protection scheme is coordinated to prevent equipment damage while allowing for normal system operation.

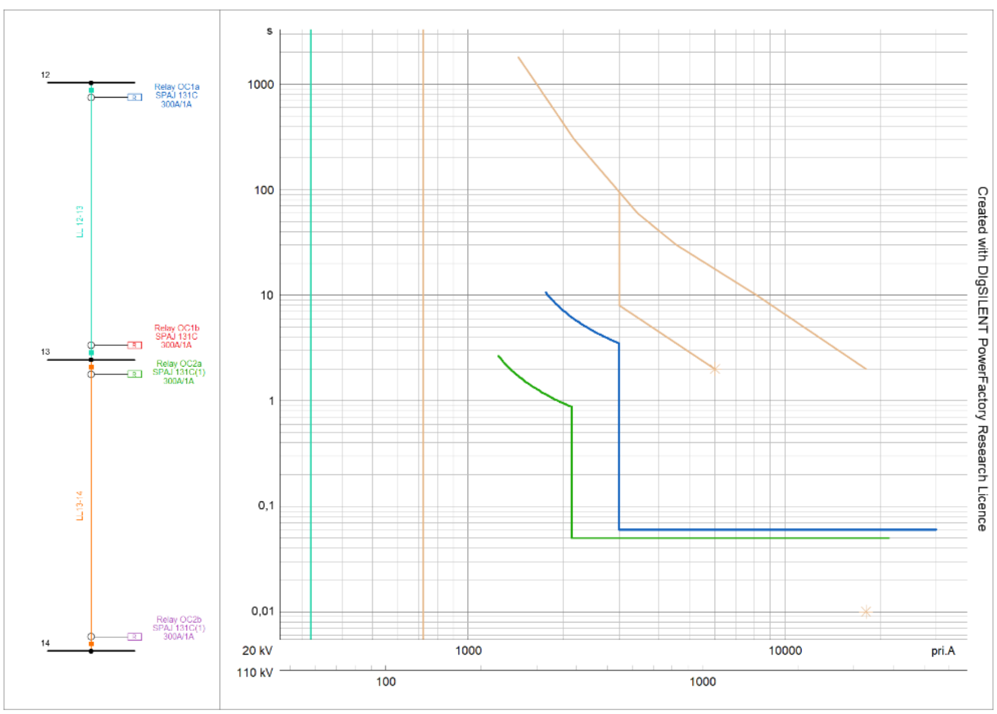


Figure 19. The Time Over Current plots of overcurrent protection relay OC1a (blue curve) and OC2a (green curve)

### 5.6. Definition and Configuration of Simulation Cases for Protection Analysis

To conduct a comprehensive study, the overcurrent protection settings were configured and applied to grid area 1, while distance protection settings were implemented in grid are 2. Subsequently, various scenarios were designed to facilitate a systematic analysis. These scenarios were simulated to evaluate the performance of the protection devices, with the results serving as the basis for the assessment.

Short-circuit calculations were conducted for grid area 1 using the short-circuit analysis tool in PowerFactory, focusing on three-phase balanced faults. These faults were simulated on lines 12-13 and 13-14 at various points along the lines : 0%, 20%, 40%, 60%, 80%, and 100% of the line length. The primary objective was to investigate the impact of faults on this grid area. The simulations yielded critical data, including the magnitude of the short-circuit current, the trip timing of the overcurrent relays (OC1a and OC2a), and other relevant parameters for further analysis.

The base case considered a system without any PV generation, where short-circuit calculations were performed, and the corresponding data were recorded. Subsequently, PV generation was incrementally introduced into the system to examine the effects of increased PV penetration on fault currents and the operation of relay protection devices. Specific scenarios, detailing the levels of PV generation added to the system, are summarized in Table 5.

The PV generation was initially implemented at bus 12 and later extended to buses 13 and 14 to investigate how the location of PV generation impacts fault behavior and relay operations within the system. These additional cases provide insights into the influence of distributed generation placement on protection coordination.

Table 5. Overview of PV Generation Scenarios in Grid area 1

| Case | PV Generation (MW) | Description |
|---|---|---|
| **Case 1** | 0 MW | Base case: No PV generation |
| **Case 2** | 4.5 MW | Low PV generation |
| **Case 3** | 45.5 MW | Moderate PV generation |
| **Case 4** | 91 MW | High PV generation |
| **Case 5** | 104 MW | Maximum PV generation |

Three phase balanced short-circuit calculations were conducted in grid area 2 using the short-circuit calculation tools in PowerFactory. These calculations were applied to all elements of the topology to ensure the correct operation of all relay protection devices in the system. The results, which are presented in the appendices (appendix 1 and appendix 2), confirm that the relay settings were properly configured and operating as intended.

For a more detailed investigation, the focus shifted to analyzing the reach of the distance protection devices, particularly their behavior in zone 3. From the short-circuit calculations, relays 3a, 5a, and 9a were selected for analysis, as they were identified as reacting within the third protection zone in different fault cases.

To study the behavior of these relays in zone 3, the measurement functionality of the distance protection in PowerFactory was utilized and RMS simulations were performed. This involved capturing variables such as current (real and imaginary components) from the current transformer and voltage (real and imaginary components) from the voltage transformer. These measurements were plotted and used to calculate the impedance magnitude and angle, enabling the derivation of resistance and reactance values.

The scenarios for the distance protection analysis are detailed in Table 6. For each relay, different PV generation levels were introduced at various locations in the grid. This approach was taken to assess the impact of both the location and magnitude of PV generation on the operation and performance of the distance protection devices. To simulate different conditions in the system, PV generation was implemented at various bus locations. For relay 3a, PV generation was introduced at bus 1, with the power levels increased as specified in Table 6. This setup was designed to evaluate the impact of PV generation on the upstream side of the relay and its influence on distance protection performance. A three-phase balanced fault was created on line 4-5 at a location 20% from bus 4.

During the RMS simulations, relays 4a and 4b were disabled to ensure that the trip from relay 3a could be captured. These relays were disabled because their settings would otherwise cause them to trip earlier (relay 4a at 0.02 s and relay 4b at 0.32 s). The fault was applied at 1 second and was expected to be cleared by relay 3a after 0.6 seconds. Subsequently, PV generation was implemented at buses 5, 11, and 8, with the cases tested according to the scenarios outlined in Table 6. This analysis aimed to investigate the impact of increasing PV generation on the downstream side of the grid and its effect on distance protection functionality.

Table 6. PV Generation Scenarios For Distance Protection Analysis In Grid area 2

| Case | PV Generation (MW) | Description |
|---|---|---|
| **Case 1** | 0 MW | Base case: No PV generation |
| **Case 2** | 13 MW | Low-level PV generation introduced. |
| **Case 3** | 27 MW | Moderate PV generation representing an increase. |
| **Case 4** | 40 MW | Higher PV generation scenario. |
| **Case 5** | 54 MW | Increased PV generation, nearing system capacity. |
| **Case 6** | 68 MW | Significant PV generation introduced. |
| **Case 7** | 82 MW | High PV generation scenario. |
| **Case 8** | 95 MW | Very high PV generation level. |
| **Case 9** | 110 MW | Maximum PV generation implemented in the system. |

Due to the inability to accurately implement the expected short-circuit contribution of the PV generators during a fault, this study focuses on presenting results with certain limitations. Specifically, for overcurrent protection, the results from the short-circuit calculations are displayed. However, for distance protection, only the RMS simulation results for the base case (Case 0) without PV generation will be presented. This approach ensures the validity of the analysis while acknowledging the limitations in accurately modeling the PV generators' behavior during fault conditions.

# 6. Results

This section presents the findings from the simulations conducted to analyze the performance of overcurrent and distance protection devices under various scenarios in the grid.

For overcurrent protection, the short-circuit calculations focus on fault current magnitudes, relay trip timings, and the impact of increasing PV generation on relay operation. These results provide insights into how overcurrent protection adapts to changes in the grid's fault characteristics.

For distance protection, RMS simulations are analyzed for the base case without PV generation to examine the performance of selected relays under three-phase balanced fault conditions. Although limitations prevented modeling the short-circuit contributions of PV generators, the presented results provide a foundation for understanding the behavior of distance protection devices in the studied grid configuration.

The findings are organized to enable a clear comparison of protection performance across different scenarios, highlighting the challenges and implications of integrating PV generation into medium-voltage grids.

## 6.1. Overcurrent protection results

### 6.1.1. Base Case – Without PV Generation

The base case represents the system without any PV generation, providing a benchmark to evaluate the behavior of overcurrent protection under balanced three-phase fault conditions. This setup allows for an analysis of the short-circuit current magnitudes and relay trip timings under typical grid conditions.

Figure 20 presents a snapshot of the results from the short-circuit calculations performed on line 12-13.

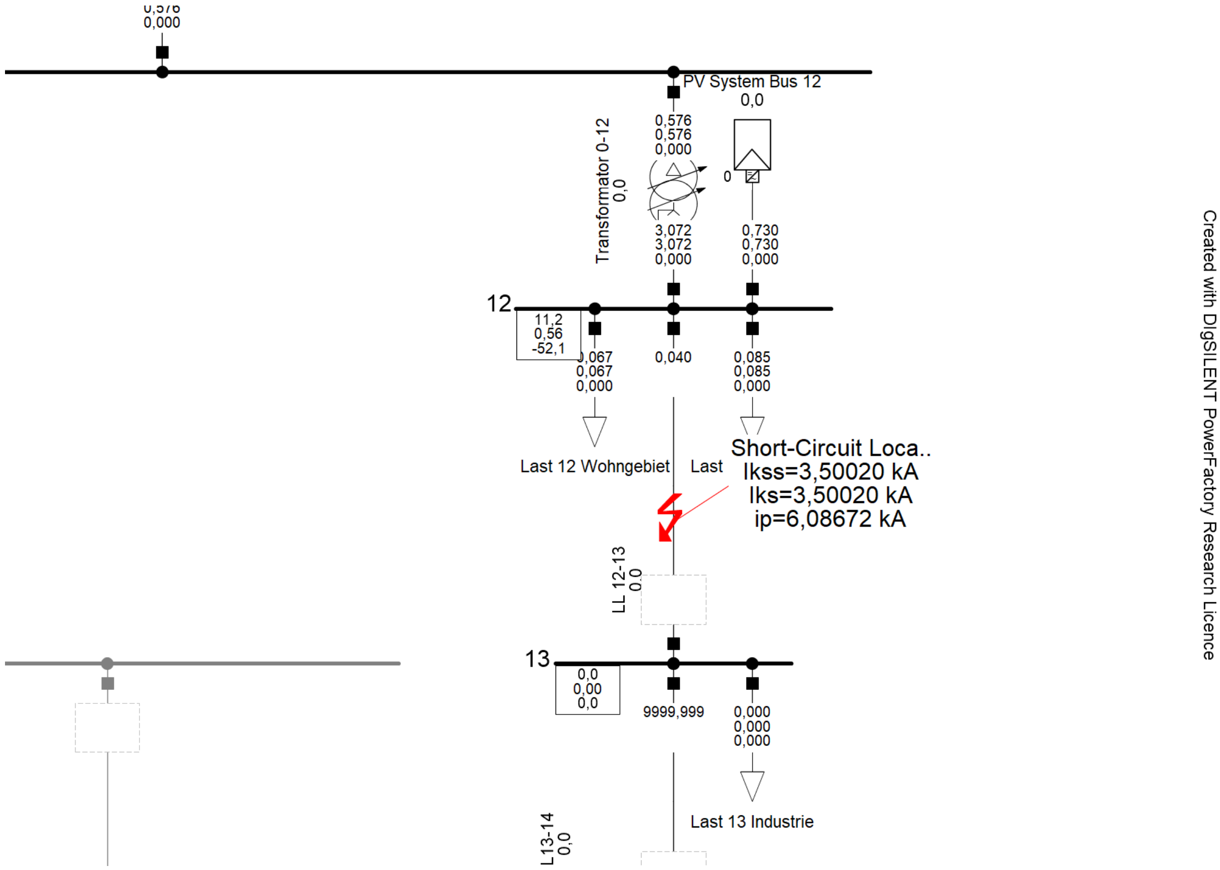


Figure 20. Short-circuit current magnitudes and relay trip timings on line 12-13 under base case conditions (no PV generation)

The results from the simulations are presented in Table 7.

Table 7. Fault Current Magnitudes and Relay Trip Timings for Short-Circuit Simulations on Line 12-13

| Fault Location (% of Line Length) | Short-Circuit Current (Iks, kA) | Relay OC1a Trip Time (s) |
|---|---|---|
| **0** | 5.809 | 1.017 |
| **20** | 4.754 | 1.120 |
| **40** | 3.942 | 1.250 |
| **60** | 3.335 | 1.393 |
| **80** | 2.875 | 1.549 |
| **100** | 2.520 | 1.721 |

The following plots provide a visual representation of the data presented in Table 7, illustrating the variation of short-circuit currents (Iks) and relay OC1a trip times at different fault locations along line 12-13 and ploted on figure 21.

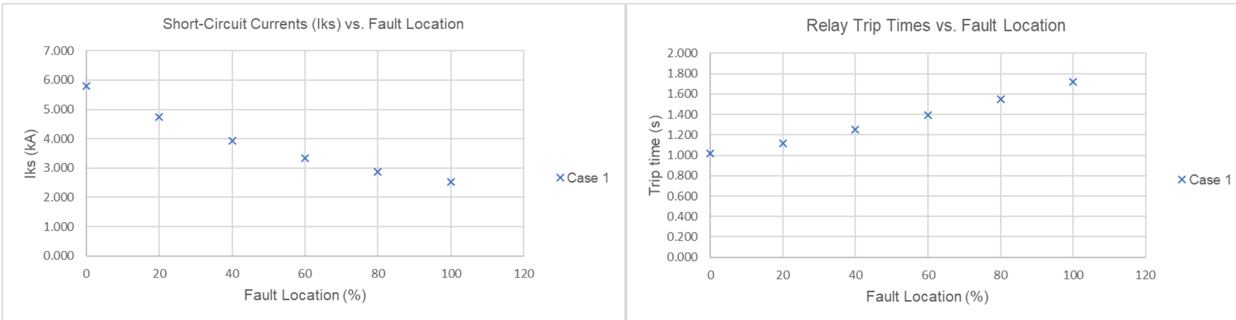


Figure 21. Short-circuit current magnitudes and relay OC1a trip times versus fault location on line 12-13

Similarly, a short-circuit fault was simulated on line 13-14, and the results of this analysis are presented in Table 8.

Table 8. Short-Circuit Current Magnitudes (Iks) and Relay Trip Times for Line 13-14 at Various Fault Locations

| Fault Location (% of Line Length) | Short-Circuit Current (Iks, kA) | Relay OC1a Trip Time (s) | Relay OC2a Trip Time (s) |
|---|---|---|---|
| **0** | 2.520 | 1.721 | 0.353 |
| **20** | 2.341 | 1.834 | 0.367 |
| **40** | 2.185 | 1.955 | 0.382 |
| **60** | 2.047 | 2.084 | 0.396 |
| **80** | 1.925 | 2.222 | 0.411 |
| **100** | 1.817 | 2.370 | 0.426 |

The values presented in Table 8 are graphically illustrated in the plots shown in Figure 22, providing a visual representation of the results.

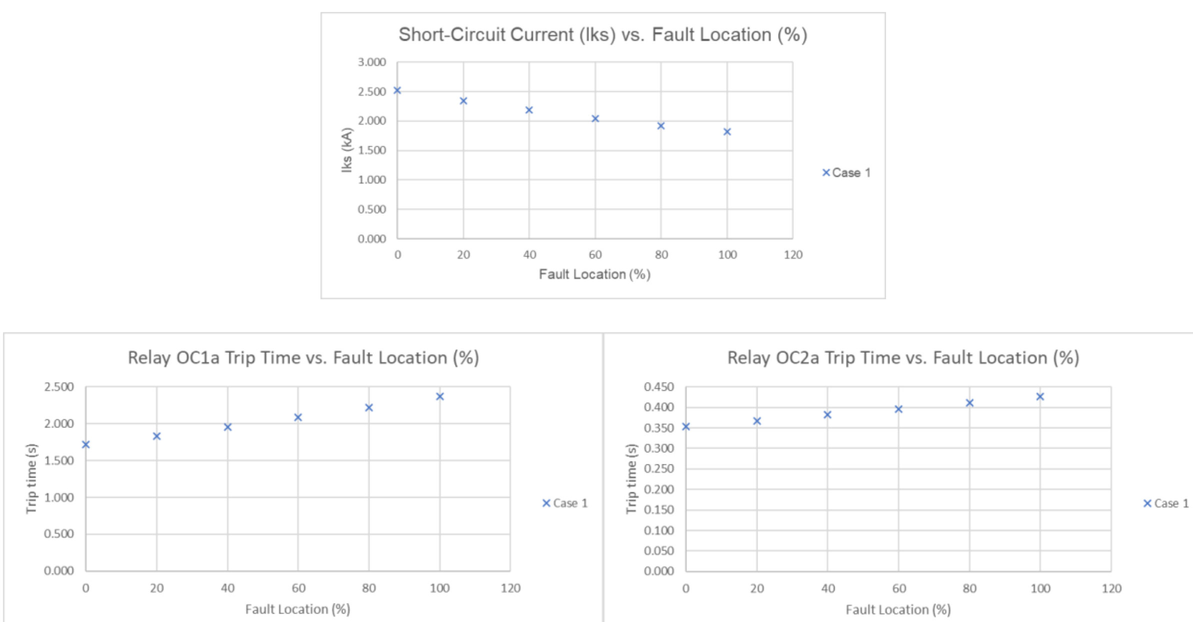


Figure 22. Short-circuit current magnitudes (Iks) and relay trip times (OC1a and OC2a) for various fault locations along line 13-14 (Case 1)

### 6.1.2. Analysis of PV Generation Increase on Bus 12

Following the methodology outlined in Section 5.6, PV generation was introduced into the model at bus 12, with generation levels increased incrementally as specified in Table 5. For each case, a three-phase balanced fault was simulated using short-circuit calculations, and the corresponding values were recorded. The results for the simulated faults on line 12-13, including the short-circuit current magnitudes and the trip times of the overcurrent relay protection (OC1a), are presented in Table 9.

Table 9. Short-circuit current magnitudes (Iks) and relay OC1a trip times for various fault locations on line 12-13 under increasing PV generation levels at Bus 12 (Cases 1–5).

| Distance (%) | Short-Circuit Current (Iks, kA) | | | | | Relay OC1a Trip Time (s) | | | | |
|---|---|---|---|---|---|---|---|---|---|---|
| | Case 1 | Case 2 | Case 3 | Case 4 | Case 5 | Case 1 | Case 2 | Case 3 | Case 4 | Case 5 |
| **0** | 5.809 | 5.804 | 5.752 | 5.697 | 5.683 | 1.017 | 1.017 | 1.018 | 1.018 | 1.019 |
| **20** | 4.754 | 4.767 | 4.894 | 5.12 | 5.29 | 1.12 | 1.119 | 1.103 | 1.076 | 1.058 |
| **40** | 3.942 | 3.96 | 4.121 | 4.374 | 4.53 | 1.25 | 1.246 | 1.216 | 1.175 | 1.115 |
| **60** | 3.335 | 3.352 | 3.5 | 3.695 | 3.781 | 1.393 | 1.358 | 1.348 | 1.301 | 1.283 |
| **80** | 2.875 | 2.891 | 3.015 | 3.146 | 3.171 | 1.549 | 1.543 | 1.496 | 1.45 | 1.442 |
| **100** | 2.52 | 2.533 | 2.635 | 2.716 | 2.701 | 1.721 | 1.714 | 1.659 | 1.619 | 1.627 |

The following results are graphically represented in figure 23, providing a clearer visualization of the data.

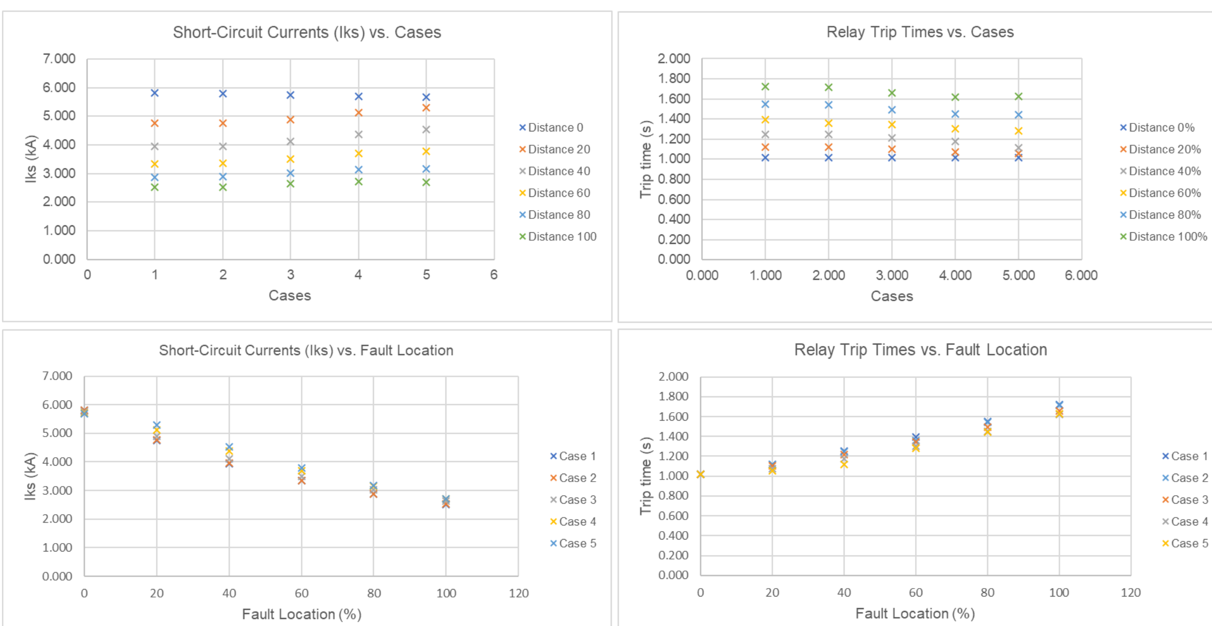


Figure 23. Short-circuit currents (Iks) and relay trip times for line 12-13. Top plots show variations with PV generation (Cases 1–5), and bottom plots show variations with fault location (% of line length)

Following the same methodology described earlier, the fault was simulated and repeated for the various cases on line 13-14, with the results presented in Table 10 and 11.

Table 10. Short-Circuit Currents (Iks) and Relay OC1a Trip Times for Line 13-14

| Distance | Short-Circuit Current (Iks, kA) | | | | | Relay OC1a Trip Time (s) | | | | |
|---|---|---|---|---|---|---|---|---|---|---|
| (%) | Case 1 | Case 2 | Case 3 | Case 4 | Case 5 | Case 1 | Case 2 | Case 3 | Case 4 | Case 5 |
| **0** | 2.52 | 2.534 | 2.695 | 2.716 | 2.701 | 1.721 | 1.714 | 1.659 | 1.619 | 1.627 |
| **20** | 2.341 | 2.353 | 2.443 | 2.499 | 2.468 | 1.834 | 1.826 | 1.767 | 1.733 | 1.752 |
| **40** | 2.185 | 2.196 | 2.275 | 2.312 | 2.268 | 1.955 | 1.946 | 1.883 | 1.855 | 1.888 |
| **60** | 2.047 | 2.057 | 2.127 | 2.148 | 2.096 | 2.084 | 2.074 | 2.006 | 1.987 | 2.036 |
| **80** | 1.925 | 1.934 | 1.997 | 2.005 | 1.946 | 2.222 | 2.211 | 2.138 | 2.129 | 2.197 |
| **100** | 1.817 | 1.825 | 1.881 | 1.878 | 1.815 | 2.37 | 2.358 | 2.28 | 2.283 | 2.372 |

Table 11. Short-Circuit Currents (Iks) and Relay OC2a Trip Times for Line 13-14

| Distance | Short-Circuit Current (Iks, kA) | | | | | Relay OC2a Trip Time (s) | | | | |
|---|---|---|---|---|---|---|---|---|---|---|
| (%) | Case 1 | Case 2 | Case 3 | Case 4 | Case 5 | Case 1 | Case 2 | Case 3 | Case 4 | Case 5 |
| **0** | 2.52 | 2.534 | 2.695 | 2.716 | 2.701 | 0.353 | 0.352 | 0.347 | 0.34 | 0.341 |
| **20** | 2.341 | 2.353 | 2.443 | 2.499 | 2.468 | 0.367 | 0.366 | 0.359 | 0.355 | 0.357 |
| **40** | 2.185 | 2.196 | 2.275 | 2.312 | 2.268 | 0.382 | 0.38 | 0.373 | 0.37 | 0.374 |
| **60** | 2.047 | 2.057 | 2.127 | 2.148 | 2.096 | 0.396 | 0.395 | 0.387 | 0.385 | 0.391 |
| **80** | 1.925 | 1.934 | 1.997 | 2.005 | 1.946 | 0.411 | 0.41 | 0.402 | 0.401 | 0.408 |
| **100** | 1.817 | 1.825 | 1.881 | 1.878 | 1.815 | 0.426 | 0.425 | 0.417 | 0.417 | 0.426 |

Based on the data presented in Tables 10 and 11, the short-circuit currents and relay trip times (OC1a and OC2a) for various fault locations and PV generation cases are graphically represented in the following plots on figure 24.

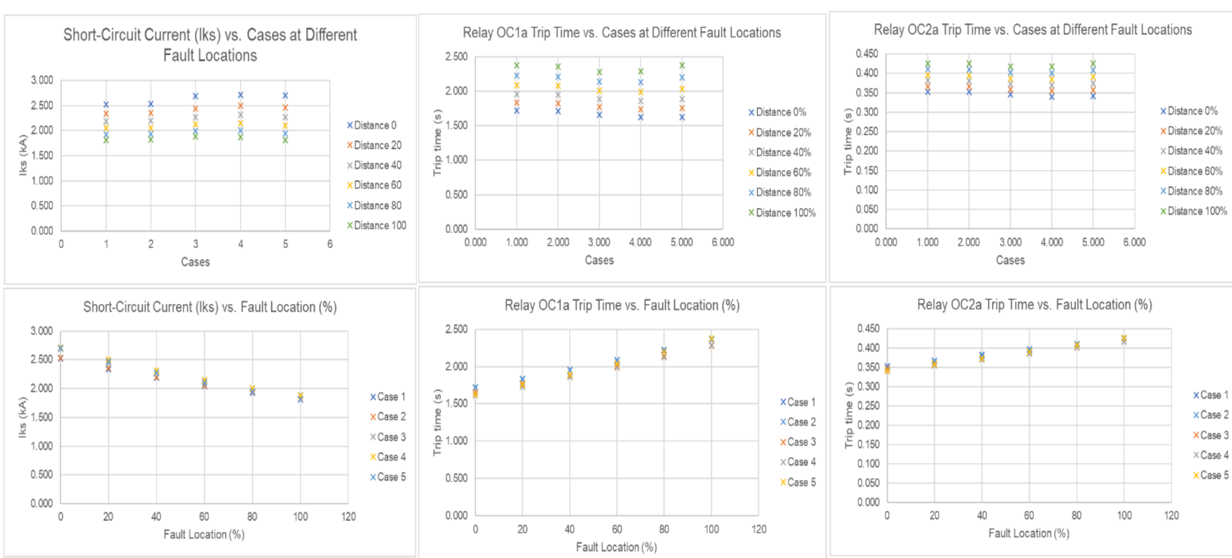


Figure 24. Short-circuit current (Iks) and relay trip times (OC1a and OC2a) for line 13-14 under increasing PV generation levels (Cases 1–5) and varying fault locations.

### 6.1.3 Analysis of PV Generation Increase on Bus 13

Following the same methodology outlined in Section 5.6, PV generation was implemented at Bus 13, with incremental increases as specified in Table 5. Three-phase balanced faults were simulated on two lines : first on line 12-13, and subsequently on line 13-14. Faults were applied at various fault locations (0%, 20%, 40%, 60%, 80%, and 100% of the line length) for increasing PV generation levels (Cases 1–5). The short-circuit current magnitudes and relay trip times for OC1a and OC2a were recorded for both fault scenarios.

The results for the simulated faults on line 12-13 with PV generation at Bus 13 are presented in Table 12.

Table 12. Short-Circuit Currents (Iks) and Relay OC1a Trip Times for Line 12-13 with PV Generation at Bus 13

| **Distance (%)** | **Short-Circuit Current (Iks, kA)** | | | | | **Relay OC1a Trip Time (s)** | | | | |
|---|---|---|---|---|---|---|---|---|---|---|
| | **Case 1** | **Case 2** | **Case 3** | **Case 4** | **Case 5** | **Case 1** | **Case 2** | **Case 3** | **Case 4** | **Case 5** |
| **0** | 5.809 | 5.809 | 5.683 | 5.741 | 5.744 | 0.049 | 0.049 | 0.049 | 0.049 | 0.049 |
| **20** | 4.754 | 4.749 | 5.29 | 4.698 | 4.701 | 1.12 | 1.121 | 1.125 | 1.128 | 1.127 |
| **40** | 3.942 | 3.939 | 4.53 | 3.896 | 3.898 | 1.25 | 1.25 | 1.256 | 1.259 | 1.258 |
| **60** | 3.335 | 3.335 | 3.781 | 3.296 | 3.298 | 1.393 | 1.394 | 1.4 | 1.404 | 1.403 |
| **80** | 2.875 | 2.875 | 3.171 | 2.842 | 2.844 | 1.549 | 1.553 | 1.559 | 1.563 | 1.563 |
| **100** | 2.52 | 2.52 | 2.701 | 2.491 | 2.492 | 1.721 | 1.722 | 1.733 | 1.738 | 1.737 |

The data from Tables 12 are graphically represented in Figure 25. The plots illustrate variations in short-circuit currents and relay trip times (OC1a) for different PV generation levels and fault locations on line 12-13.

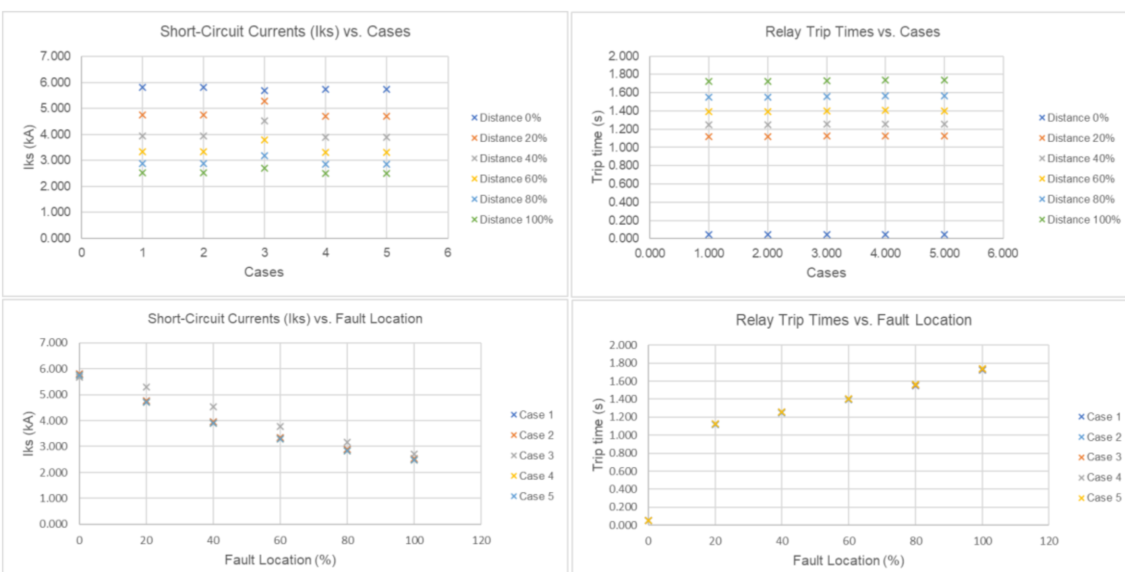


Figure 25. Short-circuit current (Iks) and relay trip times (OC1a and OC2a) for line 12-13 with PV generation at Bus 13.

The same process was repeated for faults simulated on line 13-14, with results summarized in Tables 13 and 14. Table 13 contains the short-circuit currents and relay OC1a trip times, while Table 14 presents the relay OC2a trip times.

Table 13. Short-Circuit Currents (Iks) and Relay OC1a Trip Times for Line 13-14 with PV Generation at Bus 13

| Distance (%) | Short-Circuit Current (Iks, kA) | | | | | Relay OC1a Trip Time (s) | | | | |
|---|---|---|---|---|---|---|---|---|---|---|
| | Case 1 | Case 2 | Case 3 | Case 4 | Case 5 | Case 1 | Case 2 | Case 3 | Case 4 | Case 5 |
| **0** | 2.52 | 2.518 | 2.501 | 2.491 | 2.492 | 1.721 | 1.722 | 1.733 | 1.738 | 1.737 |
| **20** | 2.341 | 2.346 | 2.375 | 2.417 | 2.439 | 1.834 | 1.837 | 1.851 | 1.861 | 1.862 |
| **40** | 2.185 | 2.195 | 2.259 | 2.34 | 2.379 | 1.955 | 1.959 | 1.986 | 2.009 | 2.015 |
| **60** | 2.047 | 2.061 | 2.15 | 2.262 | 2.313 | 2.084 | 2.091 | 2.139 | 2.183 | 2.203 |
| **80** | 1.925 | 1.941 | 2.05 | 2.183 | 2.243 | 2.222 | 2.223 | 2.314 | 2.405 | 2.438 |
| **100** | 1.817 | 1.835 | 1.957 | 2.106 | 2.171 | 2.37 | 2.387 | 2.517 | 2.673 | 2.733 |

Table 14. Short-Circuit Currents (Iks) and Relay OC2a Trip Times for Line 13-14 with PV Generation at Bus 13

| Distance (%) | Short-Circuit Current (Iks, kA) | | | | | Relay OC2a Trip Time (s) | | | | |
|---|---|---|---|---|---|---|---|---|---|---|
| | Case 1 | Case 2 | Case 3 | Case 4 | Case 5 | Case 1 | Case 2 | Case 3 | Case 4 | Case 5 |
| **0** | 2.52 | 2.518 | 2.501 | 2.491 | 2.492 | 0.353 | 0.353 | 0.354 | 0.355 | 0.355 |
| **20** | 2.341 | 2.346 | 2.375 | 2.417 | 2.439 | 0.367 | 0.367 | 0.364 | 0.361 | 0.359 |
| **40** | 2.185 | 2.195 | 2.259 | 2.34 | 2.379 | 0.382 | 0.381 | 0.374 | 0.367 | 0.364 |
| **60** | 2.047 | 2.061 | 2.15 | 2.262 | 2.313 | 0.396 | 0.395 | 0.385 | 0.374 | 0.37 |
| **80** | 1.925 | 1.941 | 2.05 | 2.183 | 2.243 | 0.411 | 0.409 | 0.396 | 0.382 | 0.376 |
| **100** | 1.817 | 1.835 | 1.957 | 2.106 | 2.171 | 0.426 | 0.423 | 0.407 | 0.39 | 0.383 |

The data from Tables 13 and 14 are graphically represented in figure 26. These plots show variations in short-circuit currents and relay trip times (OC1a and OC2a) for different PV generation levels and fault locations on line 13-14.

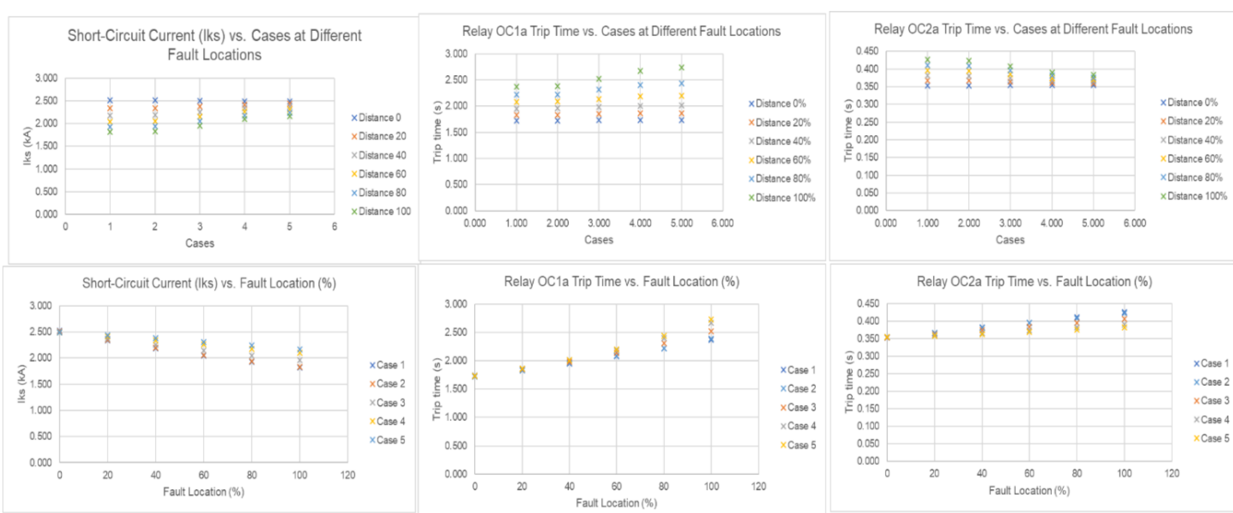


Figure 26. Short-circuit current (Iks) and relay trip times (OC1a and OC2a) for line 13-14 with PV generation at Bus 13.

### 6.1.4 Analysis of PV Generation Increase on Bus 14

Using the same methodology outlined for Bus 12 and Bus 13, PV generation was implemented at Bus 14 with incremental increases as specified in Table 5. Three-phase balanced faults were simulated on two lines : first on line 12-13, and subsequently on line 13-14. Faults were applied at various fault locations (0%, 20%, 40%, 60%, 80%, and 100% of the line length) under increasing PV generation levels (Cases 1–5). The short-circuit current magnitudes and relay trip times for OC1a and OC2a were recorded. However, during the simulation of Case 5 (maximum PV generation level), the calculations failed to converge in PowerFactory due to numerical instability or network configuration issues. As a result, data for Case 5 could not be obtained. The following results therefore include only Cases 1 through 4.

The results for the simulated faults on line 12-13 with PV generation at Bus 14 are presented in Tables 15.

The data from Tables 15 is graphically represented in figure 27. The plots illustrate variations in short-circuit currents and relay trip times (OC1a) for different PV generation levels and fault locations on line 12-13.

Table 15. Short-Circuit Currents (Iks) and Relay OC1a Trip Times for Line 12-13 with PV Generation at Bus 14

| Distance (%) | Short-Circuit Current (Iks, kA) | | | | Relay OC1a Trip Time (s) | | | |
|---|---|---|---|---|---|---|---|---|
| | Case 1 | Case 2 | Case 3 | Case 4 | Case 1 | Case 2 | Case 3 | Case 4 |
| **0** | 5.809 | 5.804 | 5.768 | 5.759 | 0.049 | 0.049 | 0.049 | 0.049 |
| **20** | 4.754 | 4.749 | 4.72 | 4.713 | 1.12 | 1.121 | 1.125 | 1.126 |
| **40** | 3.942 | 3.939 | 3.914 | 3.908 | 1.25 | 1.25 | 1.255 | 1.256 |
| **60** | 3.335 | 3.332 | 3.312 | 3.306 | 1.393 | 1.394 | 1.399 | 1.401 |
| **80** | 2.875 | 2.873 | 2.855 | 2.851 | 1.549 | 1.55 | 1.558 | 1.56 |
| **100** | 2.52 | 2.518 | 2.503 | 2.499 | 1.721 | 1.722 | 1.731 | 1.734 |

The same process was repeated for faults simulated on line 13-14, with results summarized in tables 16 and 17. Table 16 contains the short-circuit currents and relay OC1a trip times, while table 17 presents the relay OC2a trip times.

The data from Tables 16 and 17 are graphically represented in figure 28. These plots show variations in short-circuit currents and relay trip times (OC1a and OC2a) for different PV generation levels and fault locations on line 13-14.

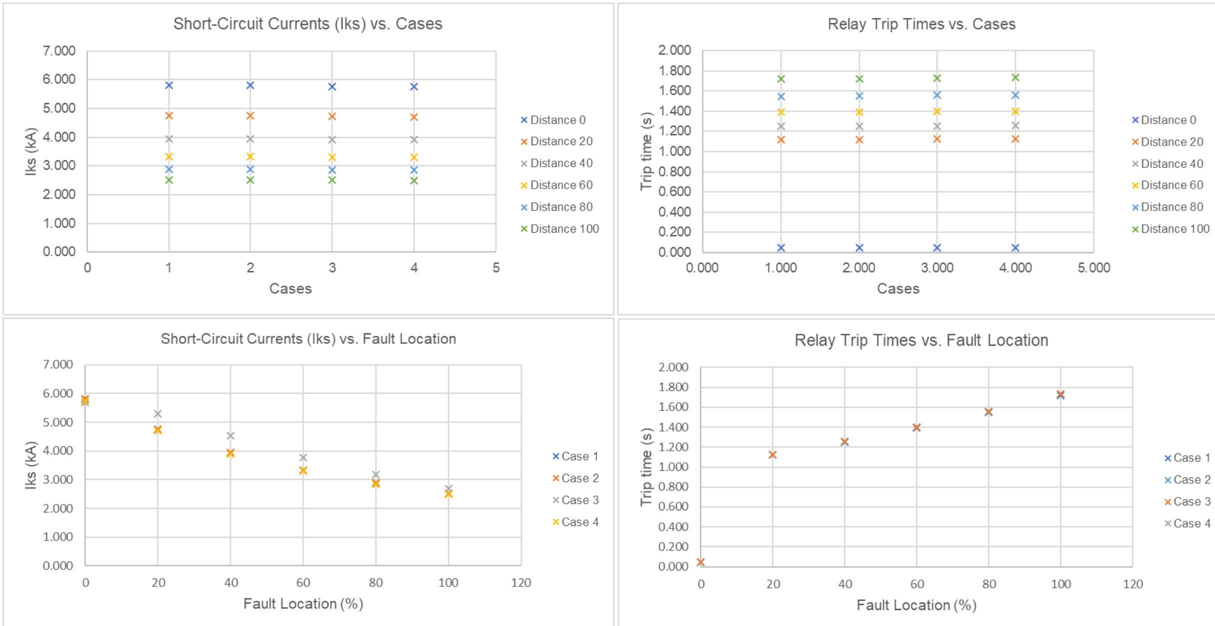


Figure 27. Short-circuit current (Iks) and relay trip times (OC1a) for line 12-13 with PV generation at Bus 14

Table 16. *Short-Circuit Currents (Iks) and Relay OC1a Trip Times for Line 13-14 with PV Generation at Bus 14*

| Distance (%) | Short-Circuit Current (Iks, kA) | | | | Relay OC1a Trip Time (s) | | | |
|---|---|---|---|---|---|---|---|---|
| | Case 1 | Case 2 | Case 3 | Case 4 | Case 1 | Case 2 | Case 3 | Case 4 |
| **0** | 2.52 | 2.518 | 2.503 | 2.499 | 1.721 | 1.722 | 1.731 | 1.734 |
| **20** | 2.341 | 2.339 | 2.325 | 2.321 | 1.834 | 1.836 | 1.846 | 1.849 |
| **40** | 2.185 | 2.183 | 2.169 | 2.166 | 1.955 | 1.957 | 1.969 | 1.972 |
| **60** | 2.047 | 2.045 | 2.033 | 2.03 | 2.084 | 2.086 | 2.099 | 2.103 |
| **80** | 1.925 | 1.924 | 1.912 | 1.909 | 2.222 | 2.224 | 2.239 | 2.243 |
| **100** | 1.817 | 1.815 | 1.804 | 1.801 | 2.37 | 2.373 | 2.39 | 2.399 |

Table 17. *Short-Circuit Currents (Iks) and Relay OC2a Trip Times for Line 13-14 with PV Generation at Bus 14*

| Distance (%) | Short-Circuit Current (Iks, kA) | | | | Relay OC2a Trip Time (s) | | | |
|---|---|---|---|---|---|---|---|---|
| | Case 1 | Case 2 | Case 3 | Case 4 | Case 1 | Case 2 | Case 3 | Case 4 |
| **0** | 2.52 | 2.518 | 2.503 | 2.499 | 0.353 | 0.353 | 0.354 | 0.355 |
| **20** | 2.341 | 2.339 | 2.325 | 2.321 | 0.367 | 0.367 | 0.369 | 0.369 |
| **40** | 2.185 | 2.183 | 2.169 | 2.166 | 0.382 | 0.382 | 0.383 | 0.383 |
| **60** | 2.047 | 2.045 | 2.033 | 2.03 | 0.396 | 0.396 | 0.398 | 0.398 |
| **80** | 1.925 | 1.924 | 1.912 | 1.909 | 0.411 | 0.411 | 0.413 | 0.413 |
| **100** | 1.817 | 1.815 | 1.804 | 1.801 | 0.426 | 0.426 | 0.428 | 0.428 |

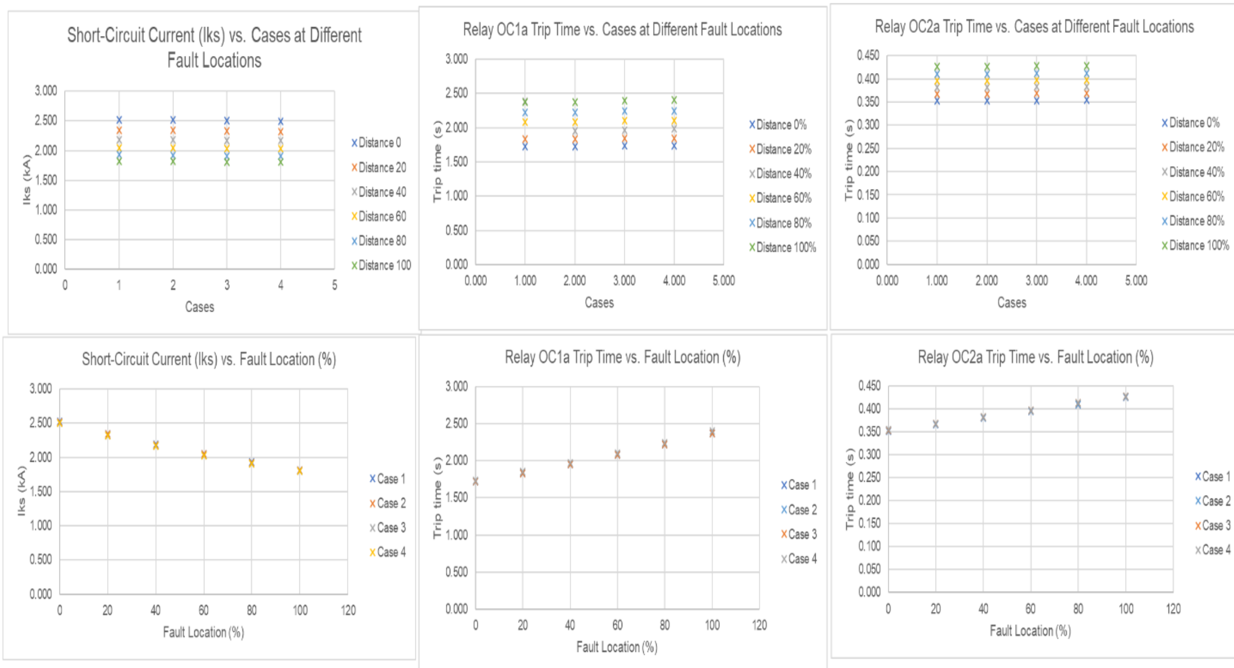


Figure 28. Short-circuit current (Iks) and relay trip times (OC1a and OC2a) for line 13-14 with PV generation at Bus 14.

## 6.2. Distance Protection Results

### 6.2.1. Base Case – Without PV Generation

In the base case scenario, no PV generation was implemented in the system, allowing the behavior of the distance protection relays to be analyzed under traditional grid conditions. Using RMS simulations in PowerFactory, a three-phase balanced fault was applied on line 4-5 at 20% of the distance from bus 4. Relay 3a was selected for detailed analysis, with relays 4a and 4b disabled to prevent premature tripping (relay 4a at 0.02 seconds and relay 4b at 0.32 seconds) and ensure that the Zone 3 operation of relay 3a could be observed. The fault was triggered at 1 second and was expected to be cleared within Zone 3, approximately 0.6 seconds after the fault application.

Variables such as the real and imaginary components of current and voltage (shown on figure 29) were captured using the measurement tools in PowerFactory. The impedance magnitude and angle, as well as the derived resistance and reactance, were calculated. These calculated results are displayed on table 18.

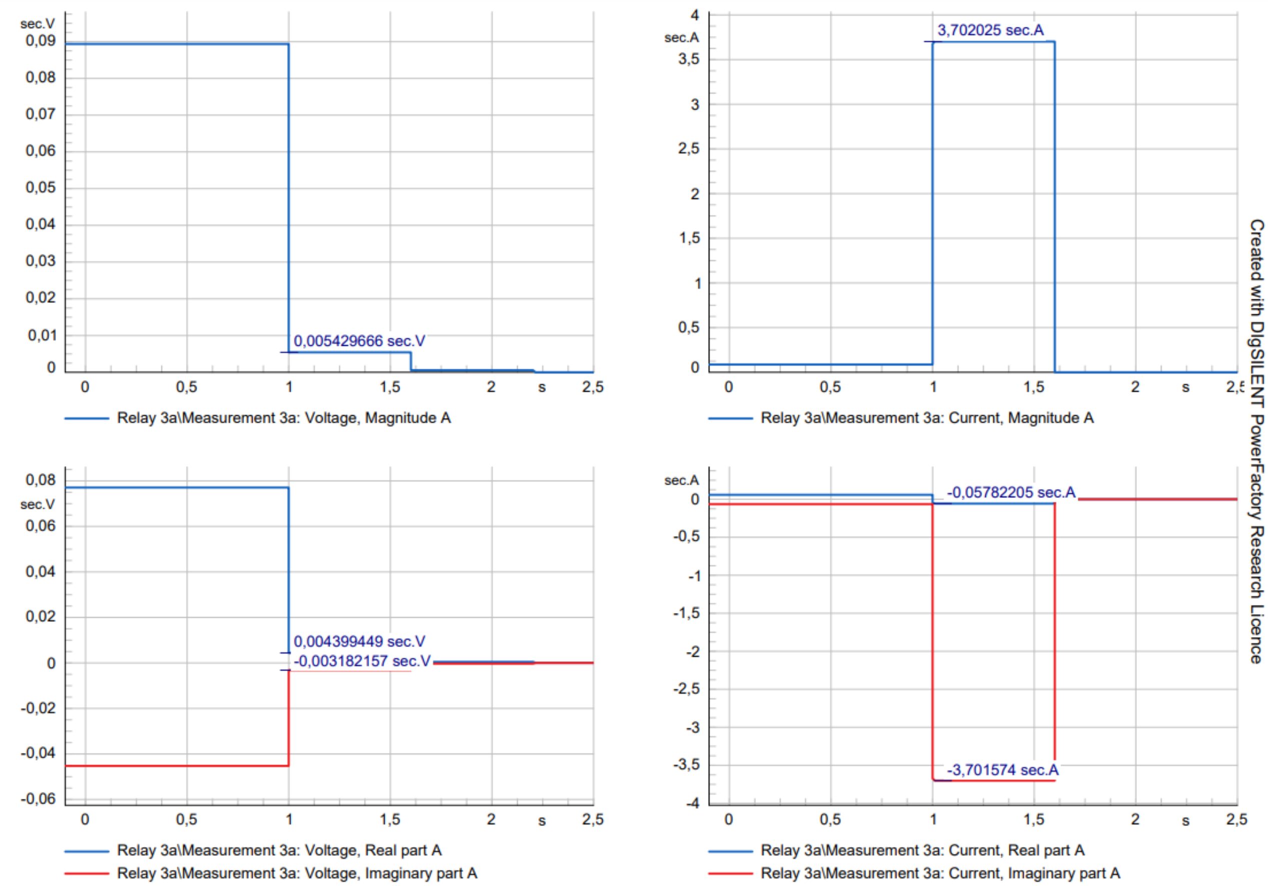


Figure 29. Visualization of real and imaginary components of current and voltage during fault conditions, captured using PowerFactory measurement tools

Table 18. Impedance and Derived Parameters for Relay 3a in the Base Case (Without PV Generation)

| **Case** | **Voltage Magnitude ($U_{mag}$, V)** | **Current Magnitude ($I_{mag}$, A)** | **Voltage Angle ($\theta_U$, °)** | **Current Angle (θI, °)** | **Impedance Magnitude ($Z_{mag}$, Ω)** | **Impedance Angle (θz, °)** | **Resistance (R, Ω)** | **Reactance (X, Ω)** |
|---|---|---|---|---|---|---|---|---|
| **Case1** | 710 | 1100.2 | -39.62 | -94.64 | 0.6452 | 55.0165 | 0.37 | 0.5287 |

Following the same methodology, relay 5a was analyzed under the base case conditions. A three-phase balanced fault was applied on line 6-7 at 20% of the distance from bus 6. Relays 6a and 6b were disabled to isolate the behavior of relay 5a and ensure its proper Zone 3 operation. Using the measurement tools in PowerFactory, the impedance values, resistance, reactance, and trip times for relay 5a were recorded and analyzed. The results are presented in Table 19.

Table 19. Impedance and Derived Parameters for Relay 5a in the Base Case (Without PV Generation)

| Case | Voltage Magnitude ($U_{mag}$, V) | Current Magnitude ($I_{mag}$, A) | Voltage Angle ($\theta_U$, °) | Current Angle ($\theta I$, °) | Impedance Magnitude ($Z_{mag}$, Ω) | Impedance Angle ($\theta z$, °) | Resistance (R, Ω) | Reactance (X, Ω) |
|---|---|---|---|---|---|---|---|---|
| **Case1** | 915.31 | 604.72 | -39.16 | -94.18 | 1.5136 | 55.0174 | 0.867 | 1.2401 |

For the base case scenario, relay 9a was analyzed under traditional grid conditions without PV generation. A three-phase balanced fault was applied on line 8-9, 20% from bus 8. To isolate the behavior of relay 9a, relays 8a and 8b were disabled to prevent premature tripping. The focus was on evaluating relay 9a's performance within Zone 3.

Using the measurement tools in PowerFactory, the real and imaginary components of current and voltage were captured during the simulation. These values were used to calculate the impedance magnitude and angle, as well as the derived resistance and reactance values. The results for relay 9a are presented in Table 20.

Table 20. Impedance and Derived Parameters for Relay 9a in the Base Case (Without PV Generation)

| Case | Voltage Magnitude ($U_{mag}$, V) | Current Magnitude ($I_{mag}$, A) | Voltage Angle ($\theta_U$, °) | Current Angle ($\theta I$, °) | Impedance Magnitude ($Z_{mag}$, Ω) | Impedance Angle ($\theta z$, °) | Resistance (R, Ω) | Reactance (X, Ω) |
|---|---|---|---|---|---|---|---|---|
| **Case1** | 346.581 | 475.563 | -39.46 | -94.48 | 0.7288 | 55.0179 | 0.417 | 0.5971 |

The analysis of distance protection devices was restricted to the base case (Case 1) due to several challenges encountered during the simulation process in PowerFactory. The primary limitation was the inability to accurately implement the short-circuit contributions of PV generators under fault conditions. These limitations in representing realistic fault ride-through behavior of PV inverters, including voltage control and reactive power support during faults, hindered the ability to analyze their impact on distance protection devices.

As a result of these challenges, the presented results are limited to the base case (Case 1) without PV generation. This provides a benchmark for the behavior of the distance protection devices under traditional grid conditions, but it does not account for the potential impact of increasing PV penetration on relay performance.

### 6.3. Built-In Model Limitations

The limitations of the built-in DSL model for photovoltaic (PV) systems in PowerFactory arise primarily from its inability to accurately simulate fault conditions and their impact on grid protection. Key issues include the deactivation of PV contributions during faults and unreliable outputs from critical measurement blocks. These limitations compromise the applicability of the model for relay protection studies, which require precise fault current data.

The first limitation is related to the “Protection” block in the model. During faults, this block deactivates the PV system, entirely removing its fault current contribution from the simulation. While this behavior might be adequate for generation studies, it renders the model unsuitable for protection studies that aim to analyze how PV systems interact with relays during faults. Disabling the “Protection” block allows the PV system to remain active, but this introduces a second limitation: the outputs from the “Power Measurement” block become inconsistent. This block, responsible for determining PV contributions, produces unreliable results under fault conditions, introducing uncertainty into the fault current data and relay behavior analysis.

To illustrate these issues, the Figure 30 below shows the internal structure of the PowerFactory DSL model for PV systems. Key components, such as the “Protection” block and “Power Measurement” block, are highlighted to emphasize their role in creating the limitations observed. The “Protection” block, when active, cuts off the PV system during faults, effectively excluding it from contributing to fault studies. On the other hand, the “Power Measurement” block, which remains operational when the “Protection” block is disabled, generates inaccurate outputs, particularly during transient conditions.

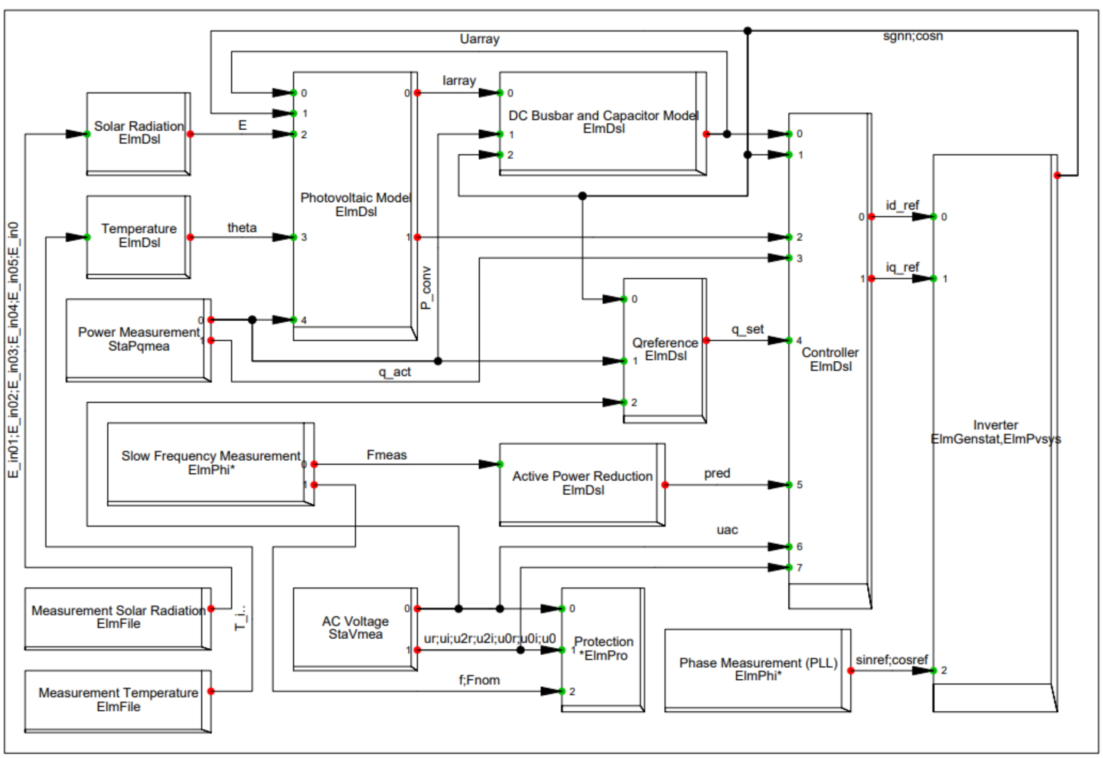


Figure 30. Internal Structure of the Built-In PowerFactory DSL Model for PV Systems [28]

This figure underscores the current model’s focus on steady-state operations rather than dynamic fault behavior, further limiting its suitability for protection analysis. The inability to simulate fault ride-through, dynamic fault contributions, and their timing hinders its use in modern protection studies. These limitations highlight the need for the development of enhanced models that accurately reflect PV behavior during faults, allowing for more reliable relay protection simulations.

## 6.4. Simplified PV Inverter Model

### 6.4.1. Model Description

To address the limitations observed in existing PV models, a new, simplified control model for the PV inverter was developed. This model aims to better represent the fault current contributions of PV systems during grid disturbances. The PV inverter is modeled as an AC Current Source, as depicted in Figure 31. This simplified approach allows for more direct control over the current contributions during fault simulations, providing flexibility and adaptability in the analysis.

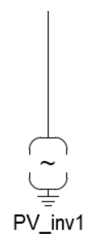


Figure 31. The PV inverter modeled as an AC Current Source [28]

The control frame of the new model is shown in Figure 32 and is composed of several key components :

- PV_inverter Block: This block is attributed to the AC Current Source net element and serves as the central element for defining the inverter’s current output.
- PV_curr_setpoint Block: This block is linked to the PV_inverter1_setpoint and is responsible for setting the current contribution manually. This functionality enables the user to define the specific current magnitude the PV inverter contributes during fault conditions.
- Voltmes Block: Attributed to PV1_termin_voltmes, this block captures voltage measurements, providing essential input for future enhancements to the model.
- Relay_trip Block: This block ensures coordination with the protective relays and facilitates interaction between the PV system and the grid’s protection mechanisms.

Figure 33 illustrates the graphical representation of the PV controller frame, showcasing the interaction between the above-mentioned blocks. Each block is designed to operate in a simplified yet effective manner, focusing on fault current contributions.

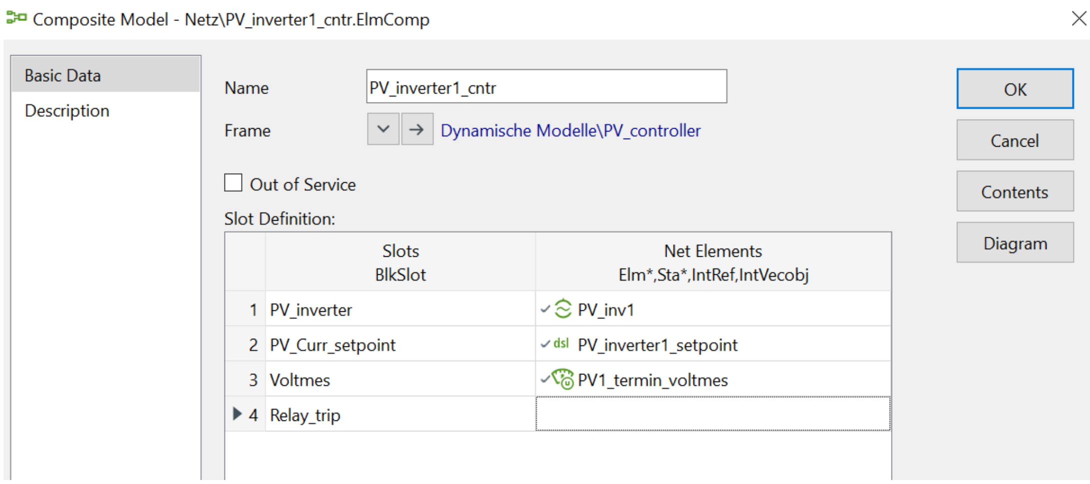


Figure 32. The controller of the PV inverter

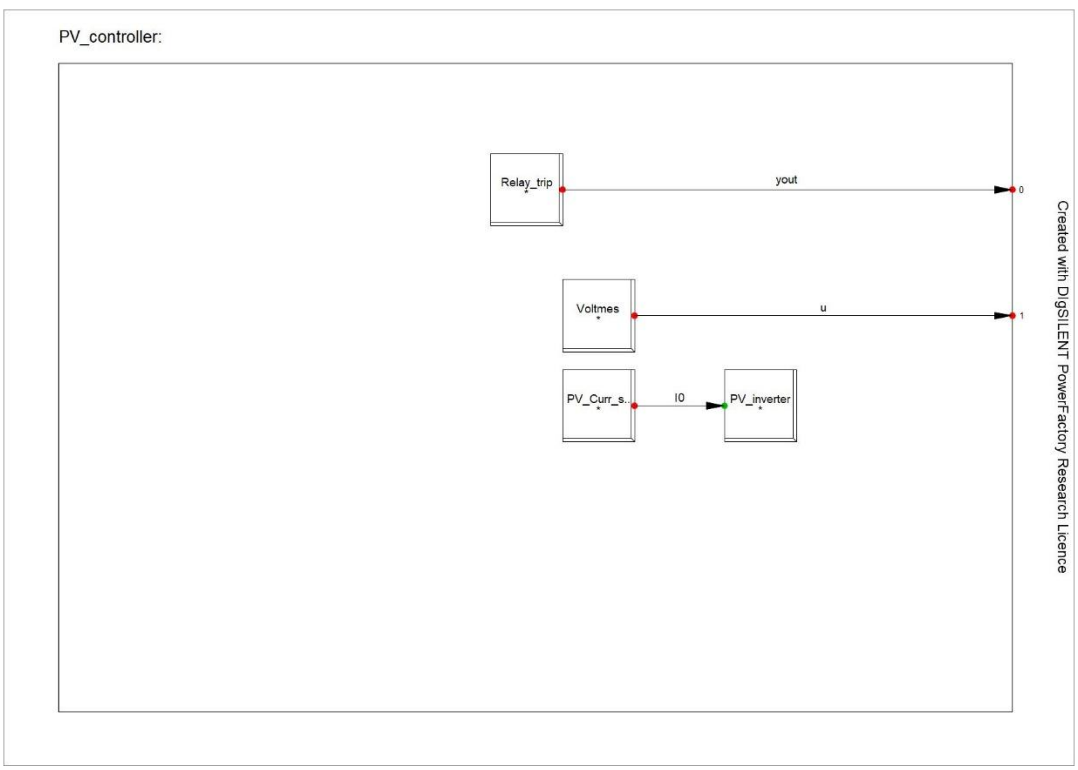


Figure 33. The control frame diagram of the PV inverter

The current model is designed to allow manual input for the current setpoint. This feature provides flexibility but also highlights areas for future improvement. Specifically, automating the current setpoint based on dynamic grid conditions is a critical next step. Additionally, the model does not yet consider the voltage measurement reference for busbar voltage limits. Incorporating this functionality will enable the PV inverter to cut off production when voltage exceeds predefined thresholds, enhancing the model's accuracy and realism.

This simplified control model serves as a foundational step towards developing a robust and adaptable PV inverter model. Its modular design and flexibility make it an ideal candidate for further refinement and integration into comprehensive protection studies.

### 6.4.2. Testing Framework

To evaluate the performance of the protection devices and analyze the impact of PV generation, a simplified grid model was designed (Figure 34). The grid consists of an external grid, three buses, three lines, and one PV inverter model utilizing the simplified DSL control framework developed in this study. This grid configuration was intentionally kept simple to isolate and clearly understand the influence of PV generation on the behavior of protection devices under the newly created PV model.

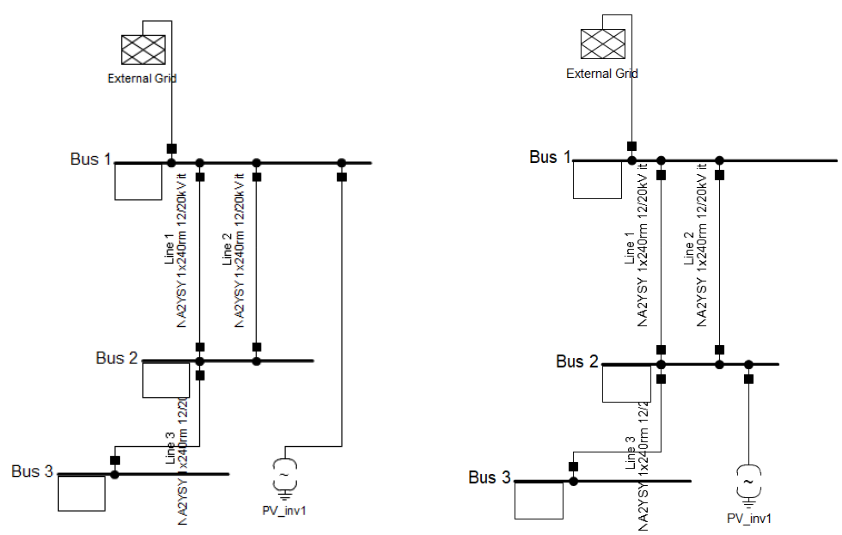


Figure 34. The grid model designed to test the PV inverter for a) upstream connection and b) downstream connection

The grid was equipped with the following protection devices:

- Distance Protection: A distance protection relay, identical to the one used in previous simulations, was installed on Line 1.

- Overcurrent Protection: An overcurrent protection relay, configured as per the models described in earlier sections of this thesis, was installed on Line 2.
- The PV inverter in the grid was modeled using the newly developed DSL control framework, where the current contribution of the PV inverter during faults was manually adjusted to test its impact under various scenarios.

The testing methodology involved varying the current setpoint of the PV inverter and observing the behavior of the protection devices. The simulations were structured to investigate the impact of PV placement on both distance and overcurrent protection. Two specific cases were defined based on the placement of the PV inverter:

- Upstream Case: The PV inverter was placed at Bus 1, closer to the external grid.
- Downstream Case: The PV inverter was placed at Bus 2, farther from the external grid.

For both protection schemes, three-phase balanced faults were applied to evaluate the performance of the relays:

- Distance Protection: Faults were introduced on Line 3, located 20% from Bus 3. The upstream and downstream cases were compared to examine how the PV's position influenced the relay's impedance calculations and fault detection capabilities.
- Overcurrent Protection: Faults were implemented on Line 2, at 50% of the line length. The current contributions from the PV inverter were varied, and the relay's tripping time and coordination were analyzed under both upstream and downstream placements.

The simulation cases were designed to vary the PV inverter's current setpoint incrementally to evaluate its contribution to fault scenarios. Seven cases were defined, as shown in Table 21:

Table 21. PV Inverter Current Setpoints for Fault Simulation Cases

| Case | Ipv [kA] |
|---|---|
| Case 1 | 0 |
| Case 2 | 1 |
| Case 3 | 2 |
| Case 4 | 4 |
| Case 5 | 8 |
| Case 6 | 16 |
| Case 7 | 20.9 |

### 6.5. Results from the Simplified PV Model

#### 6.5.1. Downstream Placement – Distance Protection

The downstream placement of the PV inverter at Bus 2 was analyzed to evaluate its impact on the distance protection relay by varying the PV inverter's current setpoint (Ipv) across seven cases, ranging from no contribution (Ipv=0) to a maximum of Ipv=20.9 kA. The results, summarized in Table 22, showed that the impedance values increased with higher PV current contributions, starting at 0.0005795 Ω for Ipv=0 and reaching 0006207Ω at Ipv=20.9 kA. This trend indicates a reduced fault current contribution from the external grid as the PV inverter injected more current during faults. Similarly, the impedance angle decreased from 40.39∘ to 38.49∘, reflecting a shift in the phase relationship between voltage and current with increasing PV penetration. The resistance and reactance components followed similar trends, as shown in the R-X plane (Figure 35b), with resistance rising from 0.0004414Ω to 0.0004858Ω, and reactance increasing from 0.0003755Ω to 0.0003863Ω. These changes highlight the influence of PV contribution on fault path characteristics, transitioning toward a more resistive-dominant nature. However, when the PV contribution exceeded 20.9 kA, the distance protection relay failed to react, underlining the significant impact of high PV penetration on relay performance. The graphical representations in Figures 35a and 35b further illustrate these trends, with the impedance plot showing a clear increase across cases and the R-X plane providing insight into the proportional changes in resistance and reactance.

Table 22. Distance Protection Relay Impedance, Angle, Resistance, and Reactance for Downstream PV Placement

| Ipv [kA] | Impedance (Ohm) | Impedance Angle (Degrees) | Resistance (Ohm) | Reactance (Ohm) |
|---|---|---|---|---|
| 0.00 | 0.0005795079 | 40.3940 | 0.00044136 | 0.00037554 |
| 1.00 | 0.0005812661 | 40.3056 | 0.00044328 | 0.00037600 |
| 2.00 | 0.0005834737 | 40.2220 | 0.00044551 | 0.00037678 |
| 4.00 | 0.0005872120 | 40.0411 | 0.00044956 | 0.00037778 |
| 8.00 | 0.0005948903 | 39.6701 | 0.00045791 | 0.00037976 |
| 16.00 | 0.0006107874 | 38.9026 | 0.00047532 | 0.00038357 |
| 20.90 | 0.0006206934 | 38.4894 | 0.00048583 | 0.00038630 |

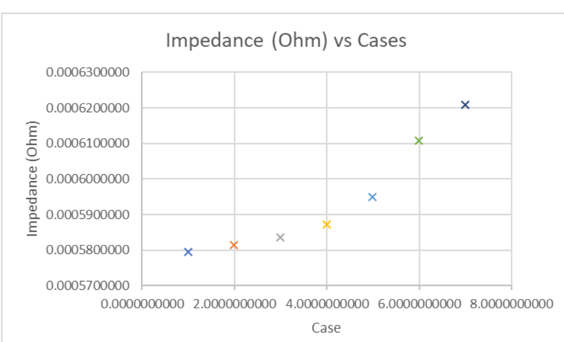


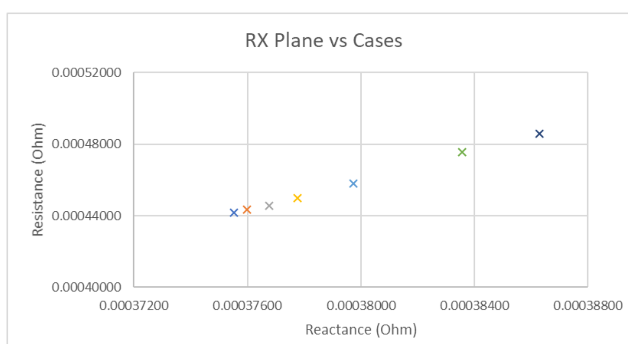


Figure 35. a) Impedance Magnitude vs. PV Current Contribution (Downstream PV Placement); b)Resistance and Reactance Trends (R-X Plane) for Downstream PV Placement

### 6.5.2. Upstream Placement – Distance Protection

To analyze the impact of the PV inverter placement upstream, the PV model was positioned at Bus 1, closer to the external grid. The results for the upstream placement of the PV inverter are presented in Table XX. The table summarizes key parameters, including the external grid current, short-circuit current (Isc), tripping time of the distance protection (DS trip), voltage and current measurements, and the computed impedance, resistance, and reactance. The results demonstrate that increasing the PV inverter's current setpoint results in slight variations in the external grid current. For example, as the PV current (Ipv) increases from 0 kA to 20.9 kA, the external grid current decreases from 58.531 kA to 50.995 kA. This indicates a reduction in the external grid's contribution to the fault current, with the PV inverter sharing a larger proportion of the fault current as its setpoint increases. The short-circuit current (Isc) at the fault location increases proportionally to the PV contribution, ranging from 58.531 kA to 67.815 kA. The impedance values show minor fluctuations, remaining around 0.000579Ω, as shown in the Impedance vs. Cases plot (Figure 36a). This indicates that the upstream PV placement does not substantially affect the apparent impedance seen by the relay. Similarly, the R-X plane plot (Figure 36b) confirms that the resistance and reactance values remain stable across all cases, with negligible variations in their magnitudes. This stability reflects the limited impact of upstream PV placement on the impedance characteristics of the faulted line.

Table 23. Distance Protection Relay Impedance, Angle, Resistance, and Reactance for Upstream PV Placement

| Ipv [kA] | Impedance (Ohm) | Impedance Angle (Degrees) | Resistance (Ohm) | Reactance (Ohm) |
|---|---|---|---|---|
| 0.00 | 0.00057951 | 40.3940 | 0.00044136 | 0.00037554 |
| 1.00 | 0.00057945 | 40.3932 | 0.00044132 | 0.00037550 |
| 2.00 | 0.00057968 | 40.4048 | 0.00044142 | 0.00037574 |
| 4.00 | 0.00057934 | 40.3948 | 0.00044123 | 0.00037544 |
| 8.00 | 0.00057960 | 40.4004 | 0.00044139 | 0.00037566 |
| 16.00 | 0.00057811 | 40.4765 | 0.00043975 | 0.00037527 |
| 20.90 | 0.00057947 | 40.3938 | 0.00044133 | 0.00037552 |

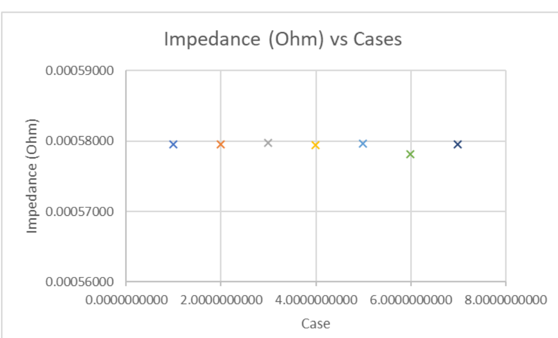

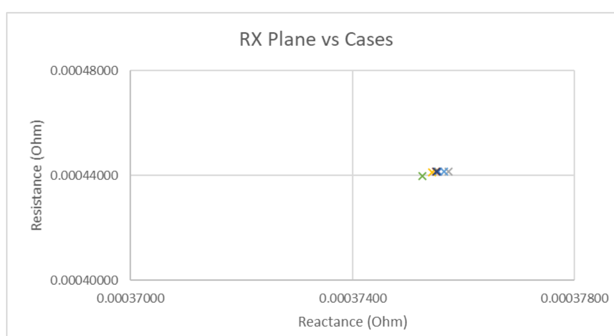


Figure 36. a) Impedance Magnitude vs. PV Current Contribution (Upstream PV Placement); b)Resistance and Reactance Trends (R-X Plane) for Upstream PV Placement

### 6.5.3. Downstream Placement – Overcurrent Protection

In the downstream PV case for overcurrent protection, the relationship between the fault current (Isc) and the tripping time of the overcurrent relay (OCtrip) was evaluated. The results are summarized in Table 24 and visually represented in Figures 37 a) and b). The analysis explores the impact of increasing PV current setpoints on the relay's performance during three-phase faults. The table demonstrates that as the PV current (Ipv) increases, there is a notable rise in the fault current (Isc). This increase in fault current correlates with a significant reduction in the relay's tripping time. For instance, at Ipv=0.00 kA, the fault current is 58.531 kA, and the relay's tripping time is 1.191731 seconds. As the PV contribution increases to Ipv=20.90 kA, the fault current rises to 75.488 kA, while the tripping time reduces to 0.102295 seconds. Figures 37a and 37b illustrate these relationships. The graph of Isc versus cases (Figure 37a) shows a clear upward trend, indicating that the PV inverter contributes significantly to the fault current as the setpoint increases. Conversely, the graph of OCtrip versus cases (Figure 37b) highlights the corresponding rapid decline in tripping time, emphasizing the heightened sensitivity of the relay under higher fault current conditions.

Table 24. Fault current magnitudes (Isc) and overcurrent relay trip times (OCtrip) for downstream PV placement with varying PV current setpoints (Ipv)

| Ipv [kA] | Isc [kA] | OC trip [s] |
|---|---|---|
| 0.00 | 58.531 | 1.191731 |
| 1.00 | 59.318 | 1.191667 |
| 2.00 | 60.106 | 1.191667 |
| 4.00 | 61.693 | 1.063317 |
| 8.00 | 64.901 | 0.102924 |
| 16.00 | 71.429 | 0.102295 |
| 20.90 | 75.488 | 0.102295 |

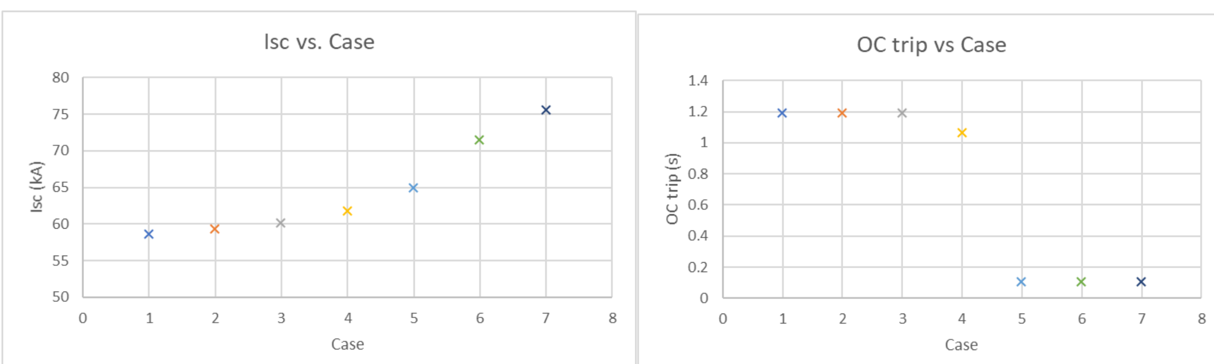


Figure 37. Relationship between PV current setpoints and overcurrent protection performance for downstream PV placement : (a) Fault current magnitudes (Isc) versus cases and (b) Overcurrent relay trip times (OCtrip) versus cases.

### 6.5.4. Upstream Placement – Overcurrent Protection

The upstream placement of the PV inverter, located at Bus 1, demonstrated notable impacts on fault current contributions and relay trip times. As shown in Table 25, the short-circuit current (Isc) progressively decreased as the PV current contribution (Ipv) increased. For the highest PV contribution (Case 8, Ipv=40 kA), the short-circuit current reduced significantly to 35.471 kA compared to 50.866 kA when Ipv=0 kA. This reduction highlights the inverse relationship between PV current contribution and fault current from the external grid in upstream configurations. Despite these changes in Isc, the overcurrent relay's trip time (OC trip) remained nearly constant across all cases, varying only slightly from 1.191701 seconds to 1.191716 seconds. The minimal variance in trip times suggests that the upstream PV contribution had a negligible effect on the overcurrent relay's operational performance. The graphs in Figures 38a and 38b illustrate these findings, with Figure 38a showing the steady decrease in Isc and Figure 38b highlighting the almost unchanged OC trip times.

Table 25. Fault current magnitudes (Isc) and overcurrent relay trip times (OCtrip) for downstream PV placement with varying PV current setpoints (Ipv).

| Ipv [kA] | Isc [kA] | OC trip [s] |
|---|---|---|
| 0.00 | 50.866 | 1.191701 |
| 1.00 | 50.481 | 1.191701 |
| 2.00 | 50.095 | 1.191702 |
| 4.00 | 49.324 | 1.191702 |
| 8.00 | 47.782 | 1.191703 |
| 16.00 | 44.699 | 1.191706 |
| 20.90 | 42.812 | 1.191708 |
| 40.00 | 35.471 | 1.191716 |

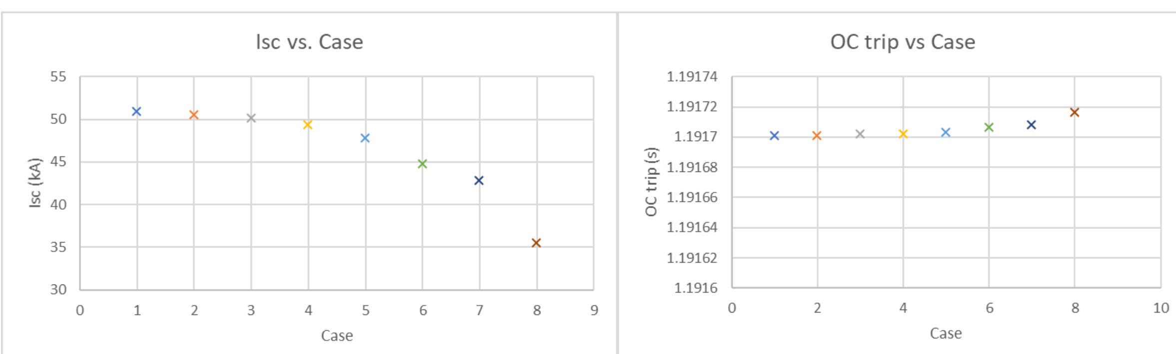


Figure 38. Relationship between PV current setpoints and overcurrent protection performance for downstream PV placement : (a) Fault current magnitudes (Isc) versus cases and (b) Overcurrent relay trip times (OCtrip) versus cases.

# 7. Discussion

This section discusses the results obtained from the analysis of overcurrent and distance protection under various scenarios, focusing on the base case and the challenges encountered during the simulations, and the insights gained from the newly developed PV model.

### 7.1. Discussion on Overcurrent Protection Results

In the base case scenario (Section 6.1.1), without PV generation, the short-circuit current magnitude exhibited a clear dependency on the fault location. Fault currents decreased as the fault location moved farther from the relay, corresponding to an increase in the line impedance. This behavior is expected in overcurrent protection systems and reflects the inverse time characteristic of relays, ensuring selective fault clearing and proper coordination. For instance, on line 13-14, faults closer to the relay resulted in higher fault currents and shorter trip times, while faults at greater distances showed reduced currents and delayed tripping (Table 8 and Figure 22). These observations establish a benchmark for evaluating the impact of PV integration.

The introduction of PV generation (Section 6.1.2) demonstrated how fault currents and relay behavior are influenced by distributed generation. With PV generation at Bus 12, the short-circuit current increased at most fault locations due to the additional current contribution from the PV inverter. However, at the relay's closest fault location (0%), a slight decrease in current was observed. This highlights the shifting reliance on local PV generation versus the external grid for fault current supply. The tripping time of relay OC1a decreased for closer faults but increased for faults farther from the relay, illustrating the complex interplay between PV contribution and relay response.

When faults were simulated on line 13-14 with PV at Bus 12, a similar pattern emerged. Fault currents increased consistently across all fault locations, reflecting the local support provided by the PV inverter. Relay trip times followed this trend, with slight delays observed for distant faults. These findings underscore the need for adaptive relay settings to account for the redistributed fault currents in PV-integrated grids.

Using the new PV model, further insights were revealed, particularly for downstream PV placement (Section 6.5.3). As the PV current setpoint (Ipv) increased from 0 to 20.9 kA, the fault current rose significantly by 28.97%. This increase reduced the overcurrent relay's tripping time by 91.42%, from 1.191731 seconds to 0.102295 seconds. While this enhanced relay responsiveness is advantageous for fault clearance, it raises concerns about coordination with upstream relays and system stability. The downstream placement highlights the potential challenges of integrating high PV penetration in grids.

Conversely, the upstream PV placement demonstrated a contrasting effect. Increasing the PV current contribution to 40 kA reduced the fault current by 30.27%, indicating a diminished reliance on the external grid. Despite this reduction, the relay trip time remained nearly constant, varying only by 0.001%. This stability suggests that the upstream placement of PV inverters may pose fewer challenges to relay coordination, offering a more predictable fault response.

## 7.2. Discussion on Distance Protection Results

The analysis of distance protection devices focused on evaluating their performance under the base case scenario without PV generation. This provided a benchmark for relay behavior under traditional grid conditions, allowing for a detailed examination of impedance characteristics, resistance, and reactance values.

The base case analysis (Section 6.2.1) provided critical benchmarks for distance protection relays under traditional grid conditions. Relays 3a, 5a, and 9a demonstrated proper operation within Zone 3 for balanced three-phase faults, with impedance, resistance, and reactance values aligning with design expectations. These results validated the reliability of distance protection devices in clearing faults under steady-state grid conditions.

The downstream PV placement (Section 6.5.2) revealed significant changes in relay behavior. As the PV current setpoint increased, the impedance progressively rose from 0.0005795 Ω to 0.0006207 Ω. This increase corresponds to a reduced fault current contribution from the external grid, with the PV inverter injecting a greater proportion of the current. The impedance angle decreased from 40.39° to 38.49°, reflecting a shift in the phase relationship between voltage and current as PV penetration grew. Resistance and reactance values increased proportionally, suggesting a transition toward a more resistive fault path. However, when the PV current exceeded 20.9 kA, the relay failed to respond, exposing its limitations in adapting to high PV penetration scenarios. This behavior is visualized in Figure 39, which illustrates the RX plane. For a PV current of 21 kA, the fault impedance falls outside the relay's third zone, clearly indicating why the relay fails to react. This underscores the need for advanced relay settings or adaptive schemes to ensure reliable fault detection in PV-dominated grids.

In the upstream PV placement scenario, the results highlighted the limited impact on distance protection. Impedance values remained consistent, with negligible fluctuations, and the impedance angle showed no variation. Despite a 15.88% increase in short-circuit current at the fault location, the relay maintained stable performance, with resistance and reactance values exhibiting minimal changes. These findings suggest that upstream PV placement exerts less influence on distance protection, making it a more predictable configuration for grid operators.

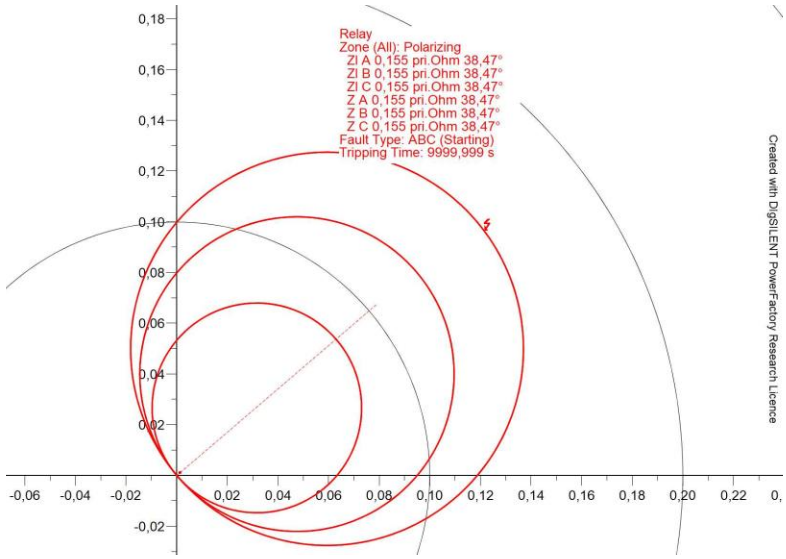


Figure 39. RX Plane Representation for a PV Current of 21 kA

## 7.3. Future Work

This thesis investigates the challenges posed by the increased integration of PV generation on traditional protection schemes, focusing on overcurrent and distance protection. The findings underscore the limitations of existing models and protection strategies under current grid conditions dominated by grid-following inverters. The research also explores a novel PV model designed to address the deficiencies of traditional DSL models, providing new insights into fault current contributions and relay behavior under varying PV placements. While this model provides valuable insights into fault current contributions and relay behavior under varying PV placements, its simplicity highlights the need for further improvement to accurately capture the dynamic and transient behavior of PV systems. These findings lay the groundwork for further research into the evolving dynamics of modern grids, particularly with the transition to grid-forming inverters.

In the context of overcurrent protection, this study identified the need for more accurate modeling of PV generators during fault conditions. Advanced models must capture the transient behavior of PV inverters, including their fault ride-through capabilities, voltage regulation, and reactive power support. These improvements will enable more realistic simulations, particularly under RMS conditions, and help evaluate the impacts of increasing PV penetration on fault currents and relay performance.

Additionally, the fault current results for overcurrent protection raised questions about the behavior of CTs under high fault current scenarios. Studies like [29] have indicated that CT saturation can significantly affect fault current measurements and relay operations. Future research should investigate the proper sizing and modeling of CTs in systems with high PV penetration to ensure accurate relay performance and reliable fault clearance.

For distance protection, the inability of the built-in PV models in PowerFactory to adequately account for PV contributions during faults highlights the need for further exploration. The new PV model developed in this study revealed that downstream PV placement significantly influences impedance characteristics, often rendering traditional relay settings ineffective under high PV penetration. Future work should prioritize the development of more detailed and complex PV models with enhanced control mechanisms to accurately capture PV behavior during faults. These refined models would enable relay engineers to better simulate and analyze fault scenarios in PowerFactory, ensuring more reliable relay settings and improved fault detection in PV-dominated grids.

Beyond the limitations identified in this study, there is a need to diversify fault scenarios to include a broader range of fault types, such as line-to-line and single-phase-to-ground faults. Earth fault simulations, in particular, are a key area for improvement, as existing tools like PowerFactory have limitations in accurately representing these fault types. [30]

The challenges posed by renewable integration also necessitate exploring advanced protection strategies. This study [31] summarizes some proposed solutions as listed on table 21:

Table 26. Scenarios, Effects, and Proposed Solutions for Addressing Protection Challenges in PV-Integrated Power Systems [31]

| Scenario Type | Effect | Proposed Solution |
|---|---|---|
| **Upstream Fault** | Unintentional tripping of feeders where PV is connected during upstream faults. | Overcurrent protection with communication link to PV units. |
| **Downstream, Low Fault Current Contribution** | Loss of overcurrent coordination, longer tripping times, under voltage, eventual islanding of PV units, frequency excursions. | Undervoltage protection, Rate-of-Change-of-Frequency protection. |
| **Downstream, High Fault Current Contribution** | Non-operation of overcurrent protection and undervoltage during downstream faults. | Improved undervoltage protection schemes. |

Furthermore, the deployment of PMUs as suggested by [32] offers promising opportunities for adaptive protection schemes. PMUs provide real-time, high-resolution data that enhance the accuracy of fault detection and relay operation. They can help distinguish power swings from faults, estimate impedance trajectories, and improve the coordination of distance and overcurrent protection. PMU-based protection strategies, supported by robust communication infrastructure, have been shown to improve fault location and enhance relay performance, even in systems with high levels of DERs. Future studies should focus on the integration of PMUs with adaptive protection schemes, leveraging protocols like IEC 61850 and IEEE C37.118 for efficient data exchange. [32]

# 8. Conclusion

This thesis investigated the challenges and behavior of overcurrent and distance protection schemes in medium-voltage grids with high levels of photovoltaic (PV) generation. Using detailed simulations in PowerFactory, various scenarios were analyzed to explore the impact of PV integration on protection coordination, fault current contributions, and relay operation. The research also introduced a novel, simplified PV model to address the limitations of traditional DSL models, providing new insights into PV behavior under fault conditions.

For overcurrent protection, the results confirmed that increasing PV penetration alters fault current distribution, significantly impacting relay operation and coordination. In downstream configurations, higher PV contributions were observed to accelerate relay tripping for nearby faults but delay tripping for distant faults, posing potential challenges for system reliability. The simplified PV model demonstrated the critical influence of PV current setpoints on fault currents and relay trip times, highlighting the need for adaptive protection schemes to maintain coordination.

In the case of distance protection, the study revealed distinct trends in impedance, resistance, and reactance with varying PV placements. Downstream PV placement led to notable changes in fault path characteristics, transitioning toward a more resistive-dominant nature. However, when PV contributions exceeded a threshold, the distance relay failed to operate, exposing the limitations of traditional protection schemes. Upstream PV placement had a minimal impact on relay performance, underscoring the resilience of existing distance protection setups in such scenarios.

The newly developed PV model, while providing valuable insights, is acknowledged as a basic representation. It lacks the ability to simulate dynamic and transient fault behavior fully. Future improvements are needed to incorporate features like voltage regulation, reactive power support, and automated current setpoints to enhance the model's realism and applicability for protection studies.

This work also emphasized broader challenges, such as the need for accurate modeling of current transformer saturation, robust communication infrastructures, and the integration of advanced technologies like phasor measurement units (PMUs). These advancements are essential for developing adaptive protection schemes capable of addressing the evolving dynamics of grids with high PV penetration.

Ultimately, this thesis provides a foundational understanding of the complexities associated with protecting modern grids in the era of renewable energy integration. It highlights the gaps and proposes potential solutions, contributing to the ongoing efforts to ensure the stability, reliability, and resilience of future distribution networks, particularly as the energy transition accelerates toward grid-forming inverters.

# References


[1] E. Union, «DIRECTIVE (EU) 2018/2001 OF THE EUROPEAN PARLIAMENT AND OF THE COUNCIL,» *Official Journal of the European Union,* pp. 2-3, 2018.

[2] E. Union, December 2019. [En ligne]. Available: https://ec.europa.eu/commission/presscorner/detail/en/ip_19_6691.

[3] B. Federal Foreign Office, 2021. [En ligne]. Available: https://www.auswaertiges-amt.de/blob/610620/5d9bfec0ab35695b9db548d10c94e57d/the-german-energiewende-data.pdf.

[4] D. A. P. E. Thomas Leopold Berg, «Analysis of the wind energy market in Denmark and future interactions with an emerging hydrogen market,» *International Journal of Hydrogen Energy,* pp. 146-156, 2021.

[5] M. V. Andreev, M. A. Denisov et A. S. Gusev, «Impact of renewable energy sources on relay protection operation,» *AIP Conference Proceedings,* pp. 1-4, 2019.

[6] J. Das, Power System Protective Relaying Volume 4, New York: CRC Press, 2018.

[7] Schneider Electric, A1 Fundamentals of Protection Practice - Network Protection & Automation Guide.

[8] M. Doyle, «Reviewing the impacts of distributed generation on distribution system protection,» *IEEE Power Engineering Society Summer Meeting,* pp. 103-105, 2002.

[9] T. J. D. J. Lewis Blackburn, Protective Relaying - Principles and Applications, New York: CRC Press , 2014.

[10] M. Comech, «Overcurrent Protection,» chez *Lecture: Protection System in Smart Grids*, 2024, Universidad de Zaragoza.

[11] P. Anderson, Power System Protection, New York: IEEE Press, 1999.

[12] E. J. H. Juan M. Gers, Protection of Electricity Distribution Networks 3rd Edition, London: The Institution of Engineering and Technology, 2011.

[13] J. K. B. Keller, «Understanding Fault Characteristics of Inverter Based Distributed Energy Resources,» *National Renewable Energy Laboratory,* 2010.

[14] IEEE , «IEEE recommended practice for electric power distribution for industrial plants,» *IEEE Std 141-1993,* pp. 109-184, 1994.

[15] IEEE, «IEEE Recommended practice for utility interface of photovoltaic (PV) systems,» *IEEE 929,* 2000.

[16] A. D. I. G. Matin Meskin, «Impact of distributed generation on the protection systems of distribution networks: analysis and remedies - review paper,» *IET Generation, Transmission and Distribution,* pp. 5944-5960, 2020.

[17] A. S. George S.P., «Multiagent based adaptive relaying for distribution network with distributed generation,» *Int. Conf. on Energy, Power and Environment Towards Sustainable Growth (ICEPE),* pp. 1-6, 2015.

[18] M. Meskin, I. Grinberg et A. Domijan, «Impact of distributed generation on the protection systems of distribution networks: analysis and remedies – review paper,» *IET Generation,Transmission & Distribution,* 2020.

[19] K. Kauhaniemi et L. Kumpulainen, «Impact of distributed generation on the protection of distribution networks,» *Eighth IEE Int. Conf. on Developments in Power System Protection,,* pp. 315-318, 2004.

[20] F. Dai, «Impacts of distributed generation on protection and autoreclosing of distribution networks,» *10th IET Int. Conf. on Developments in Power System Protection (DPSP),* pp. 1-5, 2010.

[21] O. R. et J. Yang, «Impacts of distributed generation on low-voltage distribution network protection,» *50th Int. Universities Power Engineering Conf. (UPEC),* pp. 1-6, 2015.

[22] F. Hariri et M. Crow, «New Infeed Correction Methods for Distance Protection in Distribution Systems,» *MDPI Energies,* 2021.

[23] J. Ma, J. Li et W. Z., «An adaptive distance protection scheme for distribution system with distributed generation,» *IEEE,* 2010.

[24] Cigre, «Benchmark Systems for Network Integration of Renewable and Distributed Energy Resources,» April 2014. [En ligne]. Available: http://www.e-cigre.org/Order/select.asp?ID=16639.

[25] T. Tjaden, J. Bergner, J. Weniger et Q. V., Representative electrical load profiles for residential buildings in Germany on a 1-second data basis, Berlin: HTW Berlin - University of Applied Sciences Solar Storage - Systems Research Group.

[26] A. U. B. N. U. D. K. U. S. F. Sakarwala, «Multi Agent Control Based Energy Optimization Of A Prosumer Household And A Community With Bidirectional Electric Vehicles,» *16th International Renewable Energy Storage Conference,* n° %116, pp. 434-450, 2022.

[27] W. Schossig, «Netzschutz-Magazin,» September 2017. [En ligne]. Available: https://www.netzschutz-magazin.com/leitungsschutz/distanzschutz/reichweiten-und-staffelzeiten-grundsaetze/.

[28] DIGSILENT GMBH., «POWERFACTORY 2023: TECHNICAL REFERENCE – PHOTOVOLTAIC SYSTEM TEMPLATES,» GOMARINGEN, GERMANY, 2023.

[29] R. Kamel et H. Abdullah, «In the context of overcurrent protection, this study identified the need for more accurate modeling of PV generators during fault conditions. Advanced models must capture the transient behavior of PV inverters, including their fault ride-through capabilit,» *Journal of Engineering Research,* 2022.

[30] Z. Han, «Protection Coordintion in Networks with Renewable Energy Sources,» *Manchester Research Explorer,* 2014.

[31] L. Namangolwa et E. Begumisa, «Impacts of Solar Photovoltaic on the Protection System of Distribution Networks,» *Chalmers University of Technology,* 2016.

[32] J. Rishabh, Y. N.V., K. P. et M. B., «Modern trends in power system protection for distribution grid with high DER penetration,» *e-Prime - Advances in Electrical Engineering, Electronics and Energy,* 2022.

# Appendices

Appendix 1. Fault Current and Relay Operations for Various Fault Locations and PV Levels. Part 1

| Fault Location | PV (MW) | Fault current (kA) | Relay 1 | Trip Time 1 (s) | Relay 2 | Trip Time 2 (s) | Relay 3 | Trip Time 3 (s) | Relay 4 | Trip Time 4 (s) |
|---|---|---|---|---|---|---|---|---|---|---|
| L 2-3 | 0 | 2.163 | 2a | 0.02 | N/A | N/A | N/A | N/A | N/A | N/A |
| L 2-3 | 4.5 | 2.169 | 2a | 0.02 | N/A | N/A | N/A | N/A | N/A | N/A |
| L 2-3 | 45.5 | 2.212 | 2a | 0.02 | N/A | N/A | N/A | N/A | N/A | N/A |
| L 2-3 | 91 | 2.207 | 2a | 0.02 | N/A | N/A | N/A | N/A | N/A | N/A |
| L 2-3 | 104 | 2.081 | 2a | 0.02 | N/A | N/A | N/A | N/A | N/A | N/A |
| Bus 3 | 0 | 1.464 | 2a | 0.62 | N/A | N/A | N/A | N/A | N/A | N/A |
| Bus 3 | 4.5 | 1.468 | 2a | 0.62 | N/A | N/A | N/A | N/A | N/A | N/A |
| Bus 3 | 45.5 | 1.486 | 2a | 0.62 | N/A | N/A | N/A | N/A | N/A | N/A |
| Bus 3 | 91 | 1.445 | 2a | 0.62 | N/A | N/A | N/A | N/A | N/A | N/A |
| Bus 3 | 104 | 1.382 | 2a | 0.62 | N/A | N/A | N/A | N/A | N/A | N/A |
| L 3-4 | 0 | 1.446 | 3a | 0.02 | 3b | 0.32 | 2a | 0.62 | N/A | N/A |
| L 3-4 | 4.5 | 1.450 | 3a | 0.02 | 3b | 0.32 | 2a | 0.62 | N/A | N/A |
| L 3-4 | 45.5 | 1.467 | 3a | 0.02 | 3b | 0.32 | 2a | 0.62 | N/A | N/A |
| L 3-4 | 91 | 1.426 | 3a | 0.02 | 3b | 0.32 | 2a | 0.62 | N/A | N/A |
| L 3-4 | 104 | 1.363 | 3a | 0.02 | 3b | 0.32 | 2a | 0.62 | N/A | N/A |
| Bus 4 | 0 | 1.391 | 3a | 0.32 | 4b | 0.32 | 11b | 0.32 | N/A | N/A |
| Bus 4 | 4.5 | 1.395 | 3a | 0.32 | 4b | 0.32 | 11b | 0.32 | N/A | N/A |
| Bus 4 | 45.5 | 1.411 | 3a | 0.32 | 4b | 0.32 | 11b | 0.32 | N/A | N/A |
| Bus 4 | 91 | 1.368 | 3a | 0.32 | 4b | 0.32 | 11b | 0.32 | N/A | N/A |
| Bus 4 | 104 | 1.305 | 3a | 0.32 | 4b | 0.32 | 11b | 0.32 | N/A | N/A |
| L 4-5 | 0 | 1.378 | 4a | 0.02 | 4b | 0.32 | 3a | 0.62 | N/A | N/A |
| L 4-5 | 4.5 | 1.381 | 4a | 0.02 | 4b | 0.32 | 3a | 0.62 | N/A | N/A |
| L 4-5 | 45.5 | 1.397 | 4a | 0.02 | 4b | 0.32 | 3a | 0.62 | N/A | N/A |
| L 4-5 | 91 | 1.353 | 4a | 0.02 | 4b | 0.32 | 3a | 0.62 | N/A | N/A |
| L 4-5 | 104 | 1.291 | 4a | 0.02 | 4b | 0.32 | 3a | 0.62 | N/A | N/A |
| Bus 5 | 0 | 1.333 | 4a | 0.32 | 5b | 0.32 | N/A | N/A | N/A | N/A |
| Bus 5 | 4.5 | 1.336 | 4a | 0.32 | 5b | 0.32 | N/A | N/A | N/A | N/A |
| Bus 5 | 45.5 | 1.350 | 4a | 0.32 | 5b | 0.32 | N/A | N/A | N/A | N/A |
| Bus 5 | 91 | 1.306 | 4a | 0.32 | 5b | 0.32 | N/A | N/A | N/A | N/A |
| Bus 5 | 104 | 1.244 | 4a | 0.32 | 5b | 0.32 | N/A | N/A | N/A | N/A |
| L 5-6 | 0 | 1.309 | 5a | 0.02 | 5b | 0.32 | N/A | N/A | N/A | N/A |
| L 5-6 | 4.5 | 1.313 | 5a | 0.02 | 5b | 0.32 | N/A | N/A | N/A | N/A |
| L 5-6 | 45.5 | 1.326 | 5a | 0.02 | 5b | 0.32 | N/A | N/A | N/A | N/A |
| L 5-6 | 91 | 1.282 | 5a | 0.02 | 5b | 0.32 | N/A | N/A | N/A | N/A |
| L 5-6 | 104 | 1.220 | 5a | 0.02 | 5b | 0.32 | N/A | N/A | N/A | N/A |
| Bus 6 | 0 | 1.267 | 5a | 0.32 | 6b | 0.32 | 7b | 0.62 | N/A | N/A |
| Bus 6 | 4.5 | 1.271 | 5a | 0.32 | 6b | 0.32 | 7b | 0.62 | N/A | N/A |
| Bus 6 | 45.5 | 1.283 | 5a | 0.32 | 6b | 0.32 | 7b | 0.62 | N/A | N/A |
| Bus 6 | 91 | 1.238 | 5a | 0.32 | 6b | 0.32 | 7b | 0.62 | N/A | N/A |
| Bus 6 | 104 | 1.177 | 5a | 0.32 | 6b | 0.32 | 7b | 0.62 | N/A | N/A |
| L 6-7 | 0 | 1.268 | 6b | 0.02 | 6a | 0.32 | 7b | 0.32 | 5a | 0.62 |
| L 6-7 | 4.5 | 1.271 | 6b | 0.02 | 6a | 0.32 | 7b | 0.32 | 5a | 0.62 |
| L 6-7 | 45.5 | 1.283 | 6b | 0.02 | 6a | 0.32 | 7b | 0.32 | 5a | 0.62 |
| L 6-7 | 91 | 1.238 | 6b | 0.02 | 6a | 0.32 | 7b | 0.32 | 5a | 0.62 |
| L 6-7 | 104 | 1.177 | 6b | 0.02 | 6a | 0.32 | 7b | 0.32 | 5a | 0.62 |
| Bus 7 | 0 | 1.268 | 6a | 0.32 | 7b | 0.32 | 5a | 0.62 | N/A | N/A |
| Bus 7 | 4.5 | 1.271 | 6a | 0.32 | 7b | 0.32 | 5a | 0.62 | N/A | N/A |
| Bus 7 | 45.5 | 1.284 | 6a | 0.32 | 7b | 0.32 | 5a | 0.62 | N/A | N/A |
| Bus 7 | 91 | 1.234 | 6a | 0.32 | 7b | 0.32 | 5a | 0.62 | N/A | N/A |
| Bus 7 | 104 | 1.177 | 6a | 0.32 | 7b | 0.32 | 5a | 0.62 | N/A | N/A |

Appendix 2. Fault Current and Relay Operations for Various Fault Locations and PV Levels. Part 2

| Fault Location | PV (MW) | Fault current (kA) | Relay 1 | Trip Time 1 (s) | Relay 2 | Trip Time 2 (s) | Relay 3 | Trip Time 3 (s) | Relay 4 | Trip Time 4 (s) |
|---|---|---|---|---|---|---|---|---|---|---|
| L 7-8 | 0 | 1.323 | 7b | 0.02 | 7a | 0.32 | N/A | N/A | N/A | N/A |
| L 7-8 | 4.5 | 1.327 | 7b | 0.02 | 7a | 0.32 | N/A | N/A | N/A | N/A |
| L 7-8 | 45.5 | 1.341 | 7b | 0.02 | 7a | 0.32 | N/A | N/A | N/A | N/A |
| L 7-8 | 91 | 1.296 | 7b | 0.02 | 7a | 0.32 | N/A | N/A | N/A | N/A |
| L 7-8 | 104 | 1.234 | 7b | 0.02 | 7a | 0.32 | N/A | N/A | N/A | N/A |
| Bus 8 | 0 | 1.353 | 7a | 0.32 | 12a | 0.32 | N/A | N/A | N/A | N/A |
| Bus 8 | 4.5 | 1.357 | 7a | 0.32 | 12a | 0.32 | N/A | N/A | N/A | N/A |
| Bus 8 | 45.5 | 1.371 | 7a | 0.32 | 12a | 0.32 | N/A | N/A | N/A | N/A |
| Bus 8 | 91 | 1.327 | 7a | 0.32 | 12a | 0.32 | N/A | N/A | N/A | N/A |
| Bus 8 | 104 | 1.265 | 7a | 0.32 | 12a | 0.32 | N/A | N/A | N/A | N/A |
| L 8-9 | 0 | 1.341 | 8a | 0.02 | 8b | 0.32 | 12a | 0.32 | 9a | 0.62 |
| L 8-9 | 4.5 | 1.344 | 8a | 0.02 | 8b | 0.32 | 12a | 0.32 | 9a | 0.62 |
| L 8-9 | 45.5 | 1.358 | 8a | 0.02 | 8b | 0.32 | 12a | 0.32 | 9a | 0.62 |
| L 8-9 | 91 | 1.314 | 8a | 0.02 | 8b | 0.32 | 12a | 0.32 | 9a | 0.62 |
| L 8-9 | 104 | 1.252 | 8a | 0.02 | 8b | 0.32 | 12a | 0.32 | 9a | 0.62 |
| Bus 9 | 0 | 1.338 | 8b | 0.32 | 9a | 0.32 | N/A | N/A | N/A | N/A |
| Bus 9 | 4.5 | 1.342 | 8b | 0.32 | 9a | 0.32 | N/A | N/A | N/A | N/A |
| Bus 9 | 45.5 | 1.356 | 8b | 0.32 | 9a | 0.32 | N/A | N/A | N/A | N/A |
| Bus 9 | 91 | 1.312 | 8b | 0.32 | 9a | 0.32 | N/A | N/A | N/A | N/A |
| Bus 9 | 104 | 1.250 | 8b | 0.32 | 9a | 0.32 | N/A | N/A | N/A | N/A |
| L 9-10 | 0 | 1.333 | 9a | 0.02 | 9b | 0.32 | N/A | N/A | N/A | N/A |
| L 9-10 | 4.5 | 1.337 | 9a | 0.02 | 9b | 0.32 | N/A | N/A | N/A | N/A |
| L 9-10 | 45.5 | 1.351 | 9a | 0.02 | 9b | 0.32 | N/A | N/A | N/A | N/A |
| L 9-10 | 91 | 1.307 | 9a | 0.02 | 9b | 0.32 | N/A | N/A | N/A | N/A |
| L 9-10 | 104 | 1.245 | 9a | 0.02 | 9b | 0.32 | N/A | N/A | N/A | N/A |
| Bus 10 | 0 | 1.337 | 10a | 0.32 | 9b | 0.32 | N/A | N/A | N/A | N/A |
| Bus 10 | 4.5 | 1.341 | 10a | 0.32 | 9b | 0.32 | N/A | N/A | N/A | N/A |
| Bus 10 | 45.5 | 1.355 | 10a | 0.32 | 9b | 0.32 | N/A | N/A | N/A | N/A |
| Bus 10 | 91 | 1.311 | 10a | 0.32 | 9b | 0.32 | N/A | N/A | N/A | N/A |
| Bus 10 | 104 | 1.249 | 10a | 0.32 | 9b | 0.32 | N/A | N/A | N/A | N/A |
| L 10-11 | 0 | 1.348 | 10a | 0.02 | 10b | 0.32 | 11a | 0.62 | N/A | N/A |
| L 10-11 | 4.5 | 1.351 | 10a | 0.02 | 10b | 0.32 | 11a | 0.62 | N/A | N/A |
| L 10-11 | 45.5 | 1.366 | 10a | 0.02 | 10b | 0.32 | 11a | 0.62 | N/A | N/A |
| L 10-11 | 91 | 1.322 | 10a | 0.02 | 10b | 0.32 | 11a | 0.62 | N/A | N/A |
| L 10-11 | 104 | 1.260 | 10a | 0.02 | 10b | 0.32 | 11a | 0.62 | N/A | N/A |
| Bus 11 | 0 | 1.351 | 11a | 0.32 | 10b | 0.32 | N/A | N/A | N/A | N/A |
| Bus 11 | 4.5 | 1.355 | 11a | 0.32 | 10b | 0.32 | N/A | N/A | N/A | N/A |
| Bus 11 | 45.5 | 1.370 | 11a | 0.32 | 10b | 0.32 | N/A | N/A | N/A | N/A |
| Bus 11 | 91 | 1.326 | 11a | 0.32 | 10b | 0.32 | N/A | N/A | N/A | N/A |
| Bus 11 | 104 | 1.264 | 11a | 0.32 | 10b | 0.32 | N/A | N/A | N/A | N/A |
| LL 11-4 | 0 | 1.319 | 11a | 0.02 | 11b | 0.32 | 3a | 0.62 | N/A | N/A |
| LL 11-4 | 4.5 | 1.385 | 11a | 0.02 | 11b | 0.32 | 3a | 0.62 | N/A | N/A |
| LL 11-4 | 45.5 | 1.400 | 11a | 0.02 | 11b | 0.32 | 3a | 0.62 | N/A | N/A |
| LL 11-4 | 91 | 1.357 | 11a | 0.02 | 11b | 0.32 | 3a | 0.62 | N/A | N/A |
| LL 11-4 | 104 | 1.295 | 11a | 0.02 | 11b | 0.32 | 3a | 0.62 | N/A | N/A |
| L 3-8 | 0 | 1.362 | 12a | 0.02 | 12b | 0.02 | N/A | N/A | N/A | N/A |
| L 3-8 | 4.5 | 1.366 | 12a | 0.02 | 12b | 0.02 | N/A | N/A | N/A | N/A |
| L 3-8 | 45.5 | 1.381 | 12a | 0.02 | 12b | 0.02 | N/A | N/A | N/A | N/A |
| L 3-8 | 91 | 1.337 | 12a | 0.02 | 12b | 0.02 | N/A | N/A | N/A | N/A |
| L 3-8 | 104 | 1.275 | 12a | 0.02 | 12b | 0.02 | N/A | N/A | N/A | N/A |

# Appendix 3. Distance Protection Settings Part 1

| | Protection Device | Location | Branch | Manufacturer | Model | Stage (Phase) | Impedance pri. Ohm | Impedance sec. Ohm | Angle deg | Time | Directional | Stage (Earth) |
|---|---|---|---|---|---|---|---|---|---|---|---|---|
| 1 | Relay 10a | 11 | LL 10-11 | GEC Alsthom | Micromho | PPZ1 [21] | 0.23056 | 0.000524 | 60.00 | 0.00 | Forward | PGZ1 [21] |
| | | | | | | PPZ2 [21] | 0.30272 | 0.000688 | 60.00 | 0.30 | Forward | PGZ2 [21] |
| | | | | | | PPZ3 [21] | 0.36036 | 0.000819 | 60.00 | 0.60 | Forward | PGZ3 [21] |
| 2 | Relay 10b | 10 | LL 10-11 | GEC Alsthom | Micromho | PPZ1 [21] | 0.23056 | 0.000524 | 60.00 | 0.00 | Forward | PGZ1 [21] |
| | | | | | | PPZ2 [21] | 0.30272 | 0.000688 | 60.00 | 0.30 | Forward | PGZ2 [21] |
| | | | | | | PPZ3 [21] | 0.36036 | 0.000819 | 60.00 | 0.60 | Forward | PGZ3 [21] |
| 3 | Relay 11a | 4 | LL11-4 | GEC Alsthom | Micromho | PPZ1 [21] | 0.34232 | 0.000778 | 60.00 | 0.00 | Forward | PGZ1 [21] |
| | | | | | | PPZ2 [21] | 0.44924 | 0.001021 | 60.00 | 0.30 | Forward | PGZ2 [21] |
| | | | | | | PPZ3 [21] | 0.53504 | 0.001216 | 60.00 | 0.60 | Forward | PGZ3 [21] |
| 4 | Relay 11b | 11 | LL11-4 | GEC Alsthom | Micromho | PPZ1 [21] | 0.34232 | 0.000778 | 60.00 | 0.00 | Forward | PGZ1 [21] |
| | | | | | | PPZ2 [21] | 0.44924 | 0.001021 | 60.00 | 0.30 | Forward | PGZ2 [21] |
| | | | | | | PPZ3 [21] | 0.53504 | 0.001216 | 60.00 | 0.60 | Forward | PGZ3 [21] |
| 5 | Relay 12a | 3 | LL 3-8 | GEC Alsthom | Micromho | PPZ1 [21] | 0.92686 | 0.0021065 | 60.00 | 0.00 | Forward | PGZ1 [21] |
| | | | | | | PPZ3 [21] | 1.41988 | 0.003227 | 60.00 | 0.30 | Forward | PGZ2 [21] |
| | | | | | | | | | | | | PGZ3 [21] |
| 6 | Relay 12b | 8 | LL 3-8 | GEC Alsthom | Micromho | PPZ2 [21] | 1.192796 | 0.0027109 | 60.00 | 0.30 | Forward | PGZ1 [21] |
| | | | | | | PPZ3 [21] | 1.4198801 | 0.003227 | 60.00 | 0.00 | Forward | PGZ2 [21] |
| | | | | | | | | | | | | PGZ3 [21] |
| 7 | Relay 1a | 1 | LL1-2 | GEC Alsthom | Micromho | PPZ1 DS1 [21] | 1.9712001 | 0.00448 | 60.00 | 0.00 | Forward | PGZ1 DS1 [21] |
| | | | | | | PPZ2 DS1 [21] | 2.5871998 | 0.00588 | 70.00 | 0.30 | Forward | PGZ2 DS1 [21] |
| | | | | | | PPZ3 DS1 [21] | 3.08044 | 0.007001 | 70.00 | 0.60 | Forward | PGZ3 DS1 [21] |
| 8 | Relay 1b | 2 | LL1-2 | GEC Alsthom | Micromho | PPZ1 [21] | 1.9712001 | 0.00448 | 60.00 | 0.00 | Forward | PGZ1 [21] |
| | | | | | | PPZ2 [21] | 2.5871998 | 0.00588 | 60.00 | 0.30 | Forward | PGZ2 [21] |
| | | | | | | PPZ3 [21] | 3.08044 | 0.007001 | 60.00 | 0.60 | Forward | PGZ3 [21] |
| 9 | Relay 2a | 2 | LL 2-3 | GEC Alsthom | Micromho | PPZ1 [21] | 3.08968 | 0.007022 | 60.00 | 0.00 | Forward | PGZ1 [21] |
| | | | | | | PPZ2 [21] | 3.8625266 | 0.0087785 | 60.00 | 0.30 | Forward | PGZ2 [21] |
| | | | | | | PPZ3 [21] | 4.24864 | 0.009656 | 60.00 | 0.60 | Forward | PGZ3 [21] |
| 10 | Relay 2b | 3 | LL 2-3 | GEC Alsthom | Micromho | PPZ1 [21] | 3.08968 | 0.007022 | 60.00 | 0.00 | Forward | PGZ1 [21] |
| | | | | | | PPZ2 [21] | 4.0554798 | 0.009217 | 60.00 | 0.30 | Forward | PGZ2 [21] |
| | | | | | | PPZ3 [21] | 4.8267997 | 0.01097 | 60.00 | 0.60 | Forward | PGZ3 [21] |
| 11 | Relay 3a | 3 | LL 3-4 | GEC Alsthom | Micromho | PPZ1 [21] | 0.42636 | 0.000969 | 60.00 | 0.00 | Forward | PGZ2 [21] |
| | | | | | | PPZ2 [21] | 0.55968 | 0.001272 | 60.00 | 0.30 | Forward | PGZ3 [21] |
| | | | | | | PPZ3 [21] | 0.66616 | 0.001514 | 60.00 | 0.60 | Forward | |
| 12 | Relay 3b | 4 | LL 3-4 | GEC Alsthom | Micromho | PPZ1 [21] | 0.42636 | 0.000969 | 60.00 | 0.00 | Forward | PGZ1 [21] |
| | | | | | | PPZ2 [21] | 0.55968 | 0.001272 | 60.00 | 0.30 | Forward | PGZ2 [21] |
| | | | | | | PPZ3 [21] | 0.66616 | 0.001514 | 60.00 | 0.60 | Forward | PGZ3 [21] |

Appendix 4. Distance Protection Settings Part 2

| | Protection Device | Location | Branch | Manufacturer | Model | Stage (Phase) | Impedance pri. Ohm | Impedance sec. Ohm | Angle deg | Time | Directional |
|---|---|---|---|---|---|---|---|---|---|---|---|
| 13 | Relay 4a | 4 | LL 4-5 | GEC Alsthom | Micromho | PPZ1 [21] | 0.39116 | 0.000889 | 60.00 | 0.00 | Forward |
| | | | | | | PPZ2 [21] | 0.51348 | 0.001167 | 60.00 | 0.30 | Forward |
| | | | | | | PPZ3 [21] | 0.6116 | 0.00139 | 60.00 | 0.60 | Forward |
| 14 | Relay 4b | 5 | LL 4-5 | GEC Alsthom | Micromho | PPZ1 [21] | 0.39116 | 0.000889 | 60.00 | 0.00 | Forward |
| | | | | | | PPZ2 [21] | 0.51348 | 0.001167 | 60.00 | 0.30 | Forward |
| | | | | | | PPZ3 [21] | 0.6116 | 0.00139 | 60.00 | 0.60 | Forward |
| 15 | Relay 5a | 5 | LL 5-6 | GEC Alsthom | Micromho | PPZ1 DS5 [21] | 0.9284 | 0.00211 | 60.00 | 0.00 | Forward |
| | | | | | | PPZ2 DS5 [21] | 1.46652 | 0.003333 | 60.00 | 0.30 | Forward |
| | | | | | | PPZ3 DS5 [21] | 1.81676 | 0.004129 | 60.00 | 0.60 | Forward |
| 16 | Relay 5b | 6 | LL 5-6 | GEC Alsthom | Micromho | PPZ1 DS6 [21] | 1.07624 | 0.002446 | 60.00 | 0.00 | Forward |
| | | | | | | PPZ2 DS6 [21] | 1.41284 | 0.003211 | 60.00 | 0.30 | Forward |
| | | | | | | PPZ3 DS6 [21] | 1.68212 | 0.003823 | 60.00 | 0.60 | Forward |
| 17 | Relay 6a | 6 | LL 6-7 | GEC Alsthom | Micromho | PPZ1 [21] | 0.16764 | 0.000381 | 60.00 | 0.00 | Forward |
| | | | | | | PPZ2 [21] | 0.22022 | 0.0005005 | 60.00 | 0.30 | Forward |
| | | | | | | PPZ3 [21] | 0.2618 | 0.000595 | 60.00 | 0.60 | Forward |
| 18 | Relay 6b | 7 | LL 6-7 | GEC Alsthom | Micromho | PPZ1 [21] | 0.16764 | 0.000381 | 60.00 | 0.00 | Forward |
| | | | | | | PPZ2 [21] | 0.22022 | 0.0005005 | 60.00 | 0.30 | Forward |
| | | | | | | PPZ3 [21] | 0.2618 | 0.000595 | 60.00 | 0.60 | Forward |
| 19 | Relay 7a | 7 | LL 7-8 | GEC Alsthom | Micromho | PPZ1 [21] | 1.16732 | 0.002653 | 60.00 | 0.00 | Forward |
| | | | | | | PPZ2 [21] | 1.5312001 | 0.00348 | 60.00 | 0.30 | Forward |
| | | | | | | PPZ3 [21] | 1.82424 | 0.004146 | 60.00 | 0.60 | Forward |
| 20 | Relay 7b | 8 | LL 7-8 | GEC Alsthom | Micromho | PPZ1 [21] | 1.16732 | 0.002653 | 60.00 | 0.00 | Forward |
| | | | | | | PPZ2 [21] | 1.5312001 | 0.00348 | 60.00 | 0.30 | Forward |
| | | | | | | PPZ3 [21] | 1.82424 | 0.004146 | 60.00 | 0.60 | Forward |
| 21 | Relay 8a | 9 | LL 8-9 | GEC Alsthom | Micromho | PPZ1 [21] | 0.223696 | 0.0005084 | 60.00 | 0.00 | Forward |
| | | | | | | PPZ2 [21] | 0.293612 | 0.0006673 | 60.00 | 0.30 | Forward |
| | | | | | | PPZ3 [21] | 0.349536 | 0.0007944 | 60.00 | 0.60 | Forward |
| 22 | Relay 8b | 8 | LL 8-9 | GEC Alsthom | Micromho | PPZ1 [21] | 0.223696 | 0.0005084 | 60.00 | 0.00 | Forward |
| | | | | | | PPZ2 [21] | 0.293612 | 0.0006673 | 60.00 | 0.30 | Forward |
| | | | | | | PPZ3 [21] | 0.349536 | 0.0007944 | 60.00 | 0.60 | Forward |
| 23 | Relay 9a | 10 | LL 9-10 | GEC Alsthom | Micromho | PPZ1 [21] | 0.5381199 | 0.001223 | 60.00 | 0.00 | Forward |
| | | | | | | PPZ2 [21] | 0.706508 | 0.0016057 | 60.00 | 0.30 | Forward |
| | | | | | | PPZ3 [21] | 0.841104 | 0.0019116 | 60.00 | 0.60 | Forward |
| 24 | Relay 9b | 9 | LL 9-10 | GEC Alsthom | Micromho | PPZ1 [21] | 0.5381199 | 0.001223 | 60.00 | 0.00 | Forward |
| | | | | | | PPZ2 [21] | 0.706508 | 0.0016057 | 60.00 | 0.30 | Forward |
| | | | | | | PPZ3 [21] | 0.841104 | 0.0019116 | 60.00 | 0.60 | Forward |